





Chief Guest
Prof. Bhaskar Ramamurthy

(IIT Madras)

Talk

புதிய பார்வை

of. A
Jhunjhunwala
Electrical Engineering,
IIT Madras









ऑडिटोरियम
AUDITORIUM →
नालय
MEETING HALL →





आवार्डिनेशन
AUDITORIUM
भोजनालय
DINING HALL



BPIP-1

ऑडिटोरियम
AUDITORIUM
भोजनालय
DINING HALL



Power electronic converters for Grid Interface of solar power generation

Dr. BHIM SINGH

Prof. & Head

FNAE, FNA, FNASC, FASc, FTWAS, IEEE, FIET, FIETE, FIE (I), C. ENGIL

Department of Electrical Engineering

Indian Institute of Technology Delhi

New Delhi-110016-India







NATIONAL CONFERENCE ON
RECENT TRENDS IN POWER ENGINEERING
(for Research Scholars)

Date: 29-30 December 2015

Venue : IC & SR Auditorium



Chief Guest
Prof. Bhaskar Ramamurthi

(Director, IIT Madras)

&
Plenary Talk on
"Enabling India with Electricity"
by



Prof. Ashok Jhunjhunwala
Department of Electrical Engineering,
IIT Madras



A Generalized Framework to Diagnose Displacements in Transformer Winding



Prof. L. Satish

HV Lab, Dept. of Electrical Engineering
Indian Institute of Science, Bangalore

homepage: hve.iisc.ernet.in/~satish

Credits: Mr. Pritam Mukherjee, Ph.D. scholar

National Power Engineering Research Scholars' Meet, IIT-M, 29-30 Dec, 2015



NATIONAL CONFERENCE ON
RECENT TRENDS IN POWER ENGINEERING

(for Research Scholars)

Date: 29-30 December 2015
Venue : IC & SR Auditorium



Chief Guest

Prof. Bhaskar Ramamurthi

(Director, IIT Madras)

&

Plenary Talk on

"Enabling India with Electricity"
by



Prof. Ashok Jhunjhunwala

Department of Electrical Engineering
IIT Madras

ABB and Solar Impulse
An innovation and technology alliance for a better world

With ABB and Solar Impulse share a common vision of
minimizing resource consumption and maximizing the
use of renewable energy

ABB and Solar Impulse are passionate partners of
leading-edge technology for a better world

This record-the-world flight powered by the sun

From ABB migrants were embedded in the aircraft
monitoring electrical insulators and suspension



Venue : IC & SR Auditorium





onum

Chief Guest

Bhaskar Ran

ector, IIT

&

Y



NATIONAL CONFERENCE ON
RECENT TRENDS IN POWER ENGINEERING
(for Research Scholars)
Date: 29-30 December 2015
Venue : IC & SR Auditorium



Chief Guest
Prof. Bhaskar Ramamurthi
(Director, IIT Madras)



Multilevel inverters with reduced DC link power supplies for IM drives

K. Gopakumar
Professor , DESE (formerly CEDT)
Department of Electronic systems Engineering
Indian Institute of Science
Bangalore



ENERGY AUDIT & ITS RELEVENCE TO INDIA - A CAPSULIZATION

Dr. S. THUMADHAVAN

Energy Studies, Anna University, Chennai

Int.

ITI



NATIONAL CONFERENCE ON
RECENT TRENDS IN POWER ENGINEERING
(for Research Scholars)

Date: 29-30 December 2015
Venue : IC & SR Auditorium



Chief Guest
Prof. Bhaskar Iyer Amurthi
(Director, IIIT Hyderabad)

Plenary Talk on "Green Electricity"

sunwala
Engineering.

book

of

I

II

III

IV

V

VI

VII

VIII

VII

V

VI

VII

VIII

V

VI





National Conference on Recent Trends in Power Engineering

Indian Institute of Technology Madras, Chennai 600 036, India.

29-30 December 2015

Closed Loop Control Analysis of Half Bridge LLC Resonant Converter based Battery Charger

Sumanta Kumar Show

Research Scholar, NITK Surathkal, India

P. Parthiban

Assistant Professor, NITK Surathkal, India



Introduction

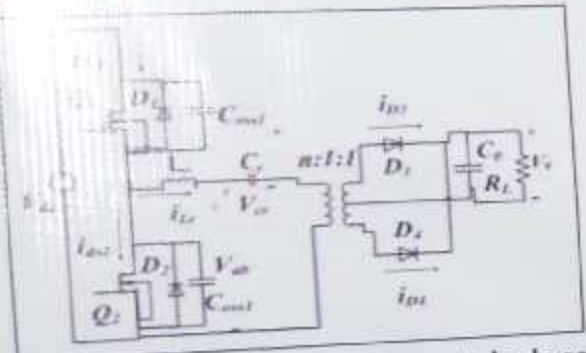


Fig. 1 Circuit diagram of LLC resonant dc-dc converter.

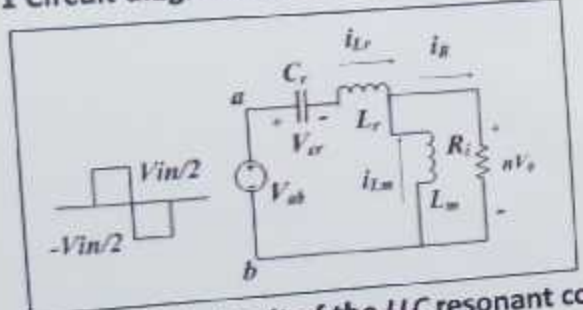


Fig. 2 Equivalent circuit of the LLC resonant converter.

Circuit Description

An LLC resonant Half-Bridge (HB) dc-dc converter consists of an LLC resonant inverter, a current-driven transformer with a center tapped rectifier.

Controller Parameters : $K_p = 0.0154$, $K_i = 10$.

Half-Bridge LLC converter Specifications

Electrical Specifications

Input Voltage (V_{in})	(380 – 420) V
Output Voltage (V_o)	(28 - 72) V
Output Current (I_o)	(16 - 25) A
Maximum Power (P_o)	1.8kW
Main Resonant Frequency (f_H)	200 kHz
Secondary Resonant Frequency (f_L)	85.287 kHz
Switching Frequency	(94.6 – 226.6) kHz

Component Parameters

Resonant Inductor (L_r)	1.855 μ H
Magnetizing Inductor (L_m)	8.356 μ H
Resonant Capacitor (C_r)	34.2 μ F
Transformer Turns Ratio	9:1:1

Results & Discussion

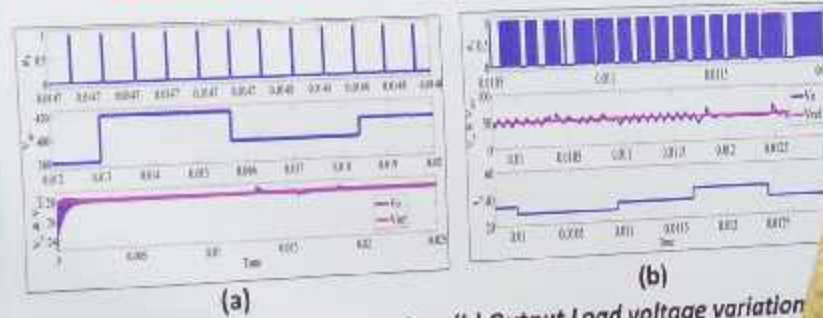


Fig. 3 (a) Input Line voltage variation, (b) Output Load voltage variation

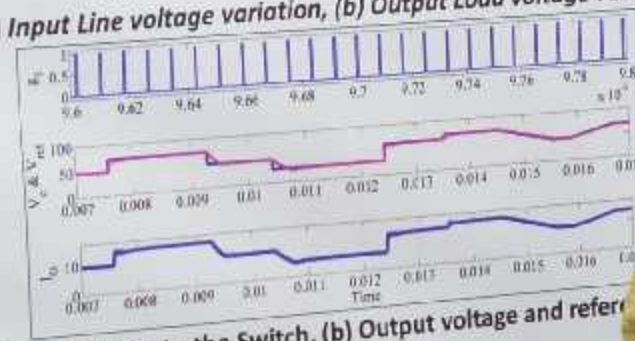


Fig. 4 (a) Gate pulses to the Switch, (b) Output voltage and reference voltage, (c) Output Load current.

Conclusions

Simulation analysis of a LLC resonant Half-Bridge (HB) dc-dc converter is presented with R-Load. Results shows the performance of Controller for adjustment of output voltage for line, load and reference.



HVE018

Calculation of Corona Generated Ionic Currents of Unipolar HVDC Transmission Lines Using New Computational Method

M. Raja Nayak, Pradeep M. Nigade, S. A. Aravind
UHVRI, Central Power Research Institute, Hyderabad
mrajanayak@yahoo.com

INTRODUCTION

The electric field environment of HVDC transmission lines is different from that existing HVAC transmission lines. In DC transmission, there space charges in the inter electrode region, contrary to that in AC transmission where the space charge created by corona is contained in the vicinity of the conductors because of the periodic reversal of the applied voltage. Hence it may be possible to predict the AC corona losses based on corona cage models. Whereas, in case of HVDC lines it is not possible to predict the DC corona losses using cage models. However, evaluation of alternate line design based on entirely experimental means proved costly and time consuming. On account of this fact, computational analysis based on experimental findings can provide a significant support for evaluation of alternate line designs.

In this current, the authors have made an attempt to develop the computational method using physical model of corona phenomenon around the line conductor with considering impacts of atmospheric parameters such as temperature and pressure.



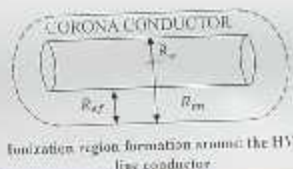
Electric Field Environment Of Unipolar HVDC Lines

METHOD OF CALCULATION:

The major equations used to estimate the parameters of electric field environment of unipolar HVDC lines are ion current equation and Poisson's equation and the governing equations of ion current and Poisson's equations are given below:

$$J = \rho b E$$
$$\nabla \cdot \mathbf{E} = \rho / \epsilon_0$$

Where J is space charge affected electric field, E is space charge free electric field, ρ is ionic current density, ϵ_0 is ion space charge density and b is mobility of ions. The average mobility of ions considered is $1.5 \text{ m}^2/\text{V}$.



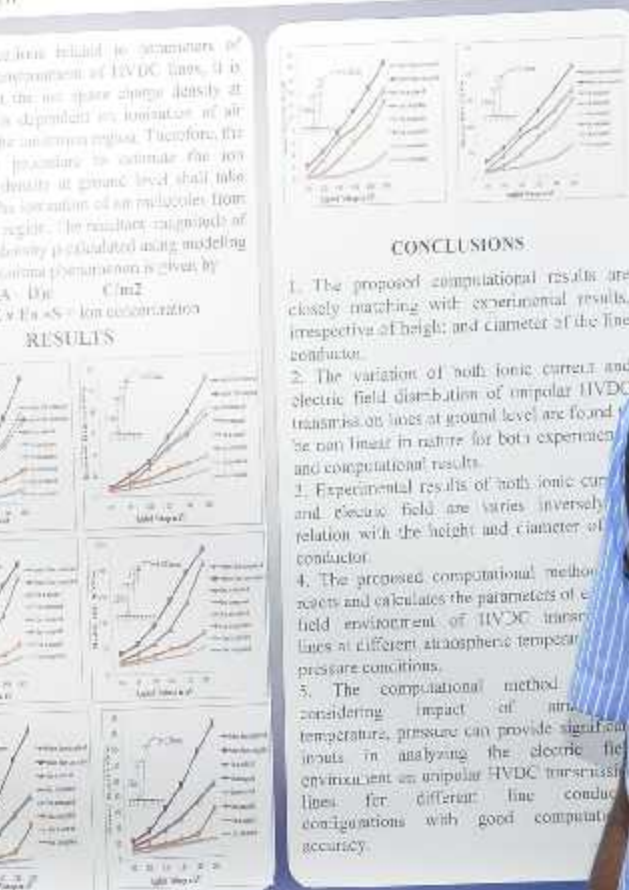
Ionization region formation around the HVDC line conductor

From the relations related to dynamics of electric field environment of HVDC lines, it is very clear that the ion space charge density at ground level is dependent on ionization of air molecules in the unipolar region. Therefore, the computational procedure to estimate the ion space charge density at ground level shall take into account the ionization of air molecules from the boundary region. The resultant ionization of space charge density is calculated using modeling of physics of corona phenomenon is given by

$$\rho = kT_e A D n \quad \text{C/m}^2$$

Where k is Boltzmann's constant, T_e is ion temperature

RESULTS



CONCLUSIONS

1. The proposed computational results are closely matching with experimental results, irrespective of height and diameter of the line conductor.

2. The variation of both ionic current and electric field distribution of unipolar HVDC transmission lines at ground level are found to be non linear in nature for both experimental and computational results.

3. Experimental results of both ionic current and electric field are varies inversely relation with the height and diameter of conductor.

4. The proposed computational method relates and calculates the parameters of electric field environment of HVDC unipolar lines at different atmospheric temperature pressure conditions.

5. The computational method considering impact of atmospheric temperature, pressure can provide significant results in analyzing the electric field environment on unipolar HVDC transmission lines for different line conductor configurations with good computational accuracy.

National Conference on Recent Trends in Power Engineering
Indian Institute of Technology Madras, Chennai 600 036, India
29-30 December 2015
Topics and Applications

TRANSMISSION LINES

2015

National Conference on Recent Trends in Power Engineering
Indian Institute of Technology Madras, Chennai 600 036, India
29-30 December 2015
Topics and Applications

SP 15

Electric and Magnetic Field Simulation of Polymer Nano-composites for Electromagnetic Shielding Effectiveness
Kavita M*, Sundara Rajan J*, Rathan** and Suganya K. R.***
*Department of Electrical Engineering, Central Power Research Institute, Bangalore, Karnataka, India; **Department of Electrical and Electronics Engineering, Anna University, Chennai 600 025, India; ***Department of EEE, Department of Electrical and Electronics Engineering, Government College of Engineering, Salem, Tamil Nadu, India

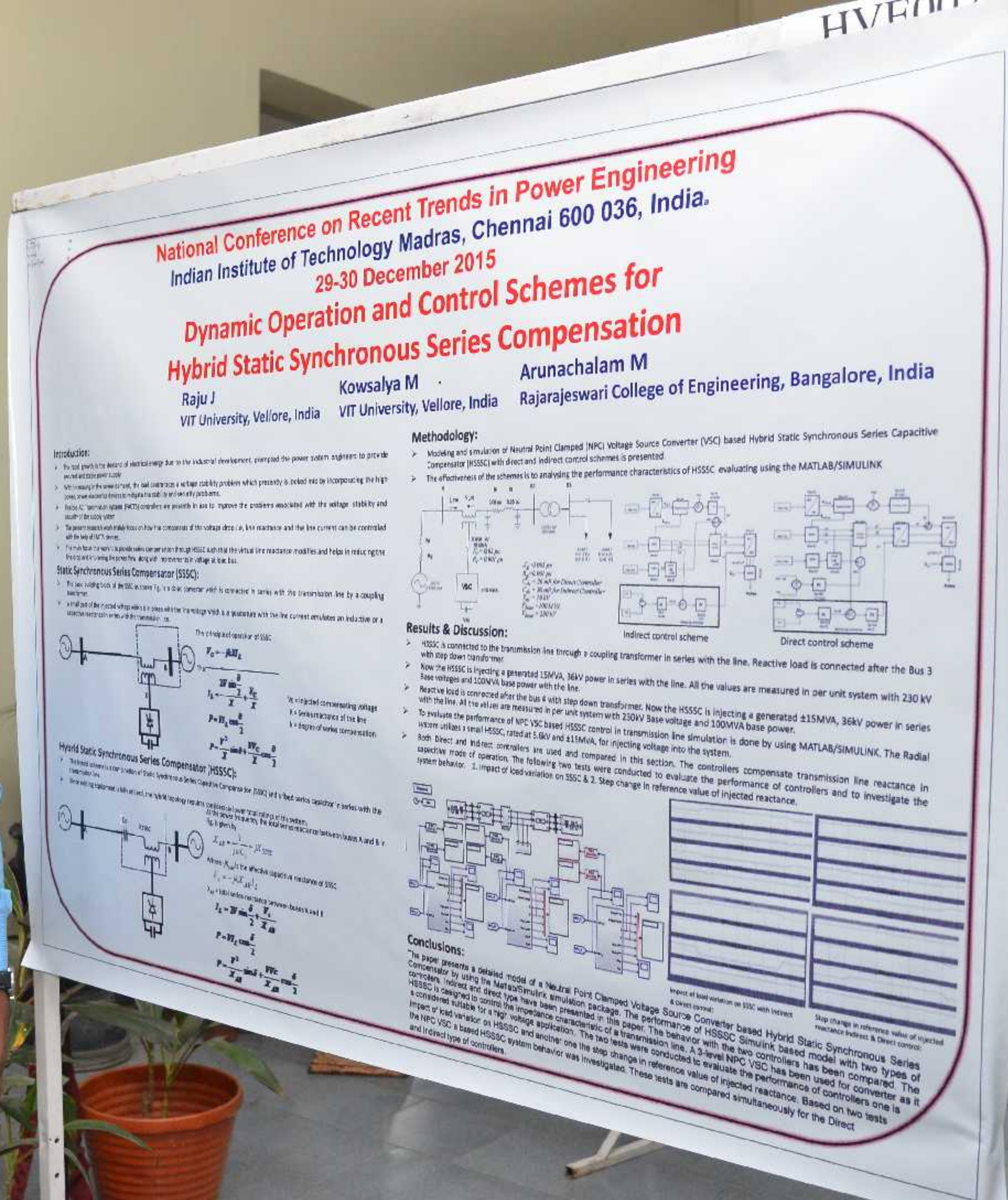
National Conference on Recent Trends in Power Engineering
Indian Institute of Technology Madras, Chennai 600 036, India
29-30 December 2015
Topics and Applications

TRANSMISSION LINES

2015

TRANSMISSION LINES

2015</p



National Conference on Recent Trends in Power Engineering
Indian Institute of Technology Madras, Chennai 600 036, India.
29-30 December 2015

H 003

Electric and Magnetic field Simulation of Polymer Nano-composites for Electromagnetic Shielding Effectiveness

Kavya M*, Sundara Rajan. J*, Rashmi** and Sailaja. R. R. N***

* Central Power Research Institute, Bangalore, Karnataka, India 560080; ** Department of Electrical and Electronics, Siddaganga Institute of Technology, Tumkur, Karnataka, 572103; *** Department EET Department, The Energy and Research Institute, Bangalore, Karnataka, 560071.

Introduction

- Electro and Magnetic interference are the serious problems faced by modern electronic systems.
- Electro magnetic compatibility is accomplished by electronic components and filters or by shielding.
- Performance of polymer composite with respect to the EM Shielding is becoming popular and is investigated in this study.
- Polymer composite used in this study is High Density Polyethylene (HDPE) and fillers used are Multi walled Carbon nanotube (MWNT) and nano Nickel.
- Filler percentage of the nano composite is varied and change in electric field distribution in static and time variant conditions and Magnetic fields are simulated and analyzed.
- Properties of pure polymer and nano Filler additives are compared to check the changes in the behaviour of composite from insulating to conductive property.
- Simulation studies have been carried out and discussed using COMSOL Multiphysics.

Methods

1. Basic Equations for Electric Field Simulation

Electric Field Simulations are based on the following equations:

$$\nabla \cdot D = P_e \\ E = \nabla V \\ D = \epsilon_0 E$$

Where D = electric field Displacement.

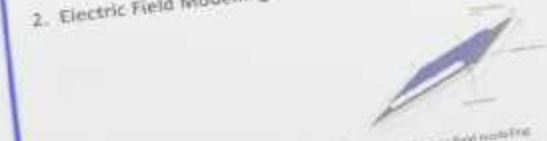
ρ_e = Charge density.

E = Electric Field

Electric field displacement is a function of the permittivity of material and electric field produced at a given input voltage.

Charge density is calculated by divergence of electric field displacement.

2. Electric Field Modelling



- Simple model using FEM is shown in Fig.1 for simulation of electric field using two parallel plate electrodes.
- The nano composite material developed is placed between the two conducting copper plate electrodes.
- Copper plate is shown in blue colour and has potential of about 10 V and Copper plate in red colour is the ground (V=0).

3. Basic Equations for Magnetic Field

$$\nabla \cdot B = 0 \\ B = \mu_0 H$$

Where B = Total Magnetic field

H = magnetic field strength

Total Magnetic field calculation is related to permeability of material and magnetic field strength.

Divergence of magnetic field is zero as magnetic monopole do not exist in space.

4. Magnetic Field Modelling

- A permanent magnet model is used for simulation of Magnetic field.
- Nano composite material developed is placed below a permanent magnet which is to be evaluated.

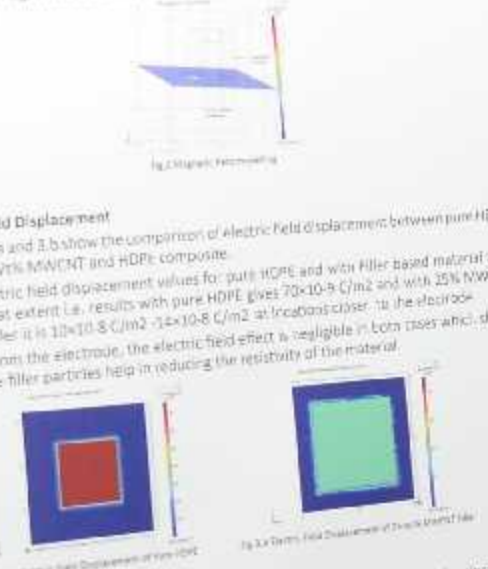
- With the help of Permanent magnet, magnetic field is generated.
- Effect of the magnetic field on pure polymer & polymer nano composites is compared.

- Polarization of HDPE with 25wt% MWNT varies from $1.5 \times 10^{-6} \text{ C/m}^2$ to $1.0 \times 10^{-6} \text{ C/m}^2$ along the sheet, which shows field is constant & it is affected due to displacement of polarization is less as compared to that of pure HDPE, which is a defect.

Results

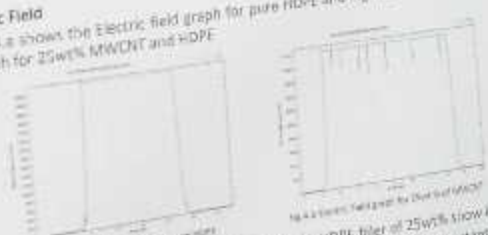
1. Electric Field Displacement

- Figure 3.a and 3.b show the comparison of electric field displacement between pure HDPE and 25 Wt% MWNT and HDPE composite.
- The electric field displacement values for pure HDPE and with filler-based material vary to a great extent i.e. results with pure HDPE gives $70 \times 10^{-6} \text{ C/m}^2$ and with 25% MWNT HDPE filer it is $10 \times 10^{-6} \text{ C/m}^2$ & $10 \times 10^{-6} \text{ C/m}^2$ at location closer to the electrode.
- Away from the electrode, the electric field effect is negligible in both cases which shows that the filler particles help in reducing the resistivity of the material.



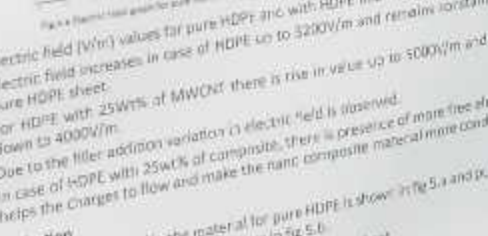
2. Electric Field

- Fig.4.a shows the Electric field graph for pure HDPE and Fig.4.b shows the electric field graph for 25wt% MWNT and HDPE.



3. Polarization

- Polarization obtained in the material for pure HDPE is shown in Fig.5.a and polarization for HDPE with 25wt% MWNT is as shown in Fig.5.b.
- Polarization in pure HDPE is $15 \times 10^{-6} \text{ C/m}^2$ along the sheet.



Conclusion

- Electrical conductivity of HDPE is low, improvement in the resistance of HDPE with MWNT.
- Magnetic property is not much affected in the presence of MWNT.
- In case of HDPE + 25wt% of MWNT composite more than double current is required to get same magnetic field as that of pure HDPE.
- The magnetic flux density of HDPE is noted to be 0.22 T for 5 and 25 A/m .
- The effect of magnetic field is low as compared to magnetic flux density.
- In case of HDPE + 25wt% of MWNT composite more than double current is required to get same magnetic field as that of pure HDPE.

Electrical conductivity of HDPE is low, improvement in the resistance of HDPE with MWNT.

Magnetic property is not much affected in the presence of MWNT.

In case of HDPE + 25wt% of MWNT composite more than double current is required to get same magnetic field as that of pure HDPE.

The magnetic flux density of HDPE is noted to be 0.22 T for 5 and 25 A/m .

The effect of magnetic field is low as compared to magnetic flux density.

In case of HDPE + 25wt% of MWNT composite more than double current is required to get same magnetic field as that of pure HDPE.

The magnetic flux density of HDPE is noted to be 0.22 T for 5 and 25 A/m .

The effect of magnetic field is low as compared to magnetic flux density.

In case of HDPE + 25wt% of MWNT composite more than double current is required to get same magnetic field as that of pure HDPE.

The magnetic flux density of HDPE is noted to be 0.22 T for 5 and 25 A/m .

The effect of magnetic field is low as compared to magnetic flux density.

In case of HDPE + 25wt% of MWNT composite more than double current is required to get same magnetic field as that of pure HDPE.

The magnetic flux density of HDPE is noted to be 0.22 T for 5 and 25 A/m .

The effect of magnetic field is low as compared to magnetic flux density.

In case of HDPE + 25wt% of MWNT composite more than double current is required to get same magnetic field as that of pure HDPE.

The magnetic flux density of HDPE is noted to be 0.22 T for 5 and 25 A/m .

The effect of magnetic field is low as compared to magnetic flux density.

In case of HDPE + 25wt% of MWNT composite more than double current is required to get same magnetic field as that of pure HDPE.

The magnetic flux density of HDPE is noted to be 0.22 T for 5 and 25 A/m .

The effect of magnetic field is low as compared to magnetic flux density.

In case of HDPE + 25wt% of MWNT composite more than double current is required to get same magnetic field as that of pure HDPE.

The magnetic flux density of HDPE is noted to be 0.22 T for 5 and 25 A/m .

The effect of magnetic field is low as compared to magnetic flux density.

In case of HDPE + 25wt% of MWNT composite more than double current is required to get same magnetic field as that of pure HDPE.

The magnetic flux density of HDPE is noted to be 0.22 T for 5 and 25 A/m .

The effect of magnetic field is low as compared to magnetic flux density.

In case of HDPE + 25wt% of MWNT composite more than double current is required to get same magnetic field as that of pure HDPE.

The magnetic flux density of HDPE is noted to be 0.22 T for 5 and 25 A/m .

The effect of magnetic field is low as compared to magnetic flux density.

In case of HDPE + 25wt% of MWNT composite more than double current is required to get same magnetic field as that of pure HDPE.

The magnetic flux density of HDPE is noted to be 0.22 T for 5 and 25 A/m .

The effect of magnetic field is low as compared to magnetic flux density.

In case of HDPE + 25wt% of MWNT composite more than double current is required to get same magnetic field as that of pure HDPE.

The magnetic flux density of HDPE is noted to be 0.22 T for 5 and 25 A/m .

The effect of magnetic field is low as compared to magnetic flux density.

In case of HDPE + 25wt% of MWNT composite more than double current is required to get same magnetic field as that of pure HDPE.

The magnetic flux density of HDPE is noted to be 0.22 T for 5 and 25 A/m .

The effect of magnetic field is low as compared to magnetic flux density.

In case of HDPE + 25wt% of MWNT composite more than double current is required to get same magnetic field as that of pure HDPE.

The magnetic flux density of HDPE is noted to be 0.22 T for 5 and 25 A/m .

The effect of magnetic field is low as compared to magnetic flux density.

In case of HDPE + 25wt% of MWNT composite more than double current is required to get same magnetic field as that of pure HDPE.

The magnetic flux density of HDPE is noted to be 0.22 T for 5 and 25 A/m .

The effect of magnetic field is low as compared to magnetic flux density.

In case of HDPE + 25wt% of MWNT composite more than double current is required to get same magnetic field as that of pure HDPE.

The magnetic flux density of HDPE is noted to be 0.22 T for 5 and 25 A/m .

The effect of magnetic field is low as compared to magnetic flux density.

In case of HDPE + 25wt% of MWNT composite more than double current is required to get same magnetic field as that of pure HDPE.

The magnetic flux density of HDPE is noted to be 0.22 T for 5 and 25 A/m .

The effect of magnetic field is low as compared to magnetic flux density.

In case of HDPE + 25wt% of MWNT composite more than double current is required to get same magnetic field as that of pure HDPE.

The magnetic flux density of HDPE is noted to be 0.22 T for 5 and 25 A/m .

The effect of magnetic field is low as compared to magnetic flux density.

In case of HDPE + 25wt% of MWNT composite more than double current is required to get same magnetic field as that of pure HDPE.

The magnetic flux density of HDPE is noted to be 0.22 T for 5 and 25 A/m .

The effect of magnetic field is low as compared to magnetic flux density.

In case of HDPE + 25wt% of MWNT composite more than double current is required to get same magnetic field as that of pure HDPE.

The magnetic flux density of HDPE is noted to be 0.22 T for 5 and 25 A/m .

The effect of magnetic field is low as compared to magnetic flux density.

In case of HDPE + 25wt% of MWNT composite more than double current is required to get same magnetic field as that of pure HDPE.

The magnetic flux density of HDPE is noted to be 0.22 T for 5 and 25 A/m .

The effect of magnetic field is low as compared to magnetic flux density.

In case of HDPE + 25wt% of MWNT composite more than double current is required to get same magnetic field as that of pure HDPE.

The magnetic flux density of HDPE is noted to be 0.22 T for 5 and 25 A/m .

The effect of magnetic field is low as compared to magnetic flux density.

In case of HDPE + 25wt% of MWNT composite more than double current is required to get same magnetic field as that of pure HDPE.

The magnetic flux density of HDPE is noted to be 0.22 T for 5 and 25 A/m .

The effect of magnetic field is low as compared to magnetic flux density.

In case of HDPE + 25wt% of MWNT composite more than double current is required to get same magnetic field as that of pure HDPE.

The magnetic flux density of HDPE is noted to be 0.22 T for 5 and 25 A/m .

The effect of magnetic field is low as compared to magnetic flux density.

In case of HDPE + 25wt% of MWNT composite more than double current is required to get same magnetic field as that of pure HDPE.

The magnetic flux density of HDPE is noted to be 0.22 T for 5 and 25 A/m .

The effect of magnetic field is low as compared to magnetic flux density.

In case of HDPE + 25wt% of MWNT composite more than double current is required to get same magnetic field as that of pure HDPE.

The magnetic flux density of HDPE is noted to be 0.22 T for 5 and 25 A/m .

HVE017

National Conference on Recent Trends in Power Engineering Indian Institute of Technology Madras, Chennai 600 036, India 29-30 December 2015

Evaluation of High Voltage Rotating Machine Stator Insulation System Using Diagnostic Tests



Ramesh P Nair* B V Sumangala** K Mallikarjunappa***
*Senior Research Fellow, Diagnostic Cables & Capacitors Division, Central Power Research Institute, Bangalore.
**Professor and Head of EEE Department, Dr. Ambedkar Institute of Technology, Bangalore.
***Joint Director and HOD, Diagnostic Cables & Capacitors Division, Central Power Research Institute, Bangalore.

Diagnostic Tests continued

B. TAN DELTA MEASUREMENT TEST

- The dielectric loss factor is a measure of dielectric loss.
- It is also known as dissipation factor.
- It is usually the winding insulation is supposed to act as a pure capacitor.
- It provides direct proof of energy dissipation in the form of heat when excited by ac voltage.
- The winding insulation can be approximated as a capacitor in parallel with a resistor.



$$\tan \delta = \frac{I_2}{I_1}$$



TABLE I TAN DELTA FOR CLASS F INSULATION		
Temperature	Line-to-line Voltage (kV)	Line-to-ground Voltage (kV)
60°C	0.25	0.25
70°C	0.25	0.25
80°C	0.25	0.25
90°C	0.25	0.25
100°C	0.25	0.25

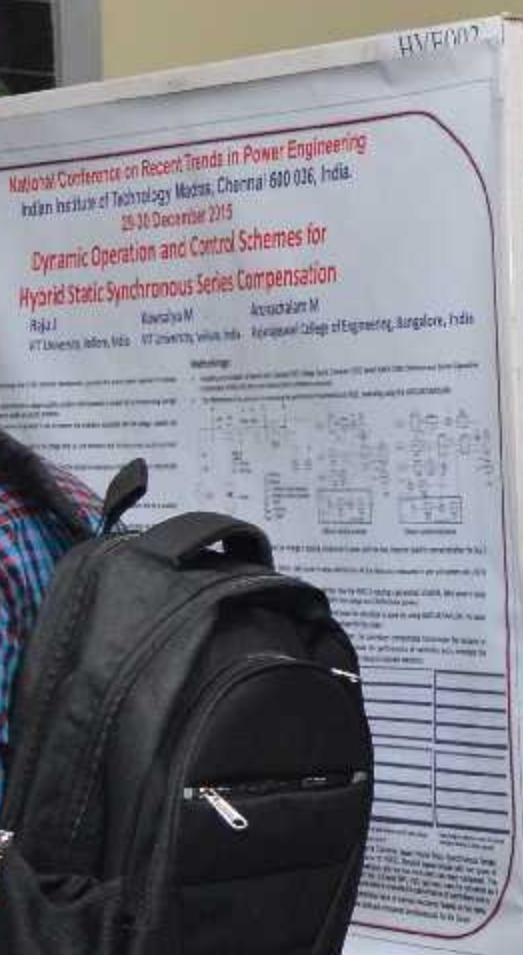


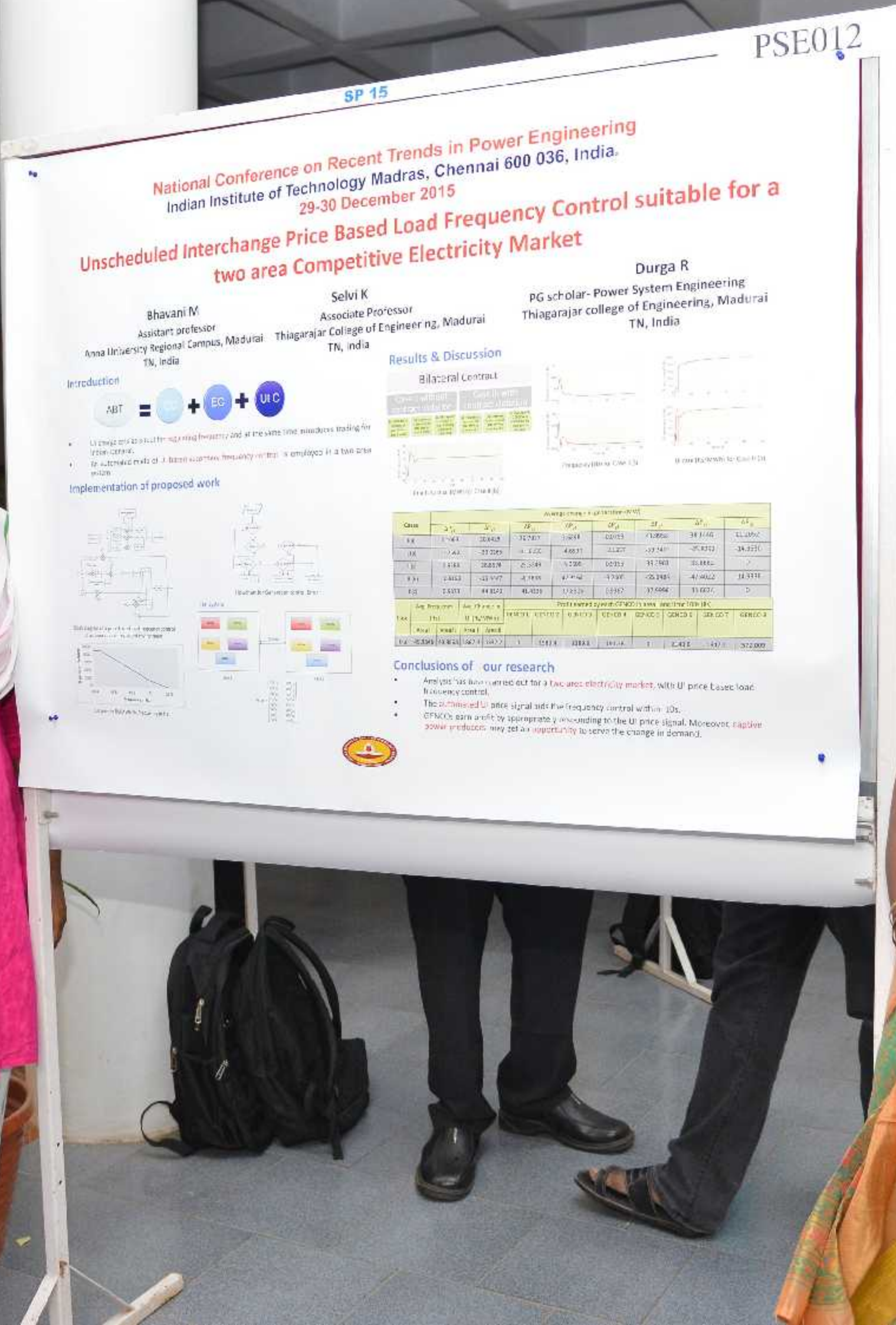
Conclusions

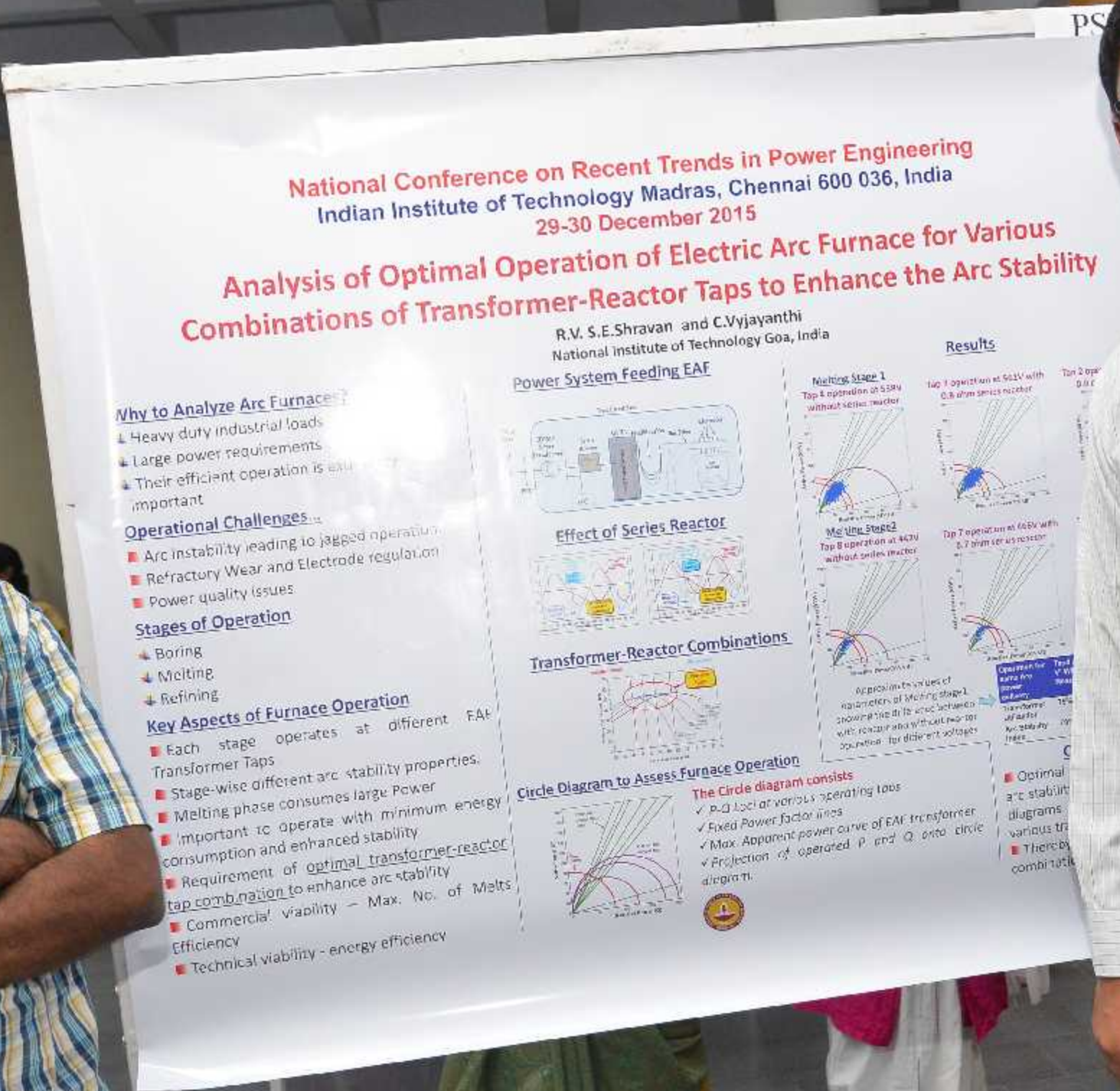
- The results obtained from the experiment indicate good correlation with insulation condition.
- Hence diagnostic tests are very good tool for monitoring the condition of rotating machines insulation system.
- These tests should be conducted in regular basis in order to trend the test data.

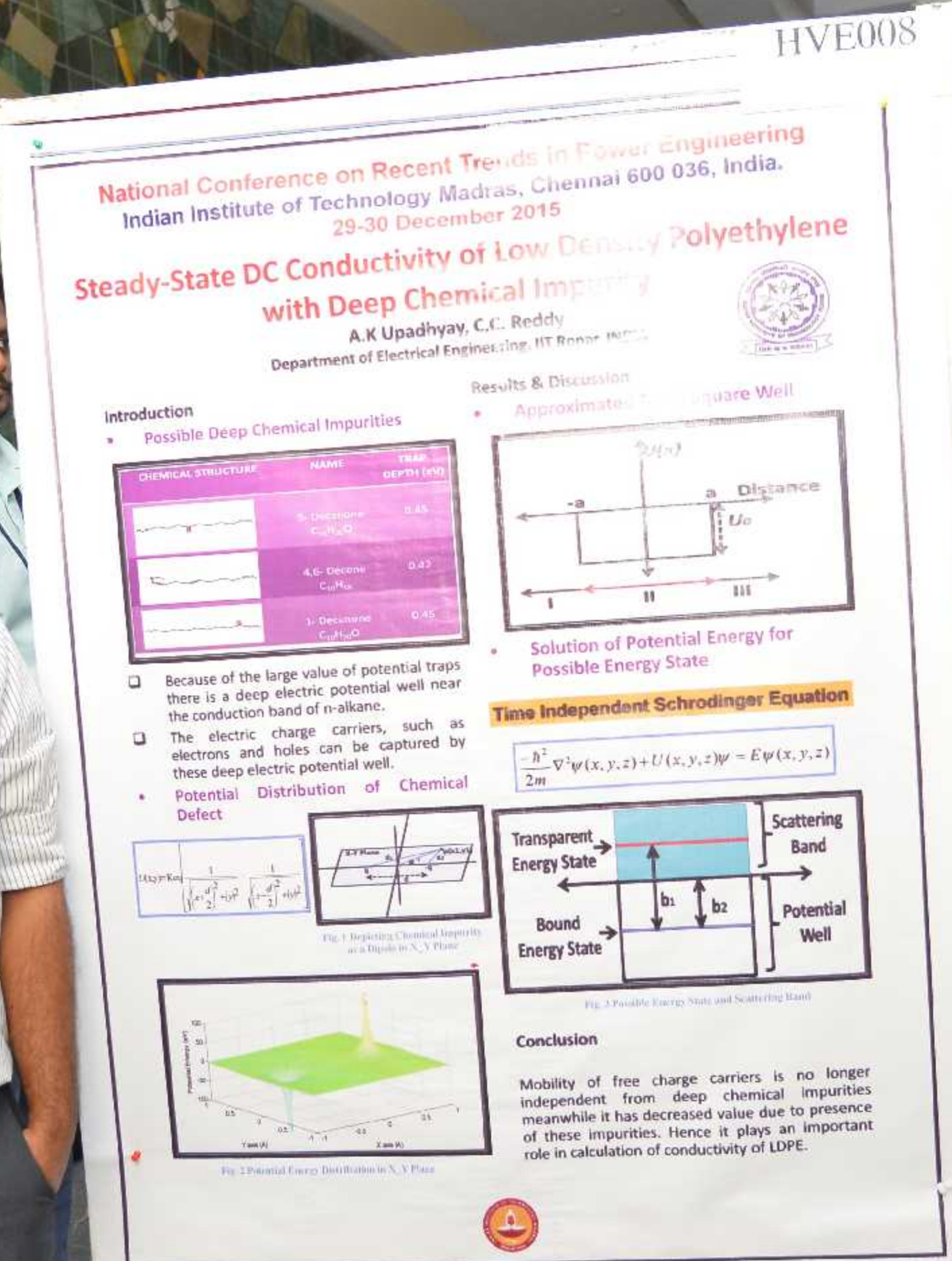
C. PARTIAL DISCHARGE TEST

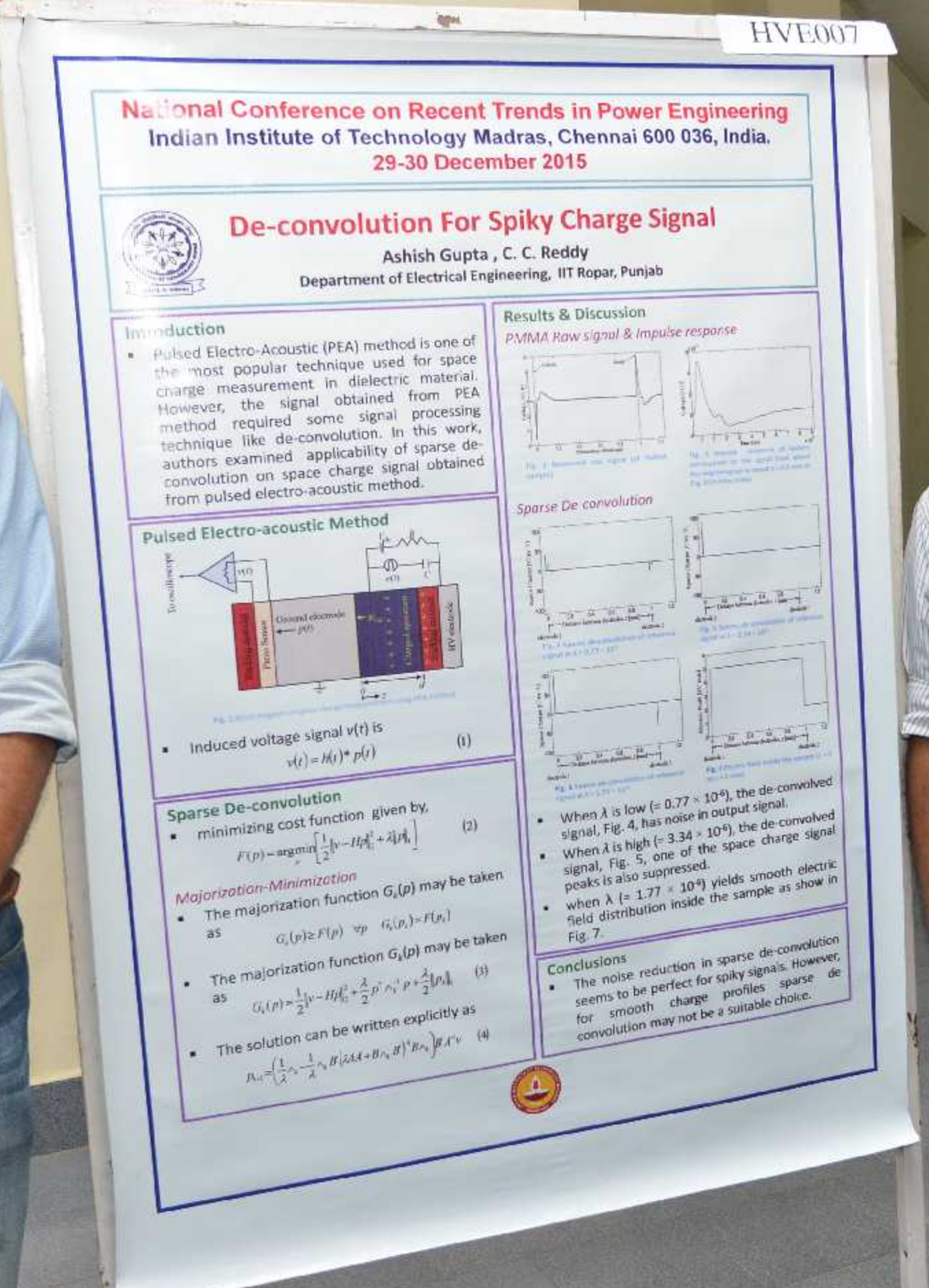
- Partial discharges are localized electrical discharge that only partially bridges the insulation between conductors and which can or cannot occur adjacent to a conductor.
- Partial discharge creates a PD pulse which are sensed by using different sensors and processed by PD detection system.
- The trend in PD magnitude over time is the most effective way of monitoring the discharge activity.













National Conference on Recent Trends in Power Engineering
Indian Institute of Technology Madras, Chennai 600 036, India.
29-30 December 2015



A study on copper corrosion and its effect on dielectric properties of paper oil insulation of transformers using simulation and laboratory experiments

S. Daisy Flora and J. Sundara Rajan
Central Power Research Institute, Bangalore – 560080.

1. Introduction

- Paper of insulation in transformer is severely affected by copper ionization - Electrochemical phenomena due to reactive sulfur species present in oil.
- Corrosive sulphur compounds react with copper conductor to form copper sulphide (Cu_2S).
- Cu_2S is initially formed on the conductor surface and then migrates towards different layers of papers.
- Dielectric properties of paper insulation are affected by Cu_2S due to its semi-conducting nature.
- The parameters of importance in this phenomenon are:
 - ✓ nature of reacting sulphur species in oil
 - ✓ surface condition of copper conductors
 - ✓ moisture
 - ✓ temperature
 - ✓ time of exposure
- Cu_2S has a semi-conductive nature in the temperature range of 300 K to 383 K and is conductive above 383 K.
- In this study, the effect of both temperature and copper sulphide contamination on the following dielectric parameters of paper oil insulation is explained:
 - ✓ Dielectric stress
 - ✓ $\tan \delta$
 - ✓ $\epsilon' - \omega \epsilon''$
 - ✓ Polarization Index
 - ✓ Insulation Resistance

2. Simulation study - FEM Model

- In this study, simulations were carried out on a planar sample configuration (Fig 1(a) and 1(b)).
- Fig 1(a) Planar sample consisting of paper covered copper conductor
- Fig 1(b) Planar size tape model with composite H6/H7
- In the proposed 3D model, paper and Cu_2S are considered as two different layers.
- Electric stress enhancement on the clear paper layer due to Cu_2S migration into each paper layer is computed.
- Surfaces were cut by representing the clear impregnated paper layer by its permittivity of 3.72 and the layer of Cu_2S by its permittivity of 40.
- The conductivity of Cu_2S layer is considered to be $50\text{m}^{-1}\text{A}\text{cm}^{-2}$ and $1 \times 10^{15}\text{S/m}$ in order to represent the metallic and semiconducting behaviour of Cu_2S respectively.
- Boundary conditions: $V=1$ Volt at the top electrode (EV)
- $V=0$ Volt at the bottom electrode (DV)

The electric stress across the Cu_2S -contaminated paper layers and clean paper layers for different values of conductivity are furnished in Table 1.

Table 1. Comparative electric stress in Cu_2S contaminated air dielectric tape for different conductivity values

Conductivity of Cu_2S in $\text{m}^{-1}\text{Acm}^{-2}$	Maximum electric stress			$\epsilon' - \omega \epsilon''$
	EV	DV	EV + DV	
0	3.02	1.16	14	0.41
0.001	2.99	1.16	14	0.39
0.01	2.98	1.16	14	0.38
0.1	2.97	1.16	14	0.37
1	2.96	1.16	14	0.36
10	2.95	1.16	14	0.35
100	2.94	1.16	14	0.34
1000	2.93	1.16	14	0.33
10000	2.92	1.16	14	0.32
100000	2.91	1.16	14	0.31
1000000	2.90	1.16	14	0.30

The variation of minimum electric stress ($\epsilon' - \omega \epsilon''$) across clean paper layers for progressive migration of Cu_2S for different conductivity values is shown in Fig 2.



Fig 2. Variation of minimum electric stress ($\epsilon' - \omega \epsilon''$) across clean paper layers for progressive migration of Cu_2S for different conductivity values

3. Experimental Study

- The dielectric measurements were carried on on laboratory model transformer winding (Fig 3). The paper layers on the High voltage (HV) conductor are fully contaminated by Cu_2S and low voltage (LV) conductor consisted of only clean paper layers.

3.1. FDS Measurements

- The FDS measurements were carried out at 200 V AC over a frequency range of 1 kHz down to 0.1 Hz.

Effect of Cu_2S on $\tan \delta$:

- The variation of $\tan \delta$ with frequency in clean and Cu_2S contaminated paper at 25 °C, 90 °C and 140 °C are shown in Fig 3, 4 and 5.

Fig 3. Variation of $\tan \delta$ with frequency in clean and Cu_2S contaminated paper at 25 °C, 90 °C and 140 °C



Fig 4. Variation of $\tan \delta$ with frequency in clean and Cu_2S contaminated paper at 25 °C, 90 °C and 140 °C

Fig 5. Variation of $\tan \delta$ with frequency in clean and Cu_2S contaminated paper at 25 °C, 90 °C and 140 °C

Effect of Cu_2S on ϵ' :

- The variation of ϵ' with frequency in clean and Cu_2S contaminated paper at 25 °C, 90 °C and 140 °C are shown in Fig 6, 7 and 8.

Fig 6. Variation of ϵ' with frequency in clean and Cu_2S contaminated paper at 25 °C, 90 °C and 140 °C

Fig 7. Variation of ϵ' with frequency in clean and Cu_2S contaminated paper at 25 °C, 90 °C and 140 °C

Fig 8. Variation of ϵ' with frequency in clean and Cu_2S contaminated paper at 25 °C, 90 °C and 140 °C

Fig 9. Variation of $\epsilon' - \omega \epsilon''$ with frequency in clean and Cu_2S contaminated paper at 25 °C, 90 °C and 140 °C

Fig 10. Variation of $\epsilon' - \omega \epsilon''$ with frequency in clean and Cu_2S contaminated paper at 25 °C, 90 °C and 140 °C

Fig 11. Variation of $\epsilon' - \omega \epsilon''$ with frequency in clean and Cu_2S contaminated paper at 25 °C, 90 °C and 140 °C

Fig 12. Variation of $\epsilon' - \omega \epsilon''$ with frequency in clean and Cu_2S contaminated paper at 25 °C, 90 °C and 140 °C

Fig 13. Variation of $\epsilon' - \omega \epsilon''$ with frequency in clean and Cu_2S contaminated paper at 25 °C, 90 °C and 140 °C

Fig 14. Variation of $\epsilon' - \omega \epsilon''$ with frequency in clean and Cu_2S contaminated paper at 25 °C, 90 °C and 140 °C

Fig 15. Variation of $\epsilon' - \omega \epsilon''$ with frequency in clean and Cu_2S contaminated paper at 25 °C, 90 °C and 140 °C

Fig 16. Variation of $\epsilon' - \omega \epsilon''$ with frequency in clean and Cu_2S contaminated paper at 25 °C, 90 °C and 140 °C

Fig 17. Variation of $\epsilon' - \omega \epsilon''$ with frequency in clean and Cu_2S contaminated paper at 25 °C, 90 °C and 140 °C

Fig 18. Variation of $\epsilon' - \omega \epsilon''$ with frequency in clean and Cu_2S contaminated paper at 25 °C, 90 °C and 140 °C

Fig 19. Variation of $\epsilon' - \omega \epsilon''$ with frequency in clean and Cu_2S contaminated paper at 25 °C, 90 °C and 140 °C

Fig 20. Variation of $\epsilon' - \omega \epsilon''$ with frequency in clean and Cu_2S contaminated paper at 25 °C, 90 °C and 140 °C

Fig 21. Variation of $\epsilon' - \omega \epsilon''$ with frequency in clean and Cu_2S contaminated paper at 25 °C, 90 °C and 140 °C

Fig 22. Variation of $\epsilon' - \omega \epsilon''$ with frequency in clean and Cu_2S contaminated paper at 25 °C, 90 °C and 140 °C

Fig 23. Variation of $\epsilon' - \omega \epsilon''$ with frequency in clean and Cu_2S contaminated paper at 25 °C, 90 °C and 140 °C

Fig 24. Variation of $\epsilon' - \omega \epsilon''$ with frequency in clean and Cu_2S contaminated paper at 25 °C, 90 °C and 140 °C

Fig 25. Variation of $\epsilon' - \omega \epsilon''$ with frequency in clean and Cu_2S contaminated paper at 25 °C, 90 °C and 140 °C

Fig 26. Variation of $\epsilon' - \omega \epsilon''$ with frequency in clean and Cu_2S contaminated paper at 25 °C, 90 °C and 140 °C

Fig 27. Variation of $\epsilon' - \omega \epsilon''$ with frequency in clean and Cu_2S contaminated paper at 25 °C, 90 °C and 140 °C

Fig 28. Variation of $\epsilon' - \omega \epsilon''$ with frequency in clean and Cu_2S contaminated paper at 25 °C, 90 °C and 140 °C

Fig 29. Variation of $\epsilon' - \omega \epsilon''$ with frequency in clean and Cu_2S contaminated paper at 25 °C, 90 °C and 140 °C

Fig 30. Variation of $\epsilon' - \omega \epsilon''$ with frequency in clean and Cu_2S contaminated paper at 25 °C, 90 °C and 140 °C

Fig 31. Variation of $\epsilon' - \omega \epsilon''$ with frequency in clean and Cu_2S contaminated paper at 25 °C, 90 °C and 140 °C

Fig 32. Variation of $\epsilon' - \omega \epsilon''$ with frequency in clean and Cu_2S contaminated paper at 25 °C, 90 °C and 140 °C

Fig 33. Variation of $\epsilon' - \omega \epsilon''$ with frequency in clean and Cu_2S contaminated paper at 25 °C, 90 °C and 140 °C

Fig 34. Variation of $\epsilon' - \omega \epsilon''$ with frequency in clean and Cu_2S contaminated paper at 25 °C, 90 °C and 140 °C

Fig 35. Variation of $\epsilon' - \omega \epsilon''$ with frequency in clean and Cu_2S contaminated paper at 25 °C, 90 °C and 140 °C

Fig 36. Variation of $\epsilon' - \omega \epsilon''$ with frequency in clean and Cu_2S contaminated paper at 25 °C, 90 °C and 140 °C

Fig 37. Variation of $\epsilon' - \omega \epsilon''$ with frequency in clean and Cu_2S contaminated paper at 25 °C, 90 °C and 140 °C

Fig 38. Variation of $\epsilon' - \omega \epsilon''$ with frequency in clean and Cu_2S contaminated paper at 25 °C, 90 °C and 140 °C

Fig 39. Variation of $\epsilon' - \omega \epsilon''$ with frequency in clean and Cu_2S contaminated paper at 25 °C, 90 °C and 140 °C

Fig 40. Variation of $\epsilon' - \omega \epsilon''$ with frequency in clean and Cu_2S contaminated paper at 25 °C, 90 °C and 140 °C

Fig 41. Variation of $\epsilon' - \omega \epsilon''$ with frequency in clean and Cu_2S contaminated paper at 25 °C, 90 °C and 140 °C

Fig 42. Variation of $\epsilon' - \omega \epsilon''$ with frequency in clean and Cu_2S contaminated paper at 25 °C, 90 °C and 140 °C

Fig 43. Variation of $\epsilon' - \omega \epsilon''$ with frequency in clean and Cu_2S contaminated paper at 25 °C, 90 °C and 140 °C

Fig 44. Variation of $\epsilon' - \omega \epsilon''$ with frequency in clean and $Cu_2S</$

HVE012

NATIONAL CONFERENCE ON RECENT TRENDS IN POWER ENGINEERING

Indian Institute of Technology Madras, Chennai 600 036, India

29-30 December 2015

ANALYSIS OF PARTICLE MOVEMENT AND PARTIAL DISCHARGE IN THE WINDING OF POWER TRANSFORMER USING CFD

N.Vasanthi Gouri¹ P.Srikanth¹ V.Shashank¹ G.Sankeerth¹ M.Ramalinga Raju²

1. CBIT, Hyderabad India 2. JNUT, Kakinada, India

I. POWER TRANSFORMER:

- An important device in electrical substation
- Electric field analysis is the most important design consideration.

II. PARTIAL DISCHARGE:

Electrical discharge that occurs between unisolated areas of the insulating system or between conducting electric components which bridging the gap. It can be caused by discontinuities in the insulation system.

It is under normal working conditions or in an abnormal environment where the insulation condition has been affected with age, or has been used prematurely by electrical over stressing, or due to improper

DISCHARGE IN TRANSFORMER OIL:

Reasons for the partial discharge in transformer oil are FREE METALLIC PARTICLE CONTAMINATIONS IN TRANSFORMER OIL



power transformer due to partial discharge.
FLUID DYNAMICS:
numerical analysis and algorithms to solve
problems involving fluid flows

geometry of the problem:

Flow occupied by the fluid into
may be uniform or non-uniform.
al modeling

use of ionization radiation i-species

y conditions:

initial conditions, fluid behavior
the boundaries of the problem,
which the equations are solved
or transient



III. SIMULATION METHOD PROPOSED:

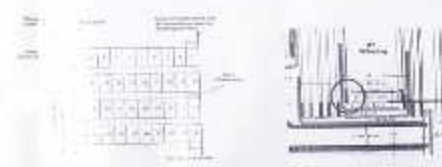


Fig. 3. HV winding of a 100 MVA, 220 KV/132 KV/11 KV transformer

- A 100 MVA/220 KV auto transformer is considered.
- Transformer has a center tap type of winding as shown.
- Only half of the HV coil is examined.
- The gap between the immediate press board cylinder and coil is 8 mm and the half height of the coil is 957 mm.
- Particle is located at any point in the base.

IV. SIMULATION OF THE TRANSFORMER:

- Two dimensional model of a HV winding of the considered transformer is obtained by ANSYS software.
- ANSYS FLUENT is used to model a flow pattern of transformer oil. Oil flow is considered in correlation with the outside flow, as the design part includes the inlet and exit way of an oil flow.
- To obtain the oil flow pattern, the HV winding part is divided into 1653 finite slots. A copper particle of spherical shape with 0.5 mm is also allowed to move along with the transformer with the oil velocity of 0.5 m/sec.



Fig. 4. Simulated oil flow streamlines at HV winding side of a transformer.

V. COLLISION OF PARTICLE WITH TRANSFORMER WINDING:

- A simulation comprising the individual insulated conductors inside the disc would require a large computational effort.
- The area of particle under collision with the winding is divided into number of elements by finite element tool.
- FEM finds the axis of area of contact with the boundary.



- Fig. 5. Model of Finite Elements of colliding area of the particle
- The particle first collides with the disc number 33 and the corresponding disc voltage is 83.466 KV.
 - As the particle touches the winding, electric stress is imposed on the particle.

VI. ELECTRIC FIELD ANALYSIS:

- ANSYS classic makes use of Finite Element Method (FEM) to obtain a structural analysis.
- The area of particle under collision with the winding is divided into number of elements by finite element tool.
- FEM finds the axis of area of contact with the boundary.
- Electrostatic energy in a bounded volume can be given by

$$2W = \epsilon_0 E^2 dv \quad (1)$$

- For a two dimensional analysis along with the axis x and y with m nodes and n number of elements can be written as,

$$2W = \epsilon_0 \int \left[\left(\frac{\partial V}{\partial x} \right)^2 + \left(\frac{\partial V}{\partial y} \right)^2 \right] dv \quad (2)$$

- The electric energy inside an element is,

$$E_{el} = \epsilon_0 \int \left[\left(\frac{\partial V}{\partial x} \right)^2 + \left(\frac{\partial V}{\partial y} \right)^2 \right] dv \quad (3)$$

- Total energy available in the contact area is given by,

$$W = W^{(1)} - W^{(2)} = W^{(1)} \quad (4)$$

- The shape function of a considered 2D geometry is,

$$L^2 = (A^2 / A^{(1)})^{1/2} \quad (5)$$

- The total node potential is given by,

$$\phi = \sum_{i=1}^m \psi_i N_i \quad (6)$$

VII. COLLISION OF PARTICLE WITH OTHER TRANSFORMER WINDING DISCS:

- With further iterations it is found that apart from disc 33 the spherical particle also collides with discs 52 and 51.
- The voltages corresponding to disc 32 and 51 are 82.34 and 83.218 KV respectively. The particle collisions with disc 52 and 51 are shown in Fig. 6 and Fig. 7 respectively.

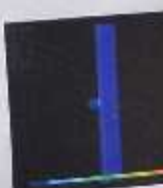


Fig. 6. Particle colliding with disc 33 and 51 of HV winding

VI. RESULTS:



Fig. 7. Particle colliding with disc 51 of HV winding

VII. CONCLUSION:

It is observed that

the particle

collides with

disc 33

and 51

of HV winding

and

disc 52

and

disc 51

of HV winding

and

disc 32

and

disc 51

of HV winding

and

disc 32

and

disc 51

of HV winding

and

disc 32

and

disc 51

of HV winding

and

disc 32

and

disc 51

of HV winding

and

disc 32

and

disc 51

of HV winding

and

disc 32

and

disc 51

of HV winding

and

disc 32

and

disc 51

of HV winding

and

disc 32

and

disc 51

of HV winding

and

disc 32

and

disc 51

of HV winding

and

disc 32

and

disc 51

of HV winding

and

disc 32

and

disc 51

of HV winding

and

disc 32

and

disc 51

of HV winding

and

disc 32

and

disc 51

of HV winding

and

disc 32

and

disc 51

of HV winding

and

disc 32

and

disc 51

of HV winding

and

disc 32

and

disc 51

of HV winding

and

disc 32

and

disc 51

of HV winding

and

disc 32

and

disc 51

of HV winding

and

disc 32

and

disc 51

of HV winding

and

disc 32

and

disc 51

of HV winding

and

disc 32

and

disc 51

of HV winding

and

disc 32

and

<p

FREQUENCY RESPONSE AND COHERENCE FUNCTION ANALYSIS FOR DETECTION OF A SINGLE TURN FAULT IN THE LINE END COIL OF 11 KV MOTOR

Md. Sajid

Cham Jah College of Engg. & Tech.

Sridhar

Institute of Aeronautical Engg.

B.P.Singh

St.Martins Engg. College

K. Shashidhar Reddy

St.Martins Engg. College

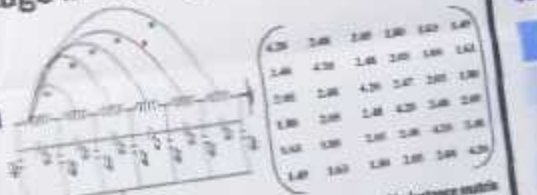
M. Surya K

JNT University, Hyd

Introduction

Power motors are reported to have failed more frequently in industries.

The reason attributed to the failure is due to fast surge generated during circuit breaker switching operations. We have published work related to transient voltage across the turns of line end coil due to incidence of surge. No method is yet proposed for location of turn failures under surge voltage in the high voltage motors.



Based on comparison of frequency response and coherence function between two frequency responses, a method is suggested to determine the failure of a specific turn.

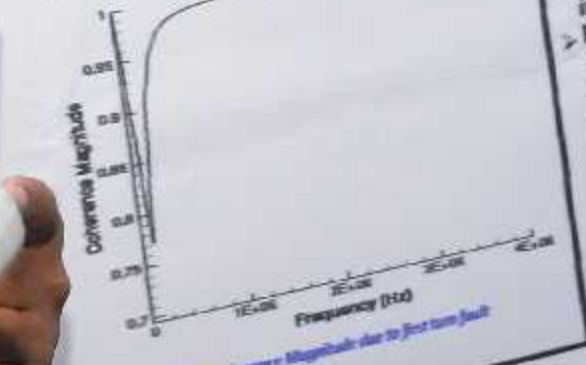


Figure 2: Coherence Magnitude due to first turn fault

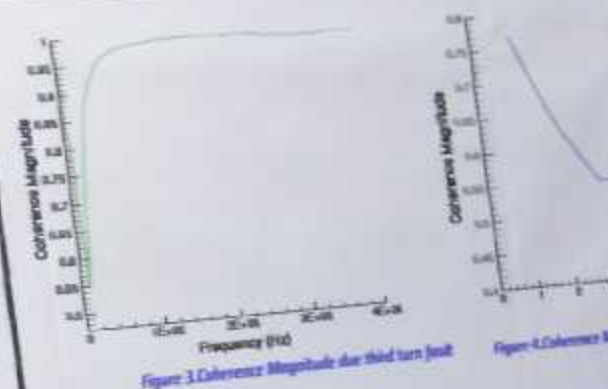


Figure 3: Coherence Magnitude due to third turn fault



Figure 4: Coherence Magnitude across two faults

Coherence magnitude for turn fault

Turn Fault	Frequency	Coherence Value
1	100.000	0.7736
2	100.000	0.6324
3	100.000	0.6324
4	100.000	0.6324
5	100.000	0.6324
6	100.000	0.6324
7	100.000	0.6324

The results related to different turn faults appears in coherence magnitude with frequency. From the above table, it is observed that coherence of inverted curve having higher coherence is lower for middle level turns.

Conclusion

The work presented in this paper function behavior of turn failure. The variation of coherence is dependant.

It is concluded that motor can give dependable results.



PED025

National Conference on Recent Trends in Power Engineering Indian Institute of Technology Madras, Chennai 600 036, India 29-30 December 2015 Study, Design and Performance Analysis of 2,3 & 4 Phase Interleaved Boost Converters in Renewable Energy Source Application

Research Scholar, School of Electrical Engineering, VIT University, Vellore, Tamil Nadu, India.
ABISHRI.P

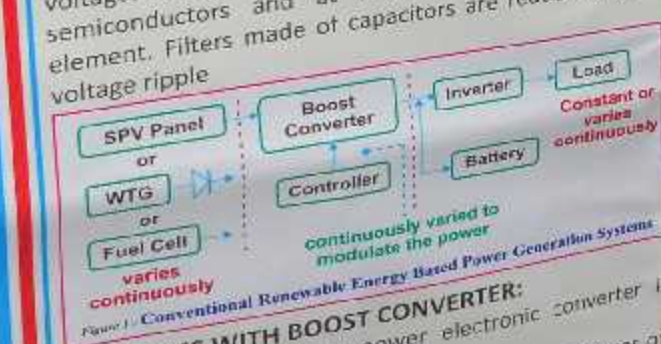
INTRODUCTION :

A suitable power conditioner is very much needed for the Renewable Energy Sources (RES), such as Solar Photovoltaic(SPV) panel, Wind Turbine Generator(WTG) and fuel cell to connect it to the load because of its non-linear current Vs voltage (I-V) characteristics, due to lower output voltage of the sources and its dependency on the sporadically varying natural phenomena. The DC-DC converter along with suitable controllers is generally used in the renewable energy sources, to maintain a constant voltage at the input of the inverter for a stable output (load) voltage, and to handle power flow control based on load requirement. The larger ripples in RES sources such as SPV panel, fuel cell etc., A detailed investigation on 2 phase, 3 phase and 4 phase interleaved boost converter is carried out with SPV , wind turbine generator , Fuel cell and battery and parameters like input current ripple, output voltage ripple and the power handling capability is analyzed. It is observed that the output voltage ripple is minimized at the points where the input current ripple is minimized. It is observed that the 4 phase IBC offers better input current and output voltage ripple reduction than the 2 and 3-phase IBC.

METHODOLOGY:

BOOST CONVERTER:

A boost converter is a DC-to-DC power converter with an output voltage greater than its input voltage. It is a class of SMPS containing at least two semiconductors and at least one energy storage element. Filters made of capacitors are reduce output voltage ripple

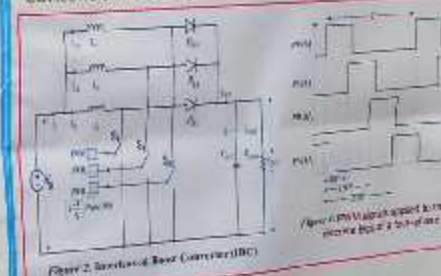


PROBLEMS WITH BOOST CONVERTER:

- The power level of a power electronic converter is limited due to several factors.
- An increase in current causes an increase in stresses on switching devices and The boost inductor should be increased to avoid saturation and overheating problems.

INTERLEAVED BOOST CONVERTER(IBC):

- Hence, for an efficient power generation and to protect the life time of the RE resources, a power conditioner that simultaneously applies voltage and power flow control along with negligible voltage and current ripple is very much necessary.
- To develop an efficient multi-phase DC-DC converters as the basic converter unit of the RES based power generation systems to increase the power processing capability with reduced ripple content, and to improve the reliability



ADVANTAGES OF IBC:

- Increase the power processing capability
- Reduced electromagnetic emission
- Fault tolerance
- Reduced conduction losses (I^2R)
- Improve the reliability of the power electronic system
- Ripple cancellation in both the input and output waveforms

RESULT:

Analysis of 2, 3 & 4 Phase are tabulated below:

Source	2 Phase	3 Phase	4 Phase
Input Current (I)	0.08 Amperes	0.05 Amperes	0.02 Amperes
Output Voltage (V)	0.86 Volts	0.62 Volts	0.50 Volts

As Seen in the both Cases, the 4 Phase IBC offers better Input Current and Output Voltage Ripple Reduction than the 2 Phase and 3 Phase Interleaved Boost Converter (IBC). Hence a 4 Phase Interleaved Boost Converter (IBC) is proposed as the Basic Converter Unit of High Power Supply





HVE010

National Conference on Recent Trends in Power Engineering
Indian Institute of Technology Madras, Chennai 600 036, India.
29-30 December 2015

Partial Discharge Characteristics of Synthetic Ester-Pressboard Insulation System: Effect of Conducting Particle

C. Thirumurugan, Ramesh Oruganti
School of Computing and Electrical Engineering,
Indian Institute of Technology Mandi,
Mandi-175001, Himachal Pradesh, India.

Ganesh Kumbhar
Department of Electrical Engineering,
Indian Institute of Technology Roorkee,
Roorkee-247667, Uttarakhand, India.

Introduction (Research Area-High Voltage Engineering)

Properties	Pressboard	Transformer Oil
DRG	calculus of high test quality	Paraffin, neophthalane
Manufacture	Industrialsilicate gelatine	extracts from petroleum
Usage	Insulation and mechanical insulation well as support	Cooling

Radar discharge: - central discharge partially bridges the insulation, sign of insulation degradation and root cause of breakdown.

From the experiment:- PD artificial defects were added (i.e. conducting particles-Cu).

Experimental work (two parts)

Figure 2: PC patterns of pressboard samples with Cu particles (PDIV=13.5kV)
a) at centre of electrodes b) near by earth electrode

Two samples- 1. Cu particles at centre of electrodes 2. Cu particle at near by earth electrode.

Measured value: PRPD pattern(Phase resolved partial discharge pattern)

Conclusions

- To check the suitability of synthetic ester for transformer insulation the PD experiment of Synthetic ester-pressboard with Cu particles has been carried out.
- As per the above PD patterns, Cu particles at the centre of the electrodes is having more repetitive pulses than Cu particles at nearby earth electrode.
- This PD patterns are used for condition monitoring of large transformers.

Reference

Sarath, R., I.P.Merin Sheema, J.sundarajan, M.G.Dakis, "Influence of harmonic ac voltage on surface discharge formation in transformer insulation", IEEE Trans. on DEI, vol. 21, No.5, pp. 2183-92, 2014.



HVE010

National Conference on Recent Trends in Power Engineering
SPET
Indian Institute of Technology Madras, Chennai 600 036, India.
29-30 December 2015

Partial Discharge Characteristics of Synthetic Ester-Pressboard Insulation System: Effect of Conducting Particle

Ganesh Kumbhar
Department of Electrical Engineering,
Indian Institute of Technology Roorkee,
Roorkee-247667, Uttarakhand, India.

C. Thirumurugan, Ramesh Oruganti
School of Computing and Electrical Engineering,
Indian Institute of Technology Mandi,
Mandi-175001, Himachal Pradesh, India.

Introduction (Research Area- High Voltage Engineering)

Properties	Pressboard	Transformer Oil
Origin	Cellulose of highest quality	Paraffinic, naphthalene
Manufacturer	Unbleached sulfate Cellulose	extracts from petroleum
Usage	Insulation and mechanical support	Insulation as well as cooling

*Partial discharge(PD)- electrical discharge partially bridges the insulation.
•PD-sign of insulation degradation and root cause of breakdown.
•In order to understand PD- artificial defects were added (i.e. conducting particles-Cu).
Experimental work (two parts)

Results & Discussion (PRPD patterns.)

Figure 2 PD patterns oil-pressboard sample with Cu particles (PDIV=13.5kV)
a) at centre of electrodes b) near by earth electrode

▪ Two samples- 1. Cu particles at centre of electrodes 2. Cu particle at near by earth electrode
▪ Measured value- PRPD pattern(Phase resolved partial discharge pattern)

Conclusions

- To check the suitability of synthetic ester for transformer insulation the PD experiment of Synthetic ester-pressboard with Cu particles has been carried out.
- As per the above PD patterns, Cu particles at the centre of the electrodes is having more repetitive pulses than Cu particles at nearby earth electrode.
- This PD patterns are used for condition monitoring of large transformers.

Reference

▪ Sarathi.R, I.P.Merlin Sheema, J.sundarajan, M.G.Daikas, "Influence of harmonic ac voltage on surface discharge formation in transformer insulation", IEEE Trans. on DEI, vol. 21, No.5, pp. 2183-92, 2014.

National Conference on Recent Trends in Power Engineering
 Indian Institute of Technology Madras, Chennai 600 036, India.

29-30 December 2015

PSE017

Optimal Siting and Sizing of DG for Loss Minimization and Voltage Stability Improvement in Distribution System

J. Senthil Kumar¹, M. Aravindhan², S. Charles Raja³, P. Venkatesh⁴

¹Research Scholar, ²PG Scholar, ³Assistant Professor, ⁴Associate Professor
 Department of Electrical and Electronics Engineering, Thiagarajar College of Engineering, Madurai, Tamil Nadu, India

Objective

- Identifying the optimal DG location by Voltage Stability Index (VSI).
- Optimal Sizing of DG to minimize power loss.
- Power loss and Voltage Stability Margin (VSM) to be analyzed for 12 and 69 bus RDS system.

Problem Formulation

DG Placement

$$VSI_c = \frac{4X_s}{V_s} \left(\frac{P_c}{Q_c} + Q_s \right) \quad \dots (1)$$

$$\text{DG Sizing} \quad \text{Minimize } P_c = \sum_k I_k^2 R_k \quad \dots (2)$$

$$\text{Power - conservation limit} \quad P_{ss} = P_D + P_L - P_{DG} \quad \dots (3)$$

Voltage Stability Margin (VSM)

$$VSM(r) = V(r)^2 - 4(P(r)X_r - Q(r)R_r)^2 - 4V(r)^2(P(r)R_r + Q(r)X_r) \quad \dots (4)$$

Where,

R=Resistance of branch k, P=Real power load(kW), Q=Reactive power load(kW), NL=Total number of branches, P_l =Total Power loss(kW), I=Current flowing in branch k, P_{ss} =Power from substation(kW), P_D =Total power demand(kW), P_{DG} =Power injected by DG(kVA)

Proposed Method



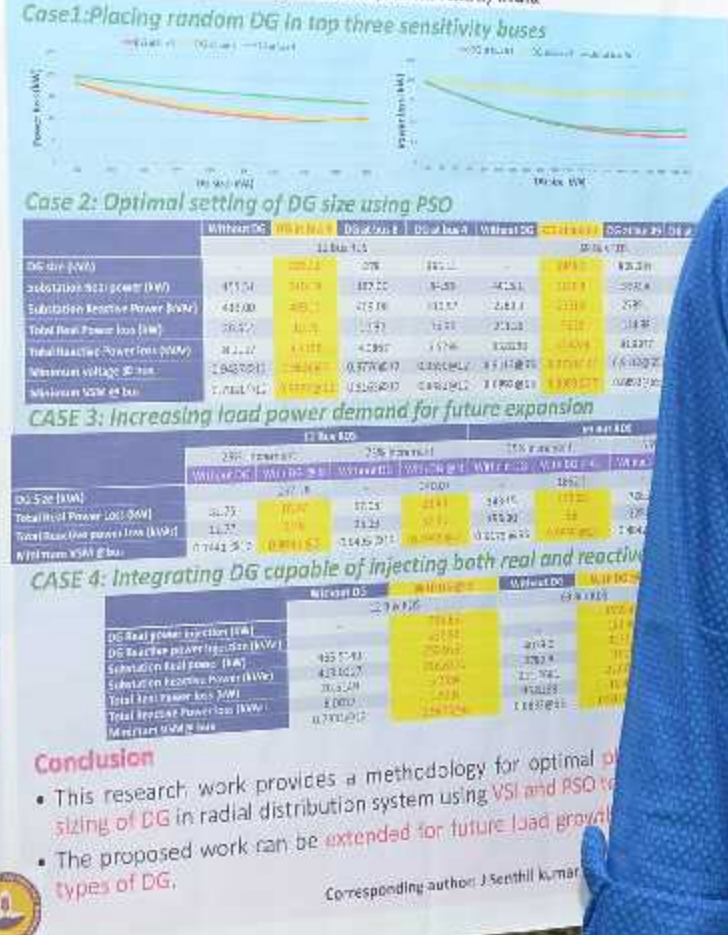
Results and Discussions

CASE 1: Placing random DG in top three sensitivity buses.

CASE 2: Optimal setting of DG size using PSO.

CASE 3: Increasing load power demand for future expansion

CASE 4: Integrating DG capable of injecting both real and reactive power



Conclusion

- This research work provides a methodology for optimal placement and sizing of DG in radial distribution system using VSI and PSO techniques.
- The proposed work can be extended for future load growth and different types of DG.

Corresponding author: J.Senthil Kumar



National Conference on Recent Trends in Power Engineering

Indian Institute of Technology Madras, Chennai 600 036, India.
29-30 December 2015

ATC Enhancement by Incorporating FACTS Devices for Deregulating Scenario in Present Power Market

PSE022

J. Jeslin Drusila Nesamalar
Research Scholar

K. Bavithra
PG Scholar

S. Charles Raja
Assistant Professor
Thiagarajar College Of Engineering, Madurai, Tamilnadu, India

P. Venkatesh
Associate Professor

Definition

- ATC is a measure of the Transfer Capability remaining in the transmission network for further commercial activity over and above already committed uses

$$ATC = TTC - ETC - TRM - CBM$$



Objective

$$\text{Maximize ATC} \quad \text{MAX} \{ ATC_{m-n} \}$$

Limits for ATC determination

- Bus Voltage limits ($V_{min} \leq V_i \leq V_{max}$)
- Line Thermal limits ($P_{ij} < P_{ij}^{max}$)
- Reactive power limits ($Q_{ui}^{min} < Q_{ui} < Q_{ui}^{max}$)

ATC Determination

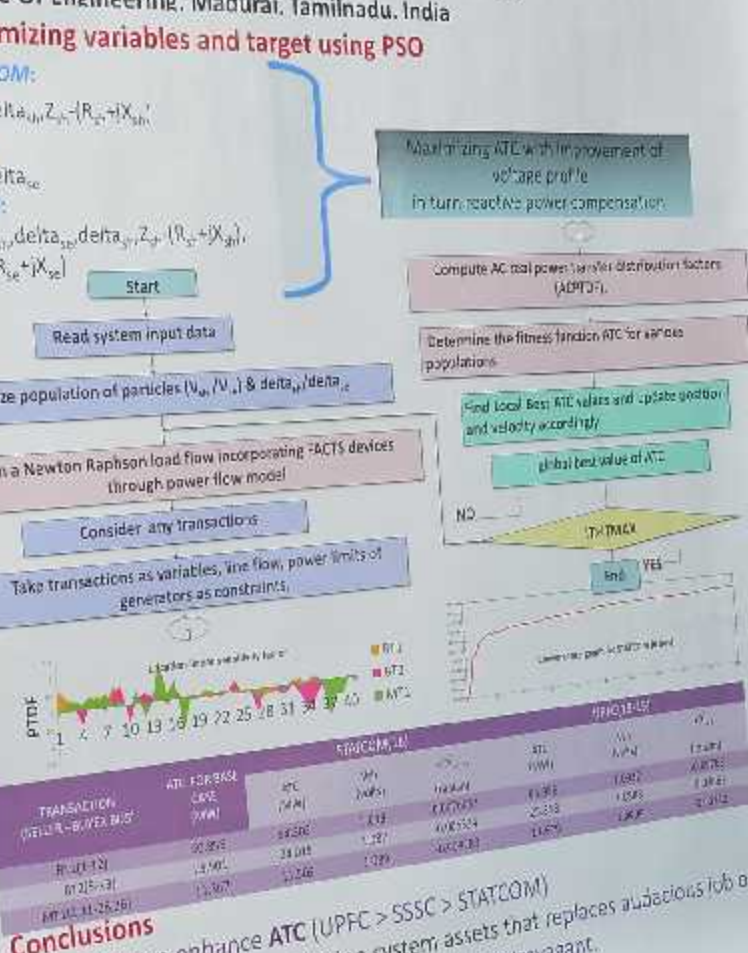
- AC-PTDF of line $i-j$ is given by, $ACPTDF_{i,j,m} = \frac{\Delta P_m}{P_m}$
- Power transfer in the line $i-j$ due to transaction $m-n$ is given by,

$$T_{i,j,m-n} = \begin{cases} \frac{(P_{i,n}^{max} - P_{i,j}^m)}{PTDF_{i,j,m}} & PTDF_{i,j,m} > 0 \\ \alpha (original) & PTDF_{i,j,m} = 0 \\ \frac{(-P_{j,n}^{max} - P_{i,j}^m)}{PTDF_{i,j,m}} & PTDF_{i,j,m} < 0 \end{cases}$$
- ATC for transaction $m-n$ is found by, $ATC_{m-n} = \min \{ T_{i,j,m-n} \}, i \in N$

Incorporating FACTS devices -power flow

- STATCOM(Shunt), SSSC(Series), UPFC(Combine)
- The change in angle and voltage is determined by change in jacobian elements.

$$\begin{bmatrix} \Delta \delta^{FACTS} \\ \Delta V^{FACTS} \end{bmatrix} = \begin{bmatrix} J_1^{FACTS} & J_2^{FACTS} \\ J_3^{FACTS} & J_4^{FACTS} \end{bmatrix} \begin{bmatrix} \Delta P \\ \Delta Q \end{bmatrix}$$



Conclusions

- FACTS can enhance ATC ($UPFC > SSSC > STATCOM$)
- Improvement in transmission system assets that replaces audacious job of erecting new transmission facility which is extravagant.



National Conference on Recent Trends in Power Engineering
Indian Institute of Technology Madras, Chennai 600 036, India.

29-30 December 2015

Optimal Siting and Sizing of DG for Loss Minimization and Voltage Stability Improvement in Distribution System

J. Senthil Kumar¹, M. Aravindhan², S. Charles Raja³, P. Venkatesh⁴

¹Research Scholar, ²PG Scholar, ³Assistant Professor, ⁴Associate Professor

Department of Electrical and Electronics Engineering, Thiagarajar College of Engineering, Madurai, Tamil Nadu, India

Objective

- Identifying the optimal DG location by Voltage Stability Index (VSI).
- Optimal Sizing of DG to minimize power loss.
- Power loss and Voltage Stability Margin (VSM) to be analyzed for 12 and 69 bus RDS system.

Problem Formulation

DG Placement: Voltage Stability Index (VSI)

$$VSI = \frac{4X_L}{P^2} \left(\frac{P_s + Q_s}{Q_s} \right) \quad \dots(1)$$

DG Sizing: $\text{Minimum } Q_s = \sum_{i=1}^{NL} I_i^2 R_i \quad \dots(2)$

Power – conservation limit: $P_{in} = P_o + P_s - P_{DG} \quad \dots(3)$

Voltage Stability Margin (VSM)

$$VSM(\theta) = |P(\theta)|^2 - 4(P(\theta)I_s - Q(\theta)R_s)^2 - 4P(\theta)(P(\theta)R_s + Q(\theta)X_s) \quad \dots(4)$$

Where,

R=Resistance of branch k, P=Real power load(kW), Q=Reactive power load(kW), NL=Total number of branches, P_t =Total Power loss(kW), I=Current load(kW), P_{DG} =Power from substation(kW), P_o =Total power flowing in branch k, P_{ss} =Power from substation(kW), P_d =Total power demand(kW), P_{DG} =Power injected by DG(kVA)

Proposed Method



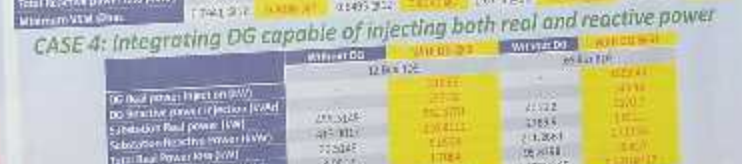
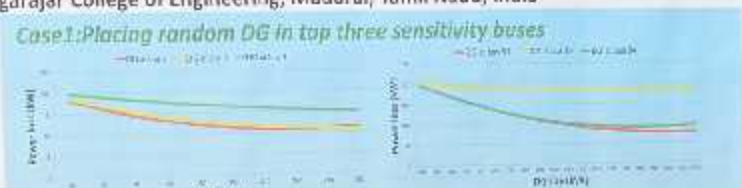
Results and Discussions

CASE 1: Placing random DG in top three sensitivity buses.

CASE 2: Optimal setting of DG size using PSO.

CASE 3: Increasing load power demand for future expansion

CASE 4: Integrating DG capable of injecting both real and reactive power

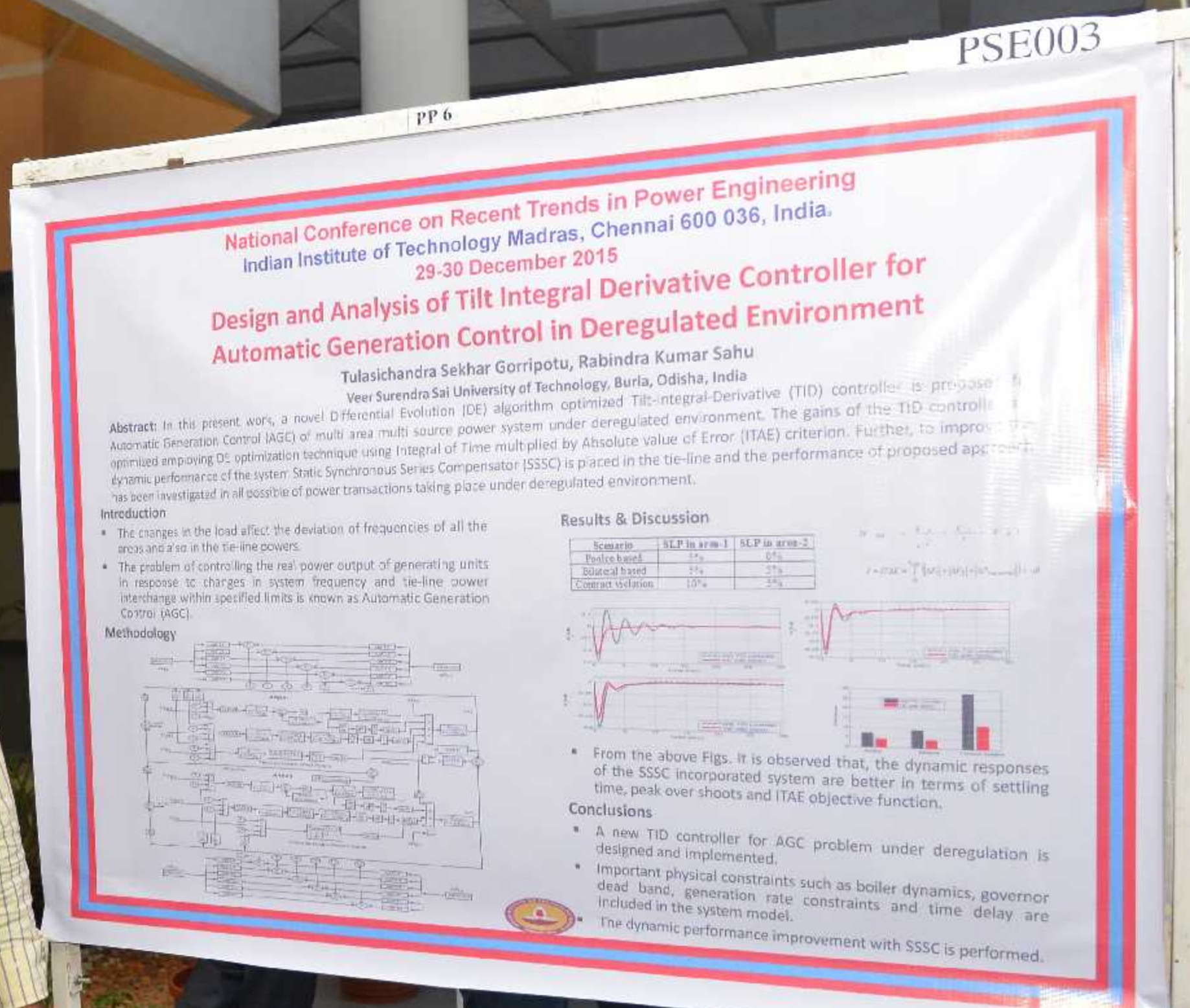


Conclusion

- This research work provides a methodology for optimal placement and sizing of DG in radial distribution system using VSI and PSO technique.
- The proposed work can be extended for future load growth and different types of DG.

Corresponding author: J.Senthil Kumar (senthil_be@maiil.com)





National Conference on Recent Trends in Power Engineering

Indian Institute of Technology Madras, Chennai 600 036, India.
29-30 December 2015

Optimal Placement and Sizing of Combined DG and Capacitor For Minimization Of Power Loss & THD in Distorted Distribution Systems

M.Swathisriranjan¹, D.Kavitha²
¹PG Scholar, ²Assistant Professor
Department of EEE, Thiagarajar College of Engineering, Madurai,Tamilnadu,India.

Introduction

- Distributed generation is an approach that employs small-scale technologies to produce electricity close to the end users of power.
- The presence of Distributed Generation (DG) in power systems may lead to several advantages such as reducing power losses and enhancing voltage profiles.
- Nowdays maximum **harmonic content** is present in the systems which inculcate power quality problems and harmonics, while placing DG in systems should be considered, hence the additional objective of THD minimization also considered. This work presents a new combined technique of minimizing the power loss and THD in distribution system by optimal DG installation together with capacitor placement by using Genetic Algorithm.

Objective

- Optimal placement & sizing of DGs & capacitors to minimize total power loss and THD
- To improve line voltage profile

Problem Formulation

Minimization of power loss:

Operational Constraints

Bus voltage limit

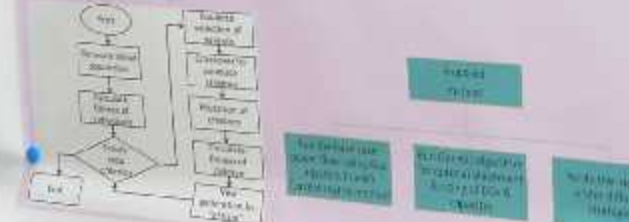
THD voltage limit

The DG capacities

Fitness function, $F = F_1 + F_2$

Implementation Of Proposed Work

Genetic algorithm steps:



Test system



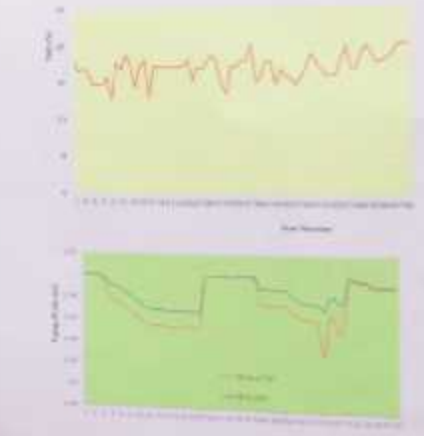
Fig. 1 69-bus radial distribution system

Results & Discussion

Bus No	P-loss (Kw)	Q-loss (Kvar)	THD (%)
Base case analysis			
(1) DG capable of injecting real power only	843.24kw	103.3	3.598
(2) any DG size utilized	1025.5kw	57.04	3.598
(3) DG utilizing both P&Q	786.05kw	84.70	3.356
Case 1: DG capable of injecting P&Q			
(1) Only DG and capacitor both being installed simultaneously	775kw, 5.11 kvar	40.15	3.086
(2) Only DG and capacitor both being installed sequentially	846.7kw, 250.4kvar	40.15	3.089
(3) DG, DG with DG and capacitor both being installed simultaneously	562.596.59kw, 56.12kvar	38.126	3.345
(4) DG, DG with DG and capacitor both being installed sequentially	511.445.87kw, 107.24kvar	38.126	3.345
Case 2: DG capable of injecting both P & Q and capacitor			
(1) Only DG and capacitor both being installed simultaneously	745.1033.1kw, 405.29kvar	44.126	3.225
(2) Only DG and capacitor both being installed sequentially	745.656.23kw, 740.24kvar	44.126	3.225
(3) DG, DG with DG and capacitor both being installed simultaneously	745.354.36kw	44.126	3.225

Conclusion

- Assistant problem formulation to place DGs and capacitor in a distorted distribution systems and to minimize the losses and THD is included.
- The results show that THD levels can be reduced along with the reduction of power loss. If DGs & capacitors are properly located and installed THD levels. In such cases, shunt capacitors are necessarily required to bring THD levels within the limits along with DG.
- The proposed technique GA gives the best solution in terms of fitness and convergence rate for minimizing the total power losses and THD.



PSE004

National Conference on Recent Trends in Power Engineering
Indian Institute of Technology Madras, Chennai 600 036, India
29-30 December 2015
Performance Analysis of Distribution Static Compensator

Sanath Saralaya
NITK, Surathkal

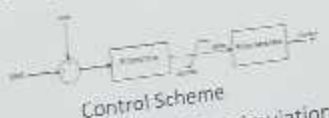
Manjunatha Sharma K
NITK, Surathkal, India

Introduction

- Distribution Static Compensator (DSTATCOM) is a shunt connected power quality improvement device.
- The performance of DSTATCOM depends on control algorithm employed.
- In this work a case study on DSTATCOM using PSCAD/EMTDC tool has been presented.

System Details

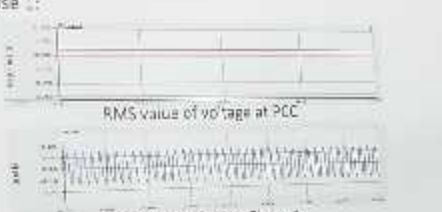
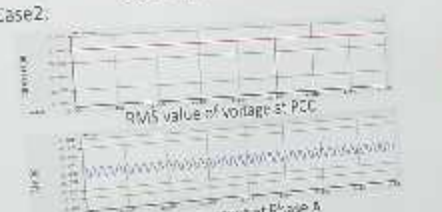
- IEEE 13 Bus System
Utility supply of 69 kV and local generation source of 13.8 kV
- Six pulse VSC with DC link Capacitor is used as DSTATCOM
- Control Method uses PI controller and generated PWM with switching frequency 5KHz.

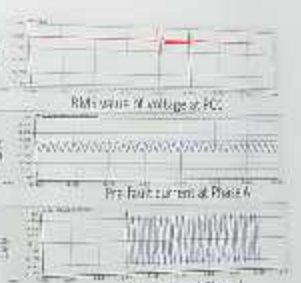


Different Cases considered for simulation

Case No.	With DSTATCOM	With LG fault
1	No	No
2	Yes	No
3	No	Yes
A	Yes	Yes

Simulation Results

- For simulation Local generator is removed from the system and Line to Ground (LG) fault is considered at bus 3.
- Case 1:

- Case2:

- Case3:

- Case 4:


Summary of Results obtained

Case No.	Voltage at Bus 3 [kV]	Current THD [%]	Voltage NO [%]
1	0.834	0.970	-
2	1	1.113	1.91
3	0.834 (ref)	0.103	-
4	1	1.141	1.52

Conclusions

- It can be observed that the DSTATCOM gives satisfactory performance in all the situations by maintaining electrical stability and maintaining within the IEEE 519 standard limit.
- THDs are maintained within the IEEE 519 standard limit.
- It is observed that VSC based control algorithm is capable for mitigating voltage related disturbances.
- For future study the DSTATCOM performance is to be analyzed with presence of distributed generation sources and different types of faults.



National Conference on Recent Trends in Power Engineering
Indian Institute of Technology Madras, Chennai 600 036, India
29-30 December 2015

Synchrophasor Estimation under Dynamic conditions and its Application in Power Systems

Dr. S. R. Bhide
Professor, VNIT,
Nagpur, India

Megha Gupta
M.Tech, VNIT,
Nagpur, India

Rajagopal Ganeshan
M.Tech, VNIT,
Nagpur, India

INTRODUCTION

This paper compares the performance of two algorithms (AMPE & LES) which have been reported in the literature to estimate the synchrophasor under dynamic conditions. Both algorithms are implemented in two of the power system applications. One is distance protection of transmission lines and other is estimation of transmission line parameters.

ALGORITHM 1: LES

Least Error Squares approach

Parameters of a digital filter determined by using LES approach are used to compute the real and imaginary components of the phasor. The signal considered is:

$$\begin{aligned} x(t) &= A_1 \cos(\omega t + \theta_1) + B e^{-t/\tau} \\ x(n) &= A_1 \cos\left(\frac{2\pi n}{N} + \theta_1\right) + B T^{-n} \end{aligned}$$

where the decaying parameter, $\Gamma = e^{-\Delta t/\tau}$

$$x(t) = A_1 \cos(\omega t + \theta_1) + B e^{-t/\tau} \quad (1)$$

$$x(n) = A_1 \cos\left(\frac{2\pi n}{N} + \theta_1\right) + B T^{-n} \quad (2)$$

Accurate real part of phasor for $(k+1)^{\text{th}}$ window

$$X_r(k) = \text{Real}(\psi(k+1)) \quad (3)$$

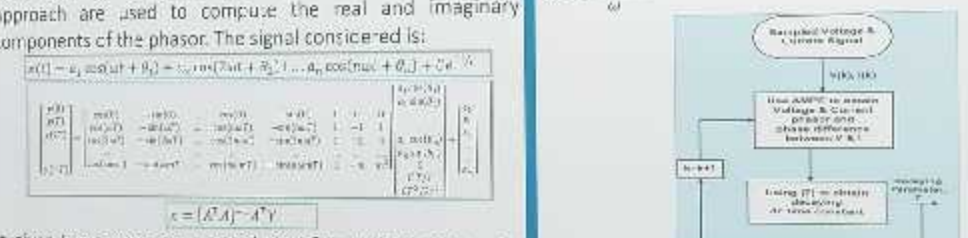
Accurate imaginary part of phasor for $(k+1)^{\text{th}}$ window

$$X_i(k) = \text{Imag}(\psi(k+1)) \quad (4)$$

$$\psi(k+1) = \frac{[X_r(k+1) - X_r(k)] + j[X_i(k+1) - X_i(k)]}{T^{-1} \cos(2\pi/N) - jT^{-1} \sin(2\pi/N)} \quad (5)$$

$$\varphi = \angle V - \angle I \quad (6)$$

$$t = \frac{\tan(\varphi)}{\omega} \quad (7)$$



It gives Least error squares solut'n for x which represents left pseudo-inverse matrix of A and minimizes the squared error E_F^2 .

ALGORITHM 2: AMPE

Adaptive Mimic Phasor Estimator

- Based on conventional sliding DFT technique to remove the decaying dc component in the signal and obtains the accurate magnitude and angle of the signal
- Uses the transmission-line parameters information hidden in the voltage and current measurements to adaptively approximate the decaying dc time constant to the accurate value

DISTANCE RELAYING

$$\begin{aligned} V_m &= 11kV, \theta = 9^\circ, \omega = 314 \\ R_{load} &= 50\Omega, L_{load} = 750mH \\ R_1 &= 50\Omega, L_1 = 733.2mH \\ R_2 &= 200\Omega, L_2 = 733.2mH \\ \text{Sampling frequency, } f_s &= 10 \text{ kHz} \end{aligned}$$



TRANSMISSION LINE PARAMETERS ESTIMATION

$$\begin{aligned} V_R &= AV_R + BI_R \\ I_Z &= CV_R + DI_R \\ A &= B = 1 + \frac{Y}{Z} = 1 + j \frac{R_c(R+jX)}{Z} \\ C &= Y \left(1 + \frac{Y}{Z} \right) = jB_c \left[1 + j \frac{R_c(R+jX)}{Z} \right] \end{aligned}$$

Parameter	Actual values		AMPE		LES	
	AMPE	LES	AMPE	LES	AMPE	LES
A	0.95 + 0.01	0.9501 + j0.0138	0.9500 + j0.0131			
B	29.97 + j0.0182	29.979 + j0.0173	29.974 + j0.0187			
C	-0.0000 + j0.0000	-4.5345e-6 + j2.2950e-4	-1.7915e-5 + j8.9004e-4			
D	0.95 + 0.01	0.9511 + j0.0137	0.9502 + j0.0175			

Parameter	Actual values		Estimated values		Error	
	AMPE	LES	AMPE	LES	AMPE	LES
R (Ω/km)	0.0997	0.0996	0.1117	0.1078	75.5%	
L (mH/km)	1.3002	1.3006	1.0914	0.0458	0.45%	0.79%
C (fF/km)	0.016	0.0002	0.31009	0.26	0.94%	

CONCLUSION

- Both methods have good harmonic rejection capability and work satisfactorily in the presence of system dynamics and decaying dc component.
- AMPE method is easier to implement under dynamic condition.
- However performance of LES is better than AMPE under large disturbances since
 - it has lower response time and lower overshoot/undershoot values.
 - requires less no of iterations to converge to the solution because convergence does not depends on the value of time constant assumed initially.
 - the decay rate during transients is not pre specified but is accounted automatically taking into consideration the effect of system resistance.





National Conference on Recent Trends in Power Engineering
Indian Institute of Technology Madras, Chennai 600 036, India.
29-30 December 2015

Power Quality Issues in Steel Re-Rolling Mills in India

Mohan V. Aware¹
Professor
Deepak S. Jain¹
M. Tech Student
¹**Electrical Engineering Department, Visvesvaraya National Institute of Technology, Nagpur, Maharashtra, India**

1. MOTIVATION

- Power Quality (PQ) issues are still largely underestimated, mainly because the losses are often hidden or not known.
- Steel re-rolling mill (SRRM) sector are prone to poor power quality and could have serious problems if not addressed in proper way.

2. OBJECTIVES

- To identify the sources of the poor PQ areas and PQ issues plaguing the sector, through power quality audit and analyse the collected data in view of its compliance with the standards available [1].
- To make the SRRMs aware about the effects of poor PQ.

3. BLOCK DIAGRAMS

Process flow of SRRM

```

graph LR
    A[Raw Material (Bogot/billet)] --> B[Furnace (IF/ EAF/CF)]
    B --> C[Rolling Mill]
    C --> D[Finished Product]
    D --> E[Project Focus]
    E --- F[Generation of PQ Impediments (2)]
    F --- G[Unnecessarily Applying Over Voltage]
    F --- H[Results: Voltage Cycles, Motor Saturation]
    H --- I[Power Quality Impediments]
  
```

4. FIELD MEASUREMENTS

PQ measurements of 15 SRRMs have been carried out in two cities (Nagpur and Raipur) of Central India by using Megger make PA9 PLUS V604 Portable PQ Analyzer. 15 SRRMs have been divided into three categories i.e. Micro, Small and Medium SRRMs. Out of 15 SRRMs, graphs and results of a plant, under Medium SRRM group, are presented .

5. IDENTIFICATION & EFFECTS OF PQ PROBLEMS

Electrical Distribution N/W of Plant

Major Power Quality impediments are voltage sag & swell and harmonics.

More pronounced PQ effects are increase in Voltage Drop (VD), transformer k-factor, & I²R loss, skin effect in cables, capacitor failure, decrease in motor lifespan & power factor.

6. OVERVIEW OF TOTAL ANALYSIS

SRRM's Type	RMS Va /V	Va /V Variation	THD Va %	THD Ia %	5 th %	7 th %
Micro	217-250	33	1.9	4-55	13-52	8-45
Small	235-264	29	1.6	3-54	8-50	5-27
Medium	234-249	15	1-16	1-70	2-30	2-11

7. ACTUAL & SIMULATION RESULTS

RMS Va & Ia Variations

Actual ($Ia_{THD} = 29.93 \%$) Simulation ($Ia_{THD} = 29.86 \%$)

8. CONCLUSIONS

- PQ analysis reveals all the PQ problems related to SRRMs.
- Real time field measurement and simulation modelling results are compared and found to be nearly same.
- This paper presents the effects of poor PQ, in SRRMs, generated due to saturation mode of motor operation.
- This paper encourages the organizations, who deal with the international standards, to make some PQ standards for controlling the PQ problems generated by the saturable devices.
- Proper design of Electrical Configuration N/Ws are also discussed to avoid the PQ issues.

9. REFERENCES

- [1] IEEE Recommended Practices and Requirements for Harmonic Control in Electrical Power Systems, IEEE Std. 519-1992, 1992.
- [2] R. C. Dugan, M. F. Mc Granahan, S. Santoso, H. W. Beauty, "Electrical Power Systems Quality", McGraw-Hill Companies, New York, 2004.
- [3] O. Salor, B. Gültækin, S. Buhar, B. Bayrakoğlu, T. İnan, T. Atalik, A. Açık, A. Terciyanlı, D. Ünsar, E. Altıntaş, Y. Akkaya, E. Özdemirli, I. Çadıroğlu, and M. Ermiş, "Electrical Power Quality of Iron and Steel industry in Turkey," in IEEE Transactions on Industry Applications, Vol. 46, No. 1, January/February 2010.



PED014

PP 1

National Conference on Recent Trends in Power Engineering
IITM Institute of Technology Madras, Chennai 600 096, India.
29-30 December 2015

National Conference on Recent Trends in Power Engineering
Indian Institute of Technology Madras, Chennai 600 036, India.
29-30 December 2015

Multiple Feedback-control-loops for Single-phase Full-bridge PWM Inverter

Jora M. Gonda and Apurva A. Londhe
 National Institute of Technology Karnataka, Surathkal, India.
 Department of Electrical & Electronics Engineering
 regondam@gmail.com, londheapurva@gmail.com

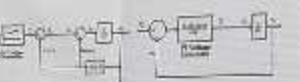


Figure 7: (a) Load current feedforward control (b)
Simplified Voltage Loop

Closed loop transfer function of the voltage loop is

$$\frac{\phi_i(s)}{\psi_i^*(s)} = \frac{\frac{K_i}{C_i} (1 + sT_i)}{s^2 - s(\frac{K_i}{C_i}) - \frac{K_i}{C_i}}$$

using the standard 2D order system, we

$$E_V = 2\zeta \omega_n C \quad \text{and} \quad T_V =$$

to tune these parameters till the actual waveform exactly follows the reference waveform. The velocity and position parameters depend on the system's required settling time and the allowable peak overshoot. The simulation parameters used in the simulation are given in Table 2.

Figure 9: Inverter output voltage with Controller for 1500 W Non-linear load

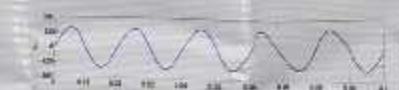


Figure 10: Inverter output voltage with Controller for 500 W Resistive Load



Figure 11: Inverter output voltage with Controller for 1500 W 0.8 lag load

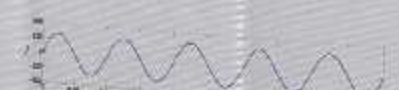


Figure 12: Inverter output voltage with capacitor



93 94 95 96 97 98 99 100 101 102



1000 W switched from resistive to non-linear load with Controller for 1500 W

B. SIMULATION

Figure 13: Inverter output voltage & load current when load is switched from resistive to non-linear load with Controller for 1500 W

7. CONCLUSION

B. SIMULATION

Figure 13: Inverter output voltage & load current when load is switched from resistive to non-linear load with Controller for 1500 W

7. CONCLUSION

T. COMIC JINH

7. CONCLUSION

PED008

National Conference on Recent Trends in Power Engineering
Indian Institute of Technology Madras, Chennai 600 036, India.
29-30 December 2015



REVIEW OF MICRO INVERTER CIRCUIT TOPOLOGY AND INFLUENCE OF TEMPERATURE

P. Elanchezian*, V. Kumar Chinnavan**, R. Sudhir Kumar*
*Central Power Research Institute, Bangalore, Karnataka, India 560080; elanchezian_srf@cpri.in
**Professor & HOD, EEE Department, KPR Institute of Engineering and Technology, Coimbatore.

Abstract
The present paper has tried to review different micro inverter circuit topologies and their influence on the system performance. The paper also highlights the influence of temperature on the system performance. The paper also highlights the influence of temperature on the system performance.

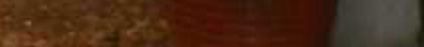
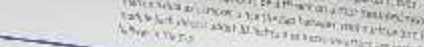
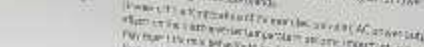
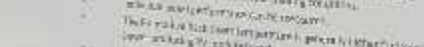
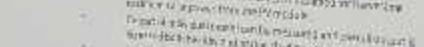
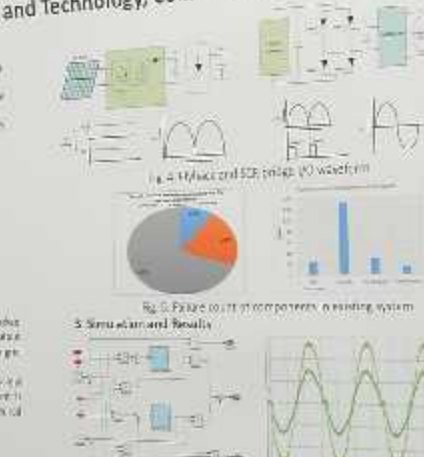
Keywords
1. Micro inverter, Micro grid

2. Micro inverter topologies
3. Micro inverter design
4. Micro inverter performance

Fig. 1. Micro inverter topologies
Fig. 2. Micro inverter design
Fig. 3. Micro inverter performance

Fig. 4. Micro inverter design
Fig. 5. Micro inverter performance

Fig. 6. Micro inverter design
Fig. 7. Micro inverter performance



National Conference on Recent Trends in Power Engineering

Indian Institute of Technology Madras, Chennai 600 036, India.

29-30 December 2015

COGNITIVE MODELED INTELLIGENT CONTROLLER FOR ELECTRICAL DRIVE

MD Qutubuddin¹ Narri Yadaiah²

Jawaharlal Nehru Technological University, Hyderabad, India^{1,2}

INTRODUCTION

In the proposed paper brain inspired emotional controller designed to control an electrical motor. As it is known fact that Emotional part of mammalian brain play vital role in balancing, movements and in speech therapy. The consequent concept can apply for an electrical motor, where the characteristics of motor varied with the disturbances occurred at internal and external variations. In the applications like hybrid vehicles, traction and variable speed applications where the control of speed is a challenging process with the change in load, different set constant speed with non linear change of stator currents and parameter variations.

OBJECTIVE

The main aim of this paper is to develop a bio-inspired intelligent controller considering the limbic system of mammalian brain. As per the mammalian brain, limbic system is responsible for emotions of an individual i.e., how faster an individual can take a decision on the issue. The emotional controller has been succeeding in many engineering applications; it is motivated to apply the emotional controller for electrical drives.

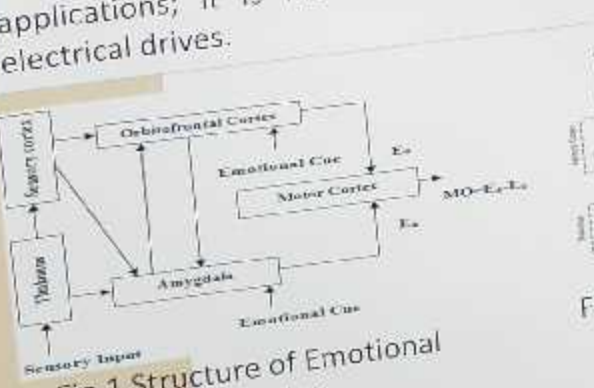


Fig.1 Structure of Emotional controller

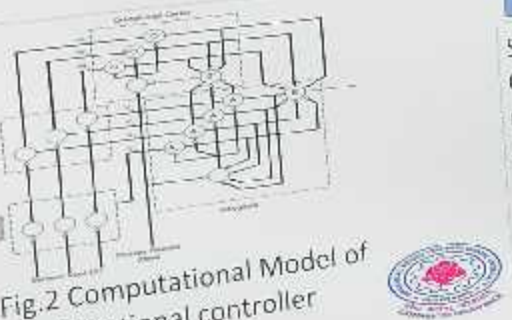


Fig.2 Computational Model of Emotional controller



RESULTS AND DISCUSSIONS

Case i) At No-Load

Case ii) Load $T = 5\text{N-m}$ is applied at $t=0.2$

Case iii) When variable Load is applied



CONCLUSIONS

Simulation results of PMSM drive with Emotional controllers are carried out at different load settings i.e. start no load to full load 5N-m and the speed tracking also carries constant load to variable load. It is observed that Emotion is very effective in controlling speed and stator current with load.



Behaviour of Water Droplets on Silicon Rubber Insulation Material

Gorla Vineeth, Palash Mishra, R.Sarathi
Indian Institute of Technology, Madras



Introduction

A spark is a brief moment of the flow of current in the insulator. However, in power systems, it can be a breakdown point. If a higher voltage is applied to the insulation, there will be a discharge process of water droplets on the insulation material.

Thus, the effect of water droplets on the insulation material is important in power systems.

The highest harmonic content is to be optimized.

To do this, we need to understand the causes of the discharge and its influences on the number of harmonics at different levels.

Thus, we analyzed the discharge using the following way:



Results and Discussion-

Wavelet Transforms of the resulting scalograms-

Time series analysis



$$CWT_f(\tau, s) = \Psi_2(\tau, s) = \frac{1}{\sqrt{s}} \int_{-\infty}^{\infty} f(t) \psi_2^*(\frac{t-\tau}{s}) dt$$

Experimental Setup



The distance between the electrodes is 2 cm.

Water drop size is of 20 µm diameter.

Some Notes-

Why wavelet transform?

- Wavelet transform possesses the ability to contract or time-frequency representation of a signal.
- It have very good time localization at high frequencies and very good frequency localization at low frequencies.
- On the other hand, Fourier transform gives the information on the energy present in each frequency.

The number of signals which present in the input wavelet is much higher than the number of signals which present in the output wavelet, even for the various surfaces examined.

The signals used for analysis-



One droplet, inception



One droplet, sparking at one electrode



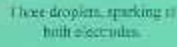
Two droplets, One electrode, sparking



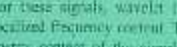
Three droplets, sparking at both electrodes



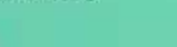
Two droplets, Both electrodes



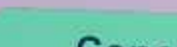
Three droplets, Both electrodes



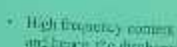
One droplet, Both electrodes



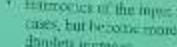
Two droplets, Both electrodes



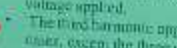
Three droplets, Both electrodes



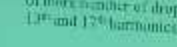
One droplet, Both electrodes



Two droplets, Both electrodes



Three droplets, Both electrodes



One droplet, Both electrodes



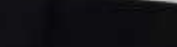
Two droplets, Both electrodes



Three droplets, Both electrodes



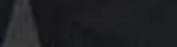
One droplet, Both electrodes



Two droplets, Both electrodes



Three droplets, Both electrodes



One droplet, Both electrodes



Two droplets, Both electrodes



Three droplets, Both electrodes



One droplet, Both electrodes



Two droplets, Both electrodes



Three droplets, Both electrodes

One droplet, Both electrodes

Two droplets, Both electrodes

Three droplets, Both electrodes

One droplet, Both electrodes

Two droplets, Both electrodes

Three droplets, Both electrodes

One droplet, Both electrodes

Two droplets, Both electrodes

Three droplets, Both electrodes

One droplet, Both electrodes

Two droplets, Both electrodes

Three droplets, Both electrodes

One droplet, Both electrodes

Two droplets, Both electrodes

Three droplets, Both electrodes

One droplet, Both electrodes

Two droplets, Both electrodes

Three droplets, Both electrodes

One droplet, Both electrodes

Two droplets, Both electrodes

Three droplets, Both electrodes

One droplet, Both electrodes

Two droplets, Both electrodes

Three droplets, Both electrodes

One droplet, Both electrodes

Two droplets, Both electrodes

Three droplets, Both electrodes

One droplet, Both electrodes

Two droplets, Both electrodes

Three droplets, Both electrodes

One droplet, Both electrodes

Two droplets, Both electrodes

Three droplets, Both electrodes

One droplet, Both electrodes

Two droplets, Both electrodes

Three droplets, Both electrodes

One droplet, Both electrodes

Two droplets, Both electrodes

Three droplets, Both electrodes

One droplet, Both electrodes

Two droplets, Both electrodes

Three droplets, Both electrodes

One

PED002

National Conference on Recent Trends in Power Engineering
Indian Institute of Technology Madras, Chennai 600 036, India.
29-30 December 2015

Field Computation of Efficiency of an Induction Machine Working on Unbalanced Conditions using Modified Non-Intrusive Air-Gap Method

G. S. Grewal and B. S. Rajpurohit
 School of Computing & Electrical Engineering, Indian Institute of Technology Mandi, Mandi-175001, Himachal Pradesh, India

Introduction

The diagram illustrates the field conditions and assumptions made for the study. Field conditions include: IM Parameters testing technique, Parameter deviation from manufacturer's data, IEEE Standard 112-1989, Equivalent circuit complexity, and Polluted power supply (voltage source harmonics). Assumptions include: Assumption based on IEEE Standard 112-1989, Need load test, Highly interactive nature, and Highly unfavorable for in-service tests.

Methods

MRAS for Speed Estimation (based on Landau concept on adaptation mechanism)

The block diagram shows a three-phase induction motor connected to a power source. The stator currents I_a , I_b , and I_c are sensed and fed into a current controller. The controller also receives feedback from a speed sensor and a torque sensor. The output of the current controller drives the motor. The speed sensor provides feedback to the controller.

Modified Non-Intrusive Air-Gap Torque Method for Efficiency Estimation

Using Parks transformations in stationary reference frame, torque is given by

Case 1: IEEE Std. 112, F&W loss = 1.2% of rated O/P & SLL = 1.8% of rated O/P.

$$T_{air-gap} = \frac{\sqrt{3}P}{6} [(I_a - I_b) \int (V_{ca} + R_s(2I_a + I_b)) dt + (2I_a + I_b) \int (V_{ab} - R_s(I_a - I_b)) dt]$$

Case 2: Indian Std. identical to IEC 60034-2-1: 2007, F&W loss + core loss = 3.5% of rated I/P and stray load loss is given by

$$S_{LL} = P_{in} \times \{0.025 - 0.005 \log_{10} \left(\frac{P_{out}}{1000} \right)\}$$

Experimental Setup

- For 45.8% unbalancing, $V_{ab} = 408$ Volts, $V_{bc} = 380$ Volts & $V_{ca} = 400$ Volts i.e. 5% Unbalancing.
- For 55.78% loading, $V_{ab} = 392$ Volts, $V_{bc} = 366$ Volts & $V_{ca} = 382$ Volts.
- Phasor computations are not required.

A photograph showing the experimental setup in a laboratory. A three-phase induction motor is connected to a power source and a control system. Various measurement instruments and sensors are visible on the bench.

Results & Discussion

Speed estimation

Speed using MRAS	Speed using optical tachometer
1370 rpm	1394 rpm

A graph plotting speed (rpm) against time (sec). The x-axis ranges from 0 to 10 seconds, and the y-axis ranges from 0 to 1500 rpm. Two curves are shown: one starting at 0 rpm and rising to approximately 1394 rpm, and another starting at approximately 1370 rpm and rising to approximately 1394 rpm. The two curves are nearly identical.

Efficiency Estimation

% Load	Operating condition	IEEE Standard 112 Method [Case 1]	BIS Identical EC 60034-2-1: 2007 [Case 2]		
		Efficiency (%)	Torque (Nm)	Efficiency (%)	Torque (Nm)
67.2	Balanced	69.92	4.392	60.73	3.08
79.45	Balanced	77.25	5.2196	73.67	4.87
96.1	Balanced	81.53	5.443	75.38	5.27
45.8	Unbalanced	71.59	3.1402	65.10	2.867
55.78	Unbalanced	68.61	1.645	58.32	2.318

IM Parameters

Resistance R1	1.1750
Resistance R2	13.73390
Inductance L1	1.2591 J
Inductance L2	12.45290
Inductance L3	146.37501

IM Nameplate

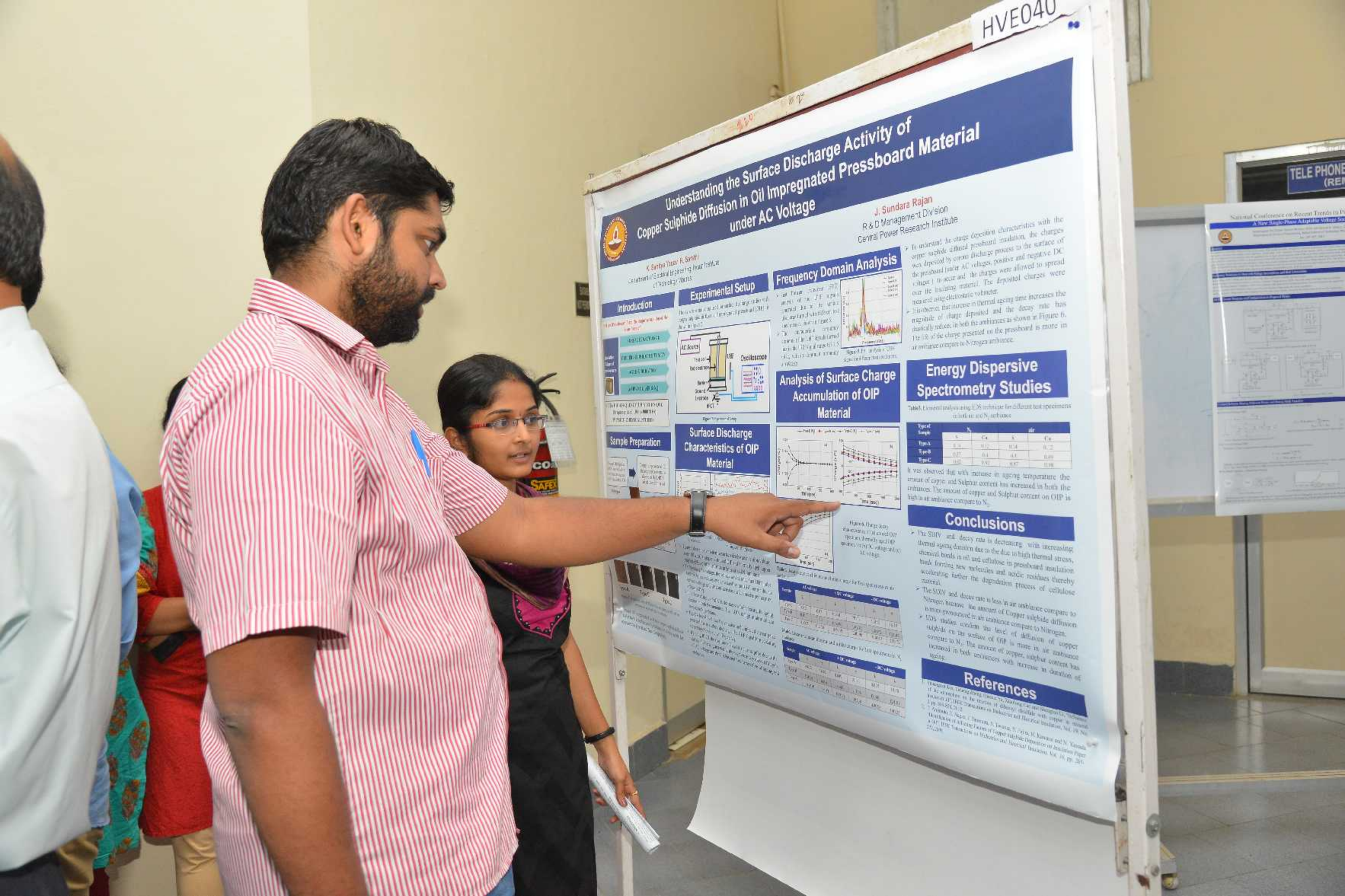
Voltage	435 VAC	Frequency	50 Hz
Rated	3.4 kW	Supply	Y
Power		Current	
Efficiency	72%	Power Factor	0.85
Power Factor		Temperature	40°C

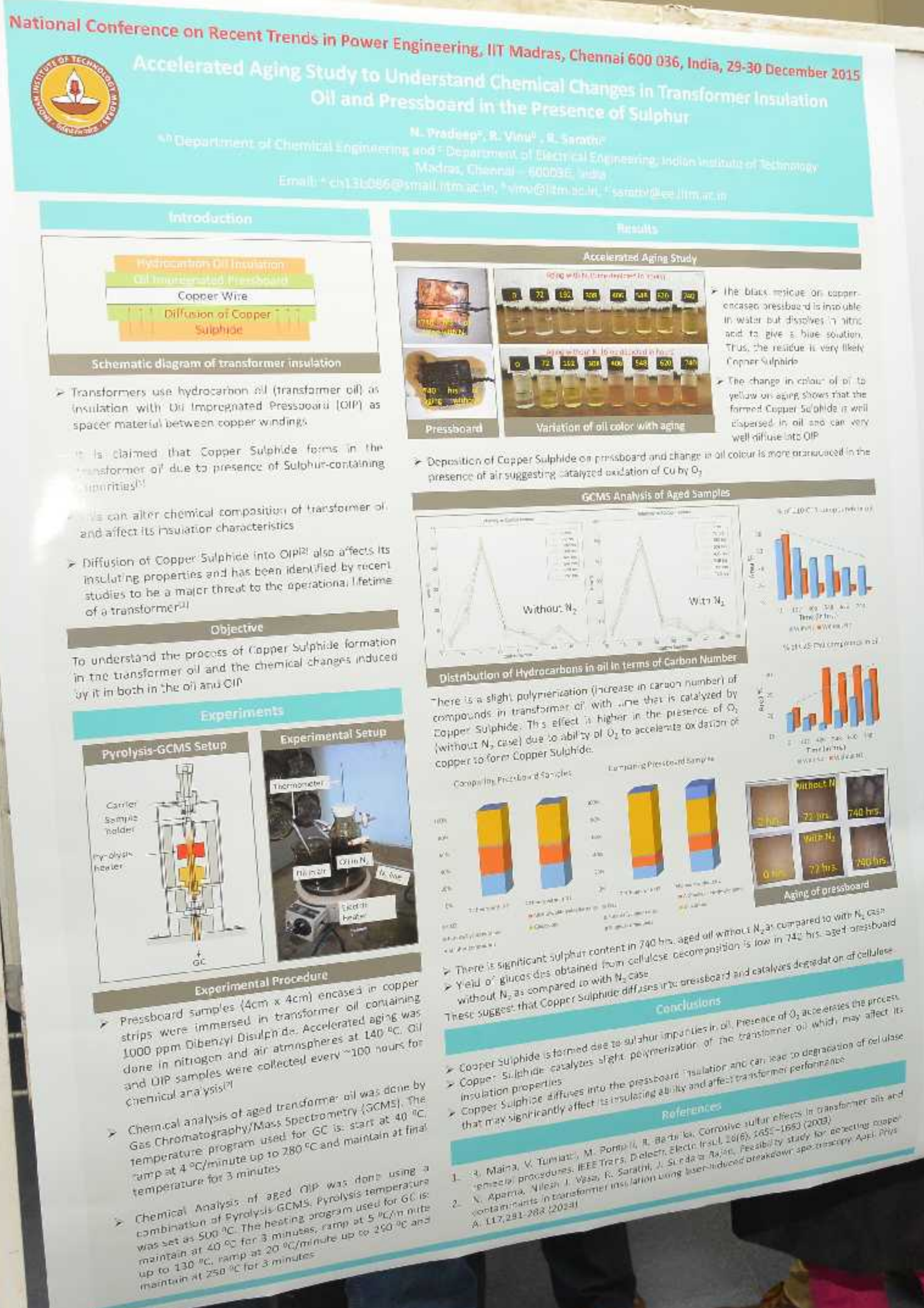
Conclusions

Proposed Non-Intrusive Air-Gap Method is advantageous

- Torque sensor is eliminated.
- No load test is not required.
- Relies only on electrical terminal quantities.
- No obvious error for nameplate inaccuracies.
- Reduces the downtime of IM.







National Conference on Recent Trends in Power Engineering A New Single-Phase Adaptable Voltage Source Inverter



Venugopalan, Sai Gopal, Student Member, IEEE and Munesh K. Midha, Senior Member, IEEE
Department of Electrical Engineering, Indian Institute of Technology Madras, Chennai, India.

Dec 29th, 30th, 2015

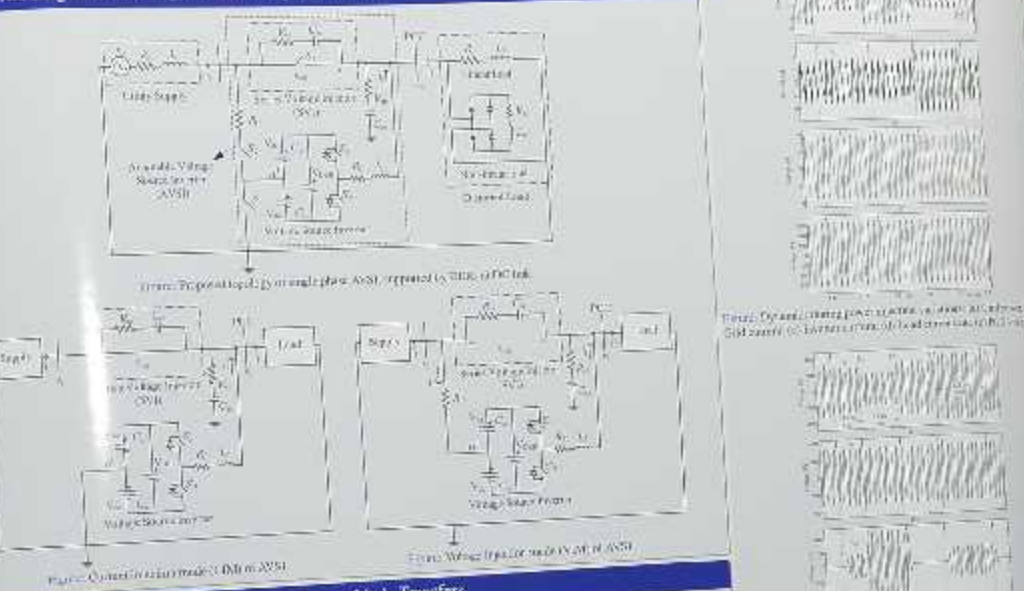
Abstract

This paper introduces while presenting power quality (PQ) aspects by using breakers, shunt and load control system to which it can be incorporated with the electrical and power electronic systems and analyse control algorithm. In the paper, a New Single Phase Source Inverter (AVSI) is proposed to mitigate distributed Energy Resources (DERs) to a single point of tie (SPT) which is used to tie AVSI, a central power plant (CPP), to utility and loads. It consists of three different modes of operation namely Grid Connected Mode (GCM), Grid Forming Mode (GFM) and Grid Supporting Mode (GSM). The AVSI along with VIM can be used for mitigation of the voltage sag and swell in the distribution system and simulation results supporting the proposed implementation of the AVSI is presented.

Existing Solutions to Deal with Voltage Interruptions and their Limitations

- Starting of POC voltage goes beyond its limit. This could cause erratic operation of grid.
- Employing a VSI for power exchange involving Dynamic Voltage Restorer (DVR) that takes about few microseconds.
- Limited Power Quality Functions (PQFs) and voltage will start from a low voltage.
- Using a single stage rectifier to voltage source inverter by making suitable changes in the source impedance.
- Grid forming voltage source inverter requires more time to track its rated voltage at the point of common coupling.

AVSI Circuit Diagram and Configurations in Proposed Modes



Control Scheme During Different Modes and During Mode Transfers

Control Strategy is divided into three sections with controls for the case of GCM, GFM and GSM.

(i) Control During GCM



(ii) Control During VIM

$$\begin{aligned} \Delta &= \phi_{VIM} - \arctan(\frac{V_{IM}}{I_{IM}}) \\ I_{IM} &\sim \sqrt{2} \cdot V_{IM} \cdot \sin(\phi_{VIM}) \end{aligned}$$

Equation (3) provides Δ which should be greater than $\pi/2$ to reduce the maximum reactive power during compensation. In (4), V_{IM} is the stage of VCC, I_{IM} is VIM current, ϕ_{VIM} is VIM angle. ϕ_{VIM} is kept constant at value θ_{VIM} .

(iii) Mode Transitions A. Grid Boundaries



Transitions from GCM to VIM happen only when V_{IM} is higher than V_{GCM} in 10 stages or less. V_{IM} is within 1.5-2.5% when $k < 0$. Transitions from GCM to VIM happen only when V_{IM} is higher than V_{GCM} in 10 stages or less. V_{IM} is within 1.5-2.5% when $k < 0$.

Simulation Results



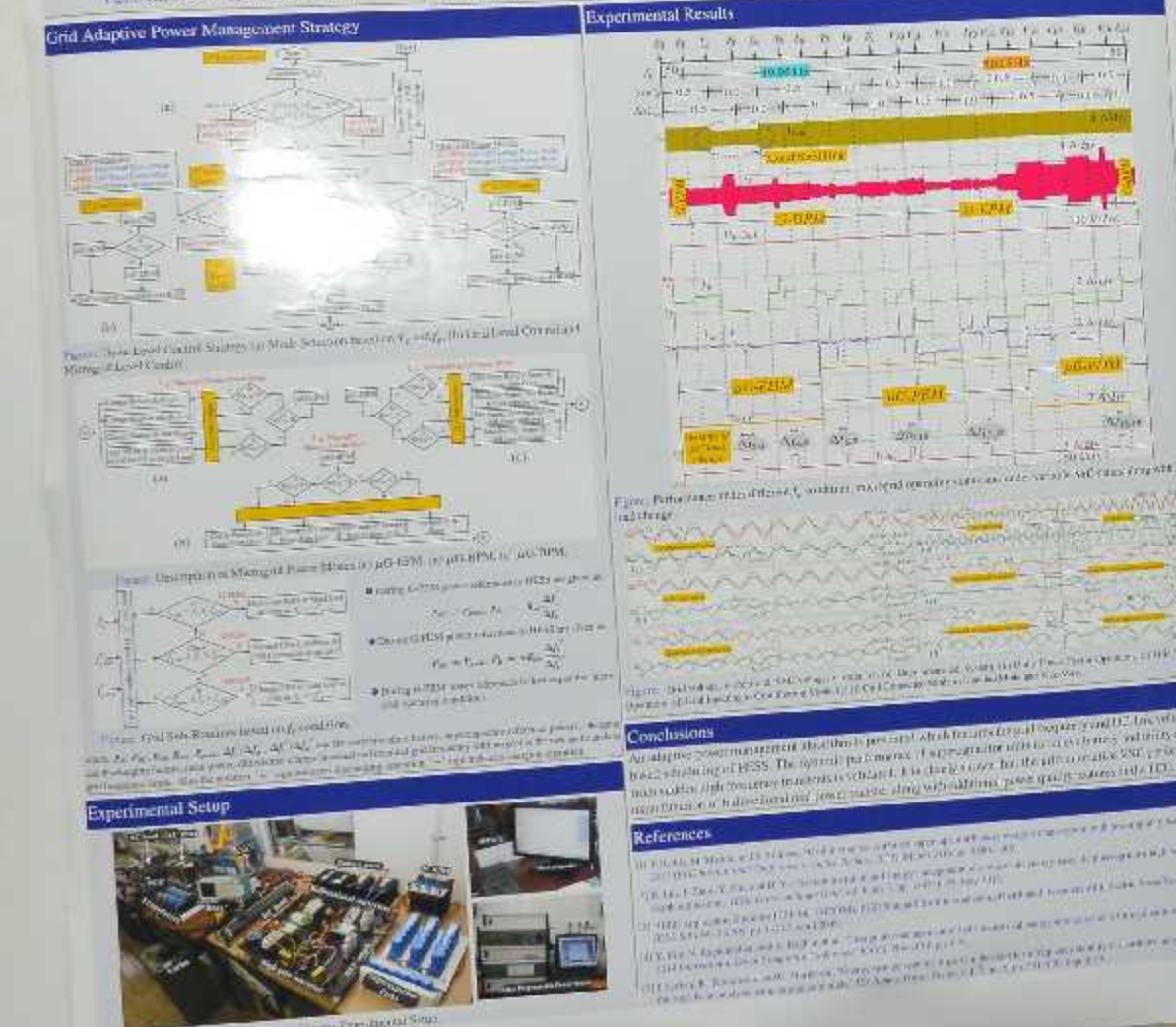
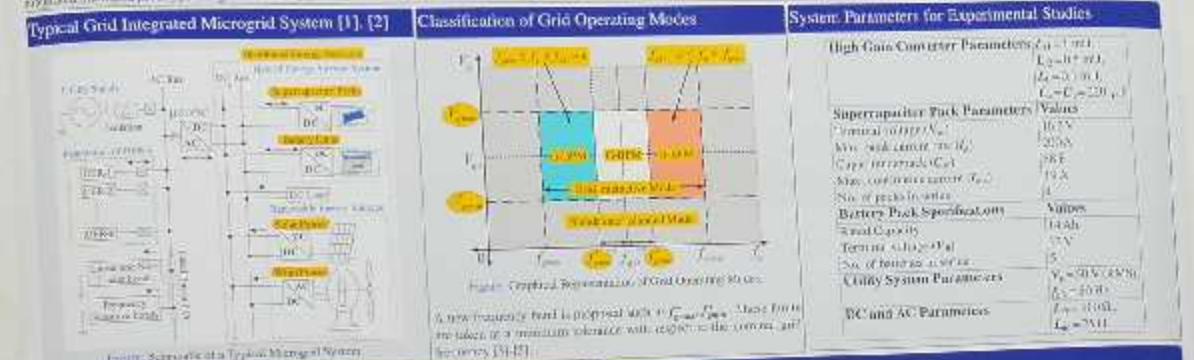
Grid Adaptive Power Management Strategy for a Renewable Tied Grid using Hybrid Storage



Nilesh Kastur, Student Member, IEEE and Nalesh K. Visarn, Senior Member, IEEE
 Department of Electrical Engineering, Indian Institute of Technology Madras, Chennai, India.
 National Conference on Recent Trends in Power Engineering
 Dec 29th-30th, 2013

Abstract

Integrated power system management systems face the challenge to meet power quality dependent load cycle. Most studies focus on supply demand mismatch to solve the issue. This paper introduces a solution to reduce the power quality issues by using a hybrid storage system. A simple control algorithm is proposed to reduce the power fluctuations and frequency variation and provides corresponding reference to the load change. Average current consumption minimization is also achieved. Another strategy of current demand mitigation reduces power export. It also achieves the objectives for utility operators in the interconnected system under grid failure conditions. Power adaptive strategies that are proposed and implemented in the integrated control program along with the energy management (ESM) and the controller under different operating processes.





National Conference on Recent Trends in Power Engineering
Supervisory Control of a Grid Interactive Microgrid

S. Biju, Kuma & Mallesh K. Marla, Senior Researcher IITB
Department of Electrical Engineering, Indian Institute of Technology, Mumbai, India
Acc. No. 201-305, 2015

Abstract:
The paper presents a supervisory control strategy for a grid interactive microgrid (GIM). The proposed GIM consists of a wind turbine, PV panel, battery bank, load and a VSC. The proposed GIM is connected to the utility grid through a VSC. The proposed GIM has two operating modes, namely, grid connected mode and island mode. The proposed GIM has two operating modes, namely, grid connected mode and island mode.

Challenges in Proliferation of a Microgrid:

- Measuring the power produced by each unit.
- All units running in IEEE.
- Interoperability among different units.
- Standardization of communication protocols.
- Standardization of energy metering.

Grid Interactive Microgrid and Proposed Control Strategy

The proposed GIM consists of a wind turbine, PV panel, battery bank, load and a VSC. The proposed GIM has two operating modes, namely, grid connected mode and island mode.

Experimental Results

Parameter	Value	Unit
Battery Pack	200 Ah	Ah
Wind Turbine Rating	200 kW	kW
VSC Rating	100 kVA	kVA
Supplementary Turbine	100 kW	kW
Wind Generator Rating	200 kW	kW
Battery Charger	200 A	A
Supplementary generator	200 kW	kW
T1-Capacity	200 kWh	kWh
GIMO parameters	200	-
VSC Parameters	200	-
Capacitor	100 kvar	kvar
AC and DC loads	100 kW, 100 kvar	kW, kvar
Bus 1	100 kV	V
Bus 2	100 kV	V
Bus 3	100 kV	V

Power Management Algorithm

The proposed GIM has two operating modes, namely, grid connected mode and island mode. The proposed GIM has two operating modes, namely, grid connected mode and island mode.

Experimental Setup

The experimental setup consists of a wind turbine, PV panel, battery bank, load and a VSC. The experimental setup consists of a wind turbine, PV panel, battery bank, load and a VSC.

Conclusion

The proposed GIM has two operating modes, namely, grid connected mode and island mode. The proposed GIM has two operating modes, namely, grid connected mode and island mode.



PED004



National Conference on Recent Trends in Power Engineering
Indian Institute of Technology Madras, Chennai 600 036, India.
29-30 December 2015

DESIGN AND IMPLEMENTATION OF A SYMMETRICAL MULTILEVEL INVERTER TOPOLOGY

JAMMALA VENKATARAMAIAH,
NITK Surathkal, Mangalore - 575025,
Karnataka, India

INTRODUCTION

A traditional CMLI require more number of components and its switching scheme become complex if the number of levels are increased. These issues have been addressed by a new symmetrical MLI topology.

Level shifted bipolar SPWM techniques(PD,POD,APOD) are implemented over the symmetrical seven level inverter topology.

SEVEN LEVEL RV TOPOLOGY

The proposed Reverse voltage (RV) topology is divided into two parts as shown in the Fig.1.

One generated part produces positive wave form (shown in fig.2) by using switching scheme as shown in table.1

Other part is a basic H-bridge inverter.

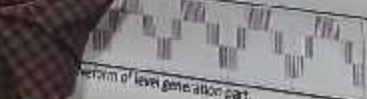
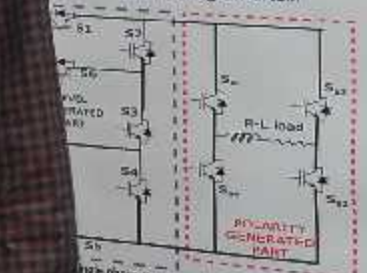


Table. 1
Switching Scheme for seven level inverter

V _d Levels	Switching States					
	S ₁	S ₂	S ₃	S ₄	S ₅	S ₆
+3V	1	0	0	0	0	1
+2V	0	1	1	0	0	1
+1V	0	1	0	1	0	1
0V	0	1	0	1	1	0

SIMULATION & EXPERIMENTAL RESULTS

Output voltages of RV topology are depicted in fig.3 based on simulated parameters $V_{dc} = 100V$, $R = 100 \Omega$, $L = 10mH$, $m_g = 0.9$ and $f_r = 25$

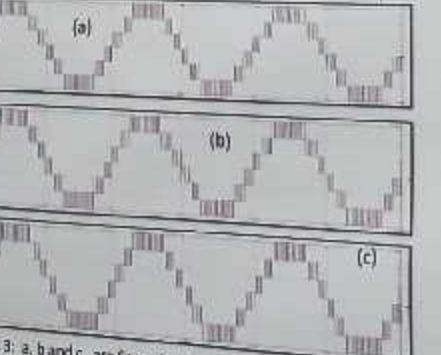


Fig. 3: a, b and c are Seven level output voltages of PD, PDD and APCD Techniques respectively.

Relationship among modulation index, %THD and output voltage for the proposed work are depicted in fig.4a, fig.4b.

The experimental results are shown in fig.5 based on resistive load of $1\text{K}\Omega$, 1 K Watt rating.

Y.Suresh,
NITK Surathkal, Mangalore - 575
025, Karnataka, India

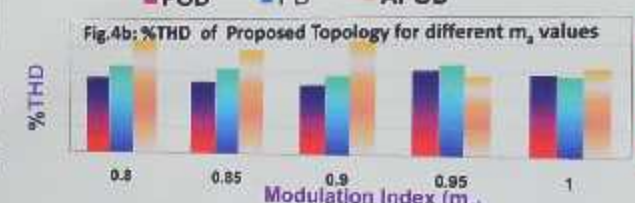
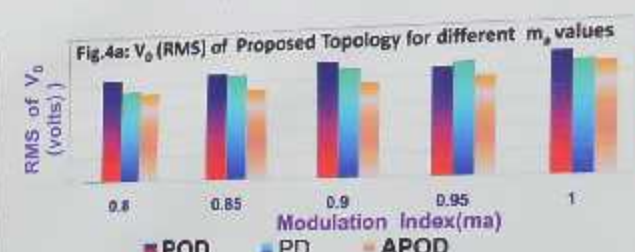


Fig. 5: (a),(b) are Photograph of prototype and Output voltage of proposed Topology respectively.

CONCLUSION

In this project, the proposed topology is simulated with different level shifted bipolar SPWM techniques.

This modified topology perform better for POD technique than PD and APOD techniques.



Electrical and Physicochemical Properties of Epoxy Sic Nano composites

Animesh Sahoo R.Sarathi and R.Jayaganthan
Indian Institute Of Technology, Madras

HVE038

1. Introduction

- Stability of any power system network is determined mainly by the high voltage equipment used. Failure of this equipment is normally related to partial discharge (PD) activity which deteriorates the system performance.
- There is a high risk of insulation system dielectric instability when PD occurs. Therefore, measurement and monitoring of PD is an important preventive tool to safeguard the high-voltage equipment from further damage.
- Various methods such as electrical, acoustic, UHF detection and optical methods have been proposed for detection and localization of PD in high voltage power apparatus.

2. Experimental Study

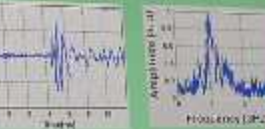


2.1. Electrical Diagnosis

a. UHF signal Analysis

- The majority of PD detection systems that are used induces Ultra High Frequency (UHF) technique.
- The UHF sensor used in the present study is a broadband type sensor, which is placed at a distance of 20 cm away from the test cell.
- The increased supply voltage enhances the electric field thus generating more electrons and ions which is understood from the increasing intensity of UHF signals.
- The UHF power which is the measure of the intensity level from 5% to 95% of peak value also increases which implies as the voltage increases the energy required for discharge is getting accumulated more and more on the surface of the sample.
- As over a same time window the peak-to-peak amplitude first signal is increasing the UHF voltage

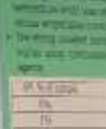
Wanted: Maximum frequency of LHF is showing less than variation in the frequency instant during the discharge process.



The PD pulse magnitudes are increasing with increasing voltage. This may indicate the increase of partial discharges in the air gap during the discharge process.



It is observed that the number of pulses per second increases with increasing voltage.



3. Conclusion

In this study, UHF power is measured.

The UHF power is measured.



सम्मेलन कक्ष 2
CONFERENCE HALL 2

EATABLES AND DRINKS
NOT PERMITTED INSIDE THE HALL

HVED39

HVE015

National Conference on Recent Trends in Power Engineering
Indian Institute of Technology Madras, Chennai 600 036, India.
29-30 December 2015

Insulation Deterioration of Twisted Pairs due to High Frequency Switching of Power Electronic Converters

K.Elanseralathan, Narashimrao,B.Amirthavalli,C.Cijith,R.Pravinraj,S.Silambarasan
Department of Electrical and Electronics Engineering, Pondicherry Engineering college, Puducherry

Introduction

- In Industries the motor speed is controlled with the help of Power Electronic Converters. But the output waveforms of the PEC's are highly distorted. It is a PWM output, which is a high frequency pulses.
- As the insulation is designed to operate with sinusoidal waveform, the life of insulation will be affected as it is stressed by PWM waveform. So the insulation must be designed in such a way that it should withstand these high distorted waveforms. This work focuses on the insulation test on primary layer of the twisted pair first followed by secondary one.

Methods

- Breakdown voltage test
- Withstand voltage test
- Thickness of primary and secondary insulation are 50 and 100 microns.
- Length of twisted pairs is 12cm and is twisted according to ASTM D 2307 standards

Figure1.Twisted pair samples



Figure2.Test setup for insulation testing



Figure3.Variation of Breakdown voltage between primary and secondary.

Results & Discussion

CURRENT	BREAKDOWN VOLTAGE (V)	TIME OF ACROSS INSULATION (ms ND)	CURRENT	BREAKDOWN VOLTAGE (V)	TIME OF VOLTAGE APPLIED (ms ND)
WITHSTAND VOLTAGE TESTS OF MAXIMUM BREAKDOWN VOLTAGES					
Primary insulation	4	12	Secondary insulation	10	1.9
Recovery insulation	5	30			
WITHSTAND VOLTAGE TESTS OF MAXIMUM BREAKDOWN VOLTAGES					
Primary insulation	7	9	Secondary insulation	13	2
Recovery insulation	8	12			

- Compare the primary and secondary insulation of magnetic wire in breakdown test by increasing the voltage gradually. From that we could identify maximum breakdown strength of the magnetic wire. So maximum breakdown strength of the secondary insulation is also measured.
- From withstand test, the maximum time duration of magnetic wire is identified at particular voltage which is found by statistical analysis by applying different voltages. From this, the maximum time duration of wire with both primary and secondary insulation are observed.

Conclusions

- Insulation degradation in electrical drives is due to various stress factors. The major stress factor considered in this study is the switching produced by the power electronic converters. It is observed that the degradation is delayed in the secondary compared to primary insulation.

References

- Francesco Gustavino, Andrea dardano, "Life Tests on Twisted Pairs in Presence of Partial Discharges: Influence of the Voltage Waveform", IEEE Transactions on Dielectrics and Electrical Insulation Vol.19 pp.45-52, No.1; February 2012.
- A.Cavalliani, D.Fabiani, and G.C.Montanari, "Power Electronics and Electrical Insulation Systems – Part 1: Phenomenology Overview", IEEE Electrical Insulation Magazine, vol.26 pp.5-14, May/June 2010



HVE010

National Conference on Recent Trends in Power Engineering
Indian Institute of Technology Madras, Chennai 600 036, India.
29-30 December 2015

Partial Discharge Characteristics of Synthetic Ester-Pressboard Insulation System: Effect of Conducting Particle

C. Thirumurugan, Ramesh Oruganti
School of Computing and Electrical Engineering,
Indian Institute of Technology Mandi,
Mandi-175001, Himachal Pradesh, India.

Ganesh Kumbhar
Department of Electrical Engineering,
Indian Institute of Technology Roorkee,
Roorkee-247667, Uttarakhand, India.

Introduction (Research Area- High Voltage Engineering)

Properties	Pressboard	Transformer Oil
Origin	Cellulose of highest quality	Paraffinic, naphthalene
Manufacture	Unbleached sulfate Cellulose	extracts from petroleum
Usage	insulation and mechanical Support	insulation well as cooling

- Partial Discharge(PD)- electrical discharge partially bridges the insulation.
- PD-sign of insulation degradation and root cause of breakdown.
- In order to understand PD, artificial defects were added (i.e. conducting particles-Cu).

Experimental work (two parts)



Figure 1. (a) Photo of two Cu particles on pressboard with Cu particles and Holes. (b) Experimental setup.

Results & Discussion (PRPD patterns)

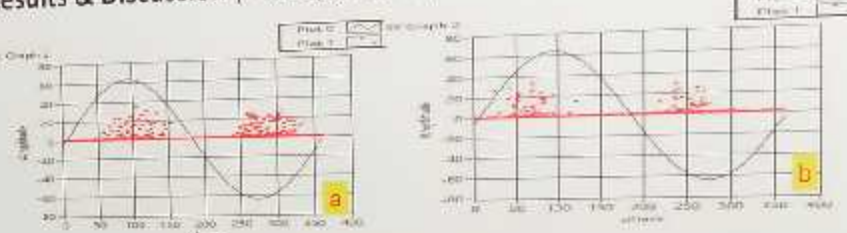


Figure 2. PRPD patterns of pressboard sample with Cu particles (PDIV=13.5kV)
a) at centre of electrodes. b) near by earth electrode.

- Two samples- 1. Cu particles at centre of electrodes. 2. Cu particle at near by earth electrode
- Measured value- PRPD pattern(Phase resolved partial discharge pattern)

Conclusions

- To check the suitability of synthetic ester for transformer insulation the PD experiment of Synthetic ester-pressboard with Cu particles has been carried out.
- As per the above PD patterns, Cu particles at the centre of the electrodes is having more repetitive pulses than Cu particles at nearby earth electrode.
- This PD patterns are used for condition monitoring of large transformers.

Reference

- Sarathi.R, I.PMerin Sheema, J.sundarajan, M.G.Daiwas, "Influence of harmonic ac voltage on surface discharge formation in transformer insulation", IEEE Trans. on DEI, vol. 21, No.5, pp. 2183-92, 2014.





National Conference on Recent Trends in Power Engineering
Indian Institute of Technology Madras, Chennai 600 036, India.
29-30 December 2015

**PROJECTING INDUCTION MOTOR AS A BEST SUITABLE
MOTOR FOR ELECTRIC VEHICLE TRACTION APPLICATION**

Dr.S.Sutha

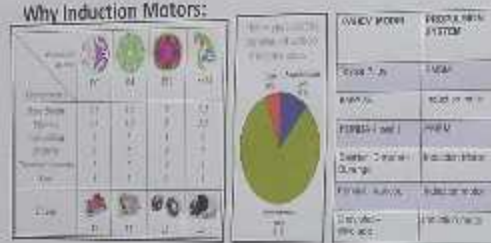
Arumugam Palanivel
AP/EEE, MAHATHAMMA INSTITUTE OF ENGINEERING
AND TECHNOLOGY, PUDUKKOTTAI, TN, INDIA

HOD/EEE, UNIVERSITY COLLEGE OF ENGINEERING
DINDIGUL,TN,INDIA

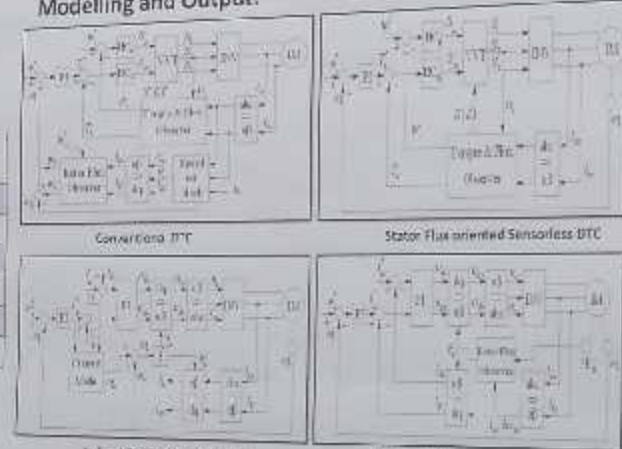
Introduction:

- This research work aims to analyze various possibility to project Induction Motor (IM) as a Suitable Drive for Electric Vehicle Traction.

Why Induction Motors:



Modelling and Output:



Artist Field cont'd. Mallard

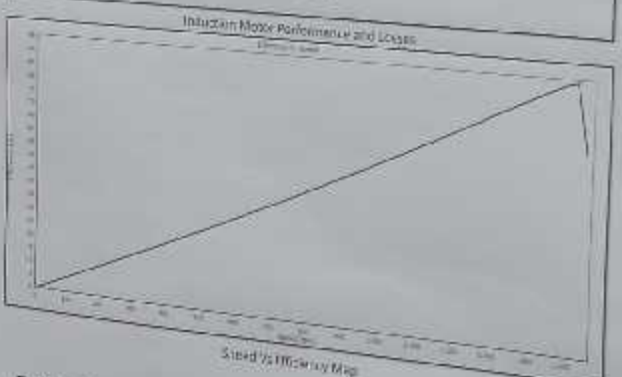


Direct-Field Control Method

Methods to achieve IM as best motor for EV

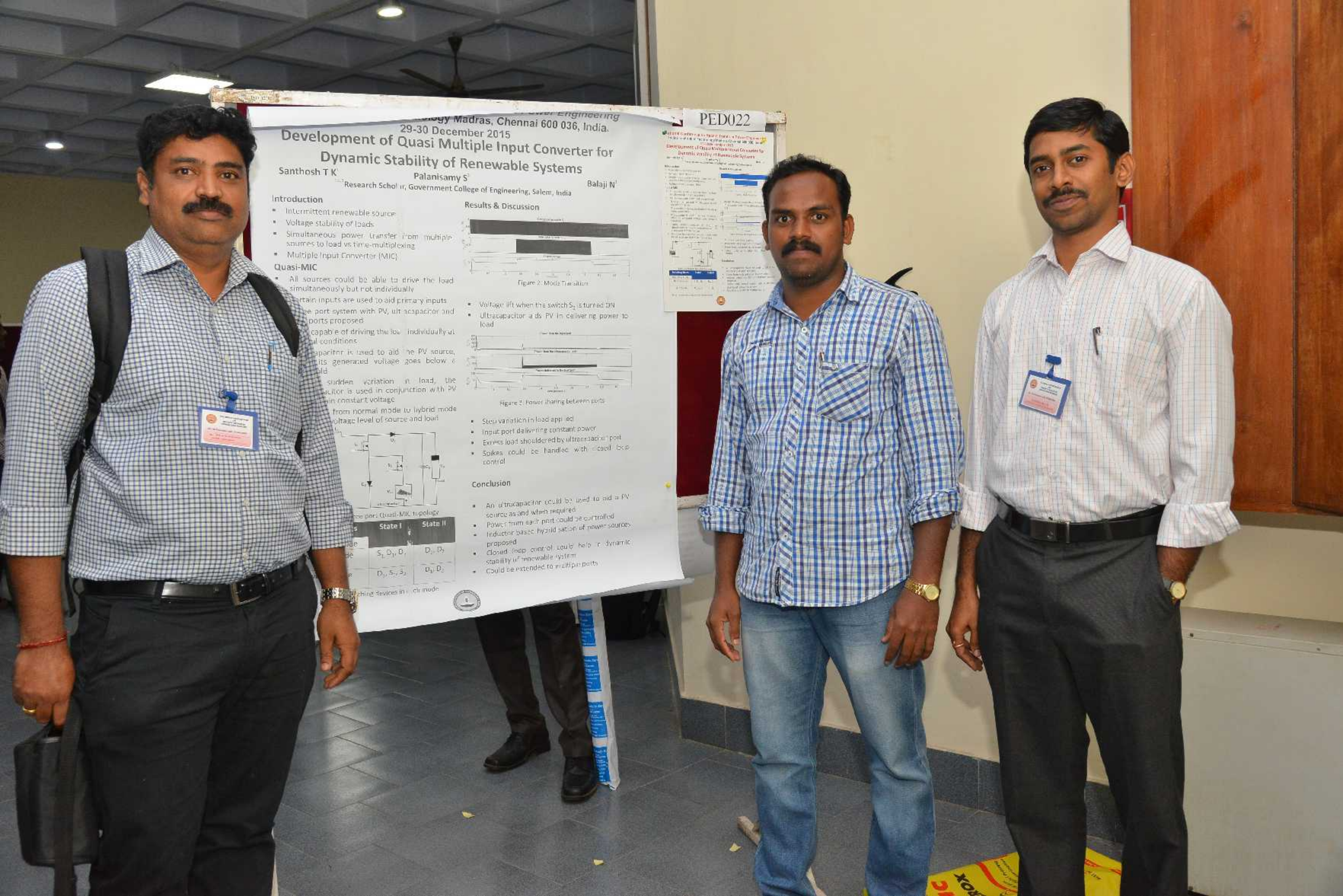


- Finding a separate and specific homologation for EV
 - Optimizing independent Variables (20)
 - Specific Nonlinear Constraints (15)
 - Solid Iron, Steel Core, Laminated Silicon Steel, Amorphous Steel
 - IEC60068-2-68, IEC60068-2-27, IEC60068-2-29, IEC60068-2-32, IEC60068-2-33, IEC60068-2-34, IEC60068-2-35, etc.
 - Capable of high fundamental frequencies (200 -2500 Hz) and harmonics up to about 25 kHz.
 - Additional heat withstand capacity for new materials.
 - High efficiency at low frequency and huge reduction in eddy current loss.
 - Direct & indirect DTC and field oriented control according to requirement and Design nature.



Conclusions of research

- ✓ Conclusions of research:
Induction Motor can perform well if design dedicated to EV propulsion.
 - ✓ When Control Methods adjusted according to requirement better performance can be achieved.
 - ✓ Induction Motor provides Economical Advantage over other motors.



Development of Quasi Multiple Input Converter for Dynamic Stability of Renewable Systems

Santhosh T K¹

Palanisamy S²
Research Scholar, Government College of Engineering, Salem, India

Balaji N¹

Introduction

- Intermittent renewable source
- Voltage stability of loads
- Simultaneous power transfer from multiple sources to load vs time-multiplexing
- Multiple Input Converter (MIC)

Quasi-MIC

- All sources could be able to drive the load simultaneously but not individually
- Certain inputs are used to aid primary inputs
- See port system with PV, ultra capacitor and AC ports proposed
- Capable of driving the load individually under certain conditions.
- Capacitor is used to aid the PV source, if its generated voltage goes below a threshold
- In sudden variation in load, the capacitor is used in conjunction with PV to maintain constant voltage

• From normal mode to hybrid mode based on voltage level of source and load



State

I

II

III

IV

V

VI

VII

VIII

IX

X

XI

XII

XIII

XIV

XV

XVI

XVII

XVIII

XIX

XX

XI

XII

XIII

XIV

XV

XVI

XVII

XVIII

XIX

XX

XI

XII

XIII

XIV

XV

XVI

XVII

XVIII

XIX

XX

XI

XII

XIII

XIV

XV

XVI

XVII

XVIII

XIX

XX

XI

XII

XIII

XIV

XV

XVI

XVII

XVIII

XIX

XX

XI

XII

XIII

XIV

XV

XVI

XVII

XVIII

XIX

XX

XI

XII

XIII

XIV

XV

XVI

XVII

XVIII

XIX

XX

XI

XII

XIII

XIV

XV

XVI

XVII

XVIII

XIX

XX

XI

XII

XIII

XIV

XV

XVI

XVII

XVIII

XIX

XX

XI

XII

XIII

XIV

XV

XVI

XVII

XVIII

XIX

XX

XI

XII

XIII

XIV

XV

XVI

XVII

XVIII

XIX

XX

XI

XII

XIII

XIV

XV

XVI

XVII

XVIII

XIX

XX

XI

XII

XIII

XIV

XV

XVI

XVII

XVIII

XIX

XX

XI

XII

XIII

XIV

XV

XVI

XVII

XVIII

XIX

XX

XI

XII

XIII

XIV

XV

XVI

XVII

XVIII

XIX

XX

XI

XII

XIII

XIV

XV

XVI

XVII

XVIII

XIX

XX

XI

XII

XIII

XIV

XV

XVI

XVII

XVIII

XIX

XX

XI

XII

XIII

XIV

XV

XVI

XVII

X



National Conference on Recent Trends in Power Engineering
Indian Institute of Technology Madras, Chennai 600 036, India
29-30 December 2015



A NOVEL TOPOLOGY FOR MULTILEVEL INVERTER BASED ON ASYMMETRIC SOURCE CONFIGURATION

Niraj Kumar Dewangan

Research Scholar, NIT Raipur, C.G, India

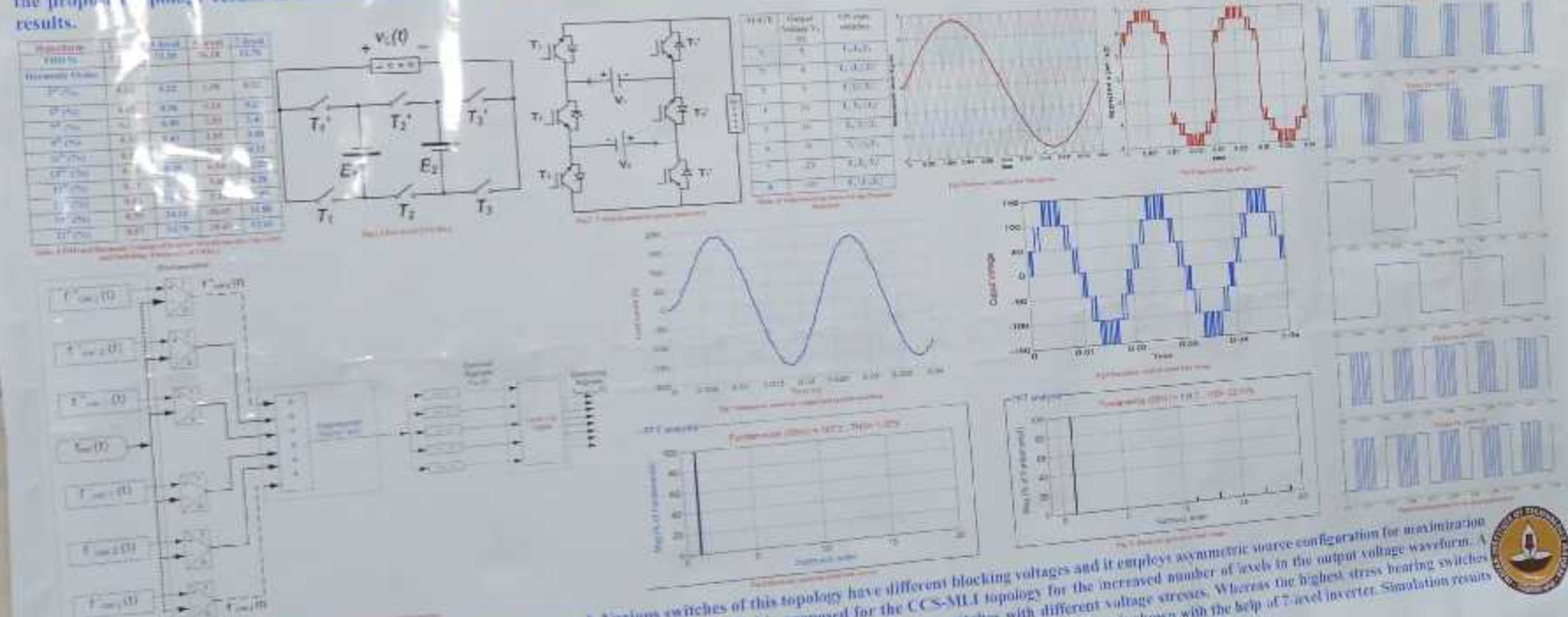
Dr. (Mrs) Shubhrata Gupta

Professor, NIT Raipur, C.G, India

Dr. Krishna Kumar Gupta

Asst. Professor, INCT Bhopal ,MP, India

Abstract As multilevel inverters are gaining importance, new topologies are being proposed especially for increased number of levels while reducing the number of power switches. In this paper, a Seven level asymmetric source based MLI is proposed for the recently proposed 'cross-connected sources based multilevel inverter (CCS-MLI)' topology. While increasing the number of levels in the output voltage, the proposed topology results in same number of power switching device count in the CCS-MLI. In this paper, an explanation of 7-level inverter is presented along with MATLAB/Simulink based simulation results.



Conclusion - A novel topology for 7-level inverter is proposed. Various switches of this topology have different blocking voltages and it employs asymmetric source configuration for maximization of levels in the output voltage waveform. Here a 7-level asymmetric source based MLI is proposed for the CCS-MLI topology for the increased number of levels in the output voltage waveform. A multicarrier PWM scheme is introduced which helps to optimize the switching frequencies of various power switches with different voltage stresses. Whereas the highest stress bearing switches operate at fundamental frequency and the lowest stress bearing switches operate at carrier frequency. Working of the switching structure is shown with the help of 7-level inverter. Simulation results based on the MATLAB/Simulink are presented to validate the proposed concept.





Novel load emulation technique for performance evaluation of isolated Solar PV system under varying load conditions

Vani Vijay*, P. Giridhar Kini **, C. Viswanatha*, R. Sudhir Kumar *

* Central Power Research Institute, Bangalore, Karnataka, India 560080; vanivijay_srf@cpri.in

** E&E department, Manipal Institute of Technology, Manipal 576104 India, 560071.

Introduction

- Performance of Renewable energy sources are highly dependent upon operating conditions
- Mostly the source side converters are designed for ideal conditions. They give degraded performance under non-ideal conditions like high THD loads, fluctuating source, low power factor etc.
- The effects of load variation can be evaluated using load emulation technique, where a flexible load model is used to create different types of loads
- Load emulation can be done using mechanical systems, power electronic systems, analogue circuits or computer models. Out of which power electronic models are most advantageous for power supply applications.

Effect of load characteristics on Stand alone Solar PV systems

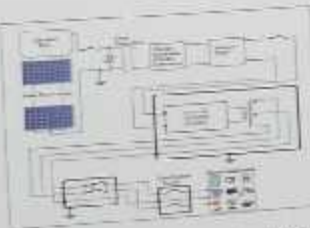


Fig. 1. Typical stand alone solar PV system

- Other than Solar variability, system design and Environmental/climatic conditions, the load variation also influence the performance of SPV systems
- Increase in core losses in transformer based systems
- Increase in current levels hence derating of equipments
- Interference with low voltage signals like control circuits and consequent malfunctioning.
- Components should be over rated to provide the required active power.
- The efficiency of power extraction from solar PV systems is reduced

Load emulation

- Emulation is the process of imitating the behaviour of a particular system using a different working principle
- Using load emulation, the operation of a system under various load conditions can be examined without the need for any electromechanical machinery or the actual load.
- A regenerative load emulator is a controllable sink which can provide a power exchange with either a grid or another power electronic converter system with characteristics as per the requirement of the user

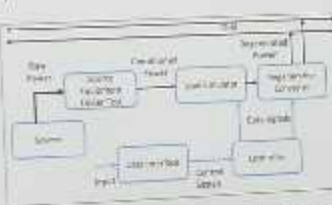


Fig. 2. Block Diagram of load emulation model

- In the proposed model, a new technique for obtaining variable power factor and variable THD load is derived using a decoupled current control method.
- The current is modulated using PWM technique to obtain in phase current, And out of phase current and variable THD

Simulation and Results

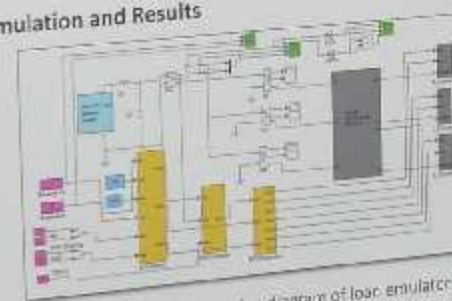


Fig. 3. Overall simulation diagram of load emulator



Fig. 4. Case studies using the simulated model at different load THD

- Efficiency is found to decrease as power factor varies from unity to 0.5 lagging
- Efficiency is found to decrease as THD increases
- The proposed load simulator can provide different power factor and loading conditions as per the requirement
- The results are verified by hardware testing using the setup shown



Fig. 5. Experimental setup for validation of results

Conclusions

- Using the method of load emulation, different types of loads can be realized easily using a single flexible platform
- The simulation results of proposed model is found to be similar to hardware results using actual load
- Unlike actual loading, the energy drawn by the load can be regenerated easily. Hence the losses in testing and hardware can be reduced to a great extent.
- They can be used as virtual load for testing and validation of applications also.
- Compared to the existing load emulator methods, the proposed gives more accurate and efficient simulation of variable power factor and variable THD loads.





HVE040

Surface Discharge Activity of Oil Impregnated Pressboard Material under AC Voltage

Copper

Aluminum

Steel

Iron

Brass

Lead

Magnesium

Zinc

tin

nickel

copper

tin





National Conference on Recent Trends in Power Engineering
 Indian Institute of Technology Madras, Chennai 600 036, India,
 29-30 December 2015

NOVEL EFFICIENT CORE RESETTING TECHNIQUES FOR ISOLATED FORWARD CONVERTER

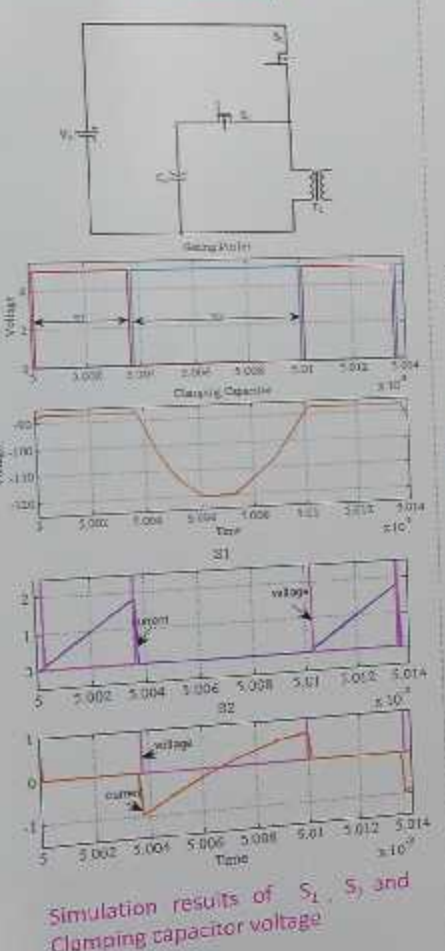
Alagu Dheeraj Dr V Rajini

Department of Electrical and Electronics Engineering
 SSN College of Engineering, Chennai, India

OBJECTIVE

To analyse various clamping cells like positive, negative and center for an isolated forward topology to optimize transformer core resetting and to enhance ZVS operation of switches.

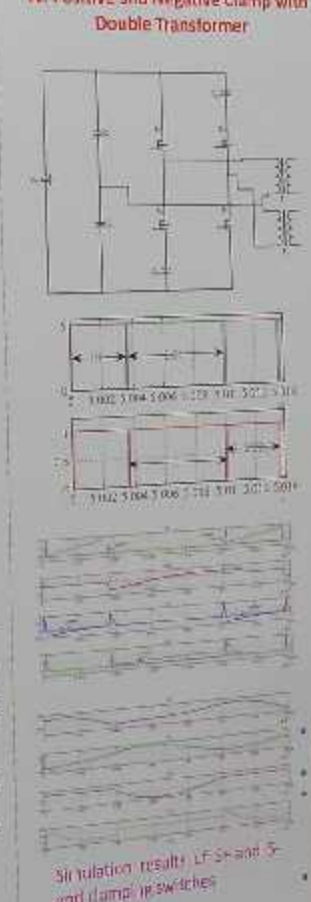
I. Positive Clamp



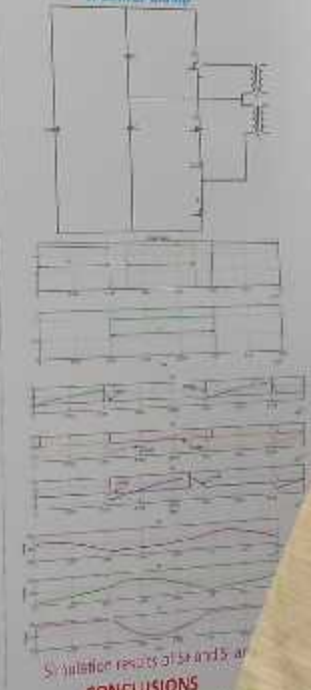
II. Negative Clamp



IV. Positive and Negative Clamp with Double Transformer



V. Center Clamp



SIGNIFICANCE

- Active Clamp Forward Converter (ACFC) core resetting depends on transformer magnetic induction B_m and clamping capacitors.
- ZVS is used to turn on switches.
- Two clamps filters for load current sharing and output junction current cancellation.
- Diode version of ACFC for all the above mentioned cells exists.

CONCLUSIONS

- Among all the clamping cells, Center clamp gives better results in terms of component reduction and load sharing.
- Multilevel Inverter based Power Conversion voltage high current reduces the magnet size.
- To increase the power density, isolated forward Comp converter with Self clamping (SFC) can be implemented.



National Conference on Recent Trends in Power Engineering
Indian Institute of Technology Madras, Chennai 600 036, India
29-30 December 2015

Harmonic Analysis in Grid connected Solar Photovoltaic system

Vigneswari M
Kamaraj College of Engg & Tech, Virudhunagar

PSE025

Dr. Kalyani S
Kamaraj College of Engg & Tech, Virudhunagar

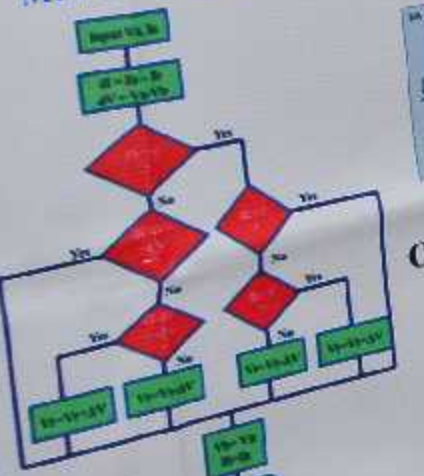
Introduction



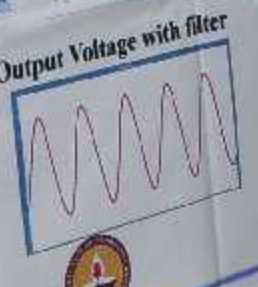
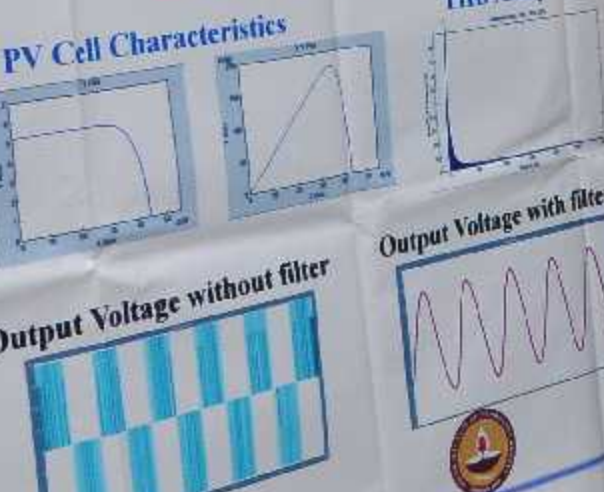
Grid connected solar PV system



MPPT Algorithm



PV Cell Characteristics



THD Analysis

Conclusion

- Incremental load used to track the load index of 0.9 to 1.0 s.
- PWM based IGBT
- Passive filter with LCL minimizes the harmonics in operation of non linear converter.
- The THD of the inverter is reduced to 3.3%

Output Voltage with filter



Parameter	Value
Current at Maximum Power	495A
Voltage at Maximum Power	352V
Line to Line Circuit Voltage	442V
Total Voltage	52A
Efficiency of System	90.5 %
Conductance	0.7
Coeficient of Open Loop Gain	0
Series Resistance	1
Inductance	1

Parameter	Value
Current at Maximum Power	495A
Voltage at Maximum Power	352V
Line to Line Circuit Voltage	442V
Total Voltage	52A
Efficiency of System	90.5 %
Conductance	0.7
Coeficient of Open Loop Gain	0
Series Resistance	1
Inductance	1

Parameter	Value
Current at Maximum Power	495A
Voltage at Maximum Power	352V
Line to Line Circuit Voltage	442V
Total Voltage	52A
Efficiency of System	90.5 %
Conductance	0.7
Coeficient of Open Loop Gain	0
Series Resistance	1
Inductance	1

Parameter	Value
Current at Maximum Power	495A
Voltage at Maximum Power	352V
Line to Line Circuit Voltage	442V
Total Voltage	52A
Efficiency of System	90.5 %
Conductance	0.7
Coeficient of Open Loop Gain	0
Series Resistance	1
Inductance	1

Parameter	Value
Current at Maximum Power	495A
Voltage at Maximum Power	352V
Line to Line Circuit Voltage	442V
Total Voltage	52A
Efficiency of System	90.5 %
Conductance	0.7
Coeficient of Open Loop Gain	0
Series Resistance	1
Inductance	1

Parameter	Value
Current at Maximum Power	495A
Voltage at Maximum Power	352V
Line to Line Circuit Voltage	442V
Total Voltage	52A
Efficiency of System	90.5 %
Conductance	0.7
Coeficient of Open Loop Gain	0
Series Resistance	1
Inductance	1

Parameter	Value
Current at Maximum Power	495A
Voltage at Maximum Power	352V
Line to Line Circuit Voltage	442V
Total Voltage	52A
Efficiency of System	90.5 %
Conductance	0.7
Coeficient of Open Loop Gain	0
Series Resistance	1
Inductance	1

Parameter	Value
Current at Maximum Power	495A
Voltage at Maximum Power	352V
Line to Line Circuit Voltage	442V
Total Voltage	52A
Efficiency of System	90.5 %
Conductance	0.7
Coeficient of Open Loop Gain	0
Series Resistance	1
Inductance	1

Parameter	Value
Current at Maximum Power	495A
Voltage at Maximum Power	352V
Line to Line Circuit Voltage	442V
Total Voltage	52A
Efficiency of System	90.5 %
Conductance	0.7
Coeficient of Open Loop Gain	0
Series Resistance	1
Inductance	1

Parameter	Value
Current at Maximum Power	495A
Voltage at Maximum Power	352V
Line to Line Circuit Voltage	442V
Total Voltage	52A
Efficiency of System	90.5 %
Conductance	0.7
Coeficient of Open Loop Gain	0
Series Resistance	1
Inductance	1

Parameter	Value
Current at Maximum Power	495A
Voltage at Maximum Power	352V
Line to Line Circuit Voltage	442V
Total Voltage	52A
Efficiency of System	90.5 %
Conductance	0.7
Coeficient of Open Loop Gain	0
Series Resistance	1
Inductance	1

Parameter	Value
Current at Maximum Power	495A
Voltage at Maximum Power	352V
Line to Line Circuit Voltage	442V
Total Voltage	52A
Efficiency of System	90.5 %
Conductance	0.7
Coeficient of Open Loop Gain	0
Series Resistance	1
Inductance	1

Parameter	Value
Current at Maximum Power	495A
Voltage at Maximum Power	352V
Line to Line Circuit Voltage	442V
Total Voltage	52A
Efficiency of System	90.5 %
Conductance	0.7
Coeficient of Open Loop Gain	0
Series Resistance	1
Inductance	1

Parameter	Value
Current at Maximum Power	495A
Voltage at Maximum Power	352V
Line to Line Circuit Voltage	442V
Total Voltage	52A
Efficiency of System	90.5 %
Conductance	0.7
Coeficient of Open Loop Gain	0
Series Resistance	1
Inductance	1

Parameter	Value
Current at Maximum Power	495A
Voltage at Maximum Power	3

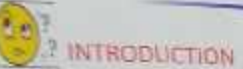
National Conference on Recent Trends in Power Engineering Indian Institute of Technology Madras,
Chennai - 600 036, India. 29-30 December 2015

FAULT DETECTION AND IDENTIFICATION ON SMART GRID BY USING SYNCHRONIZED MEASUREMENT UNIT

Keerthana.G¹

Dr.Umayal.S²

¹PG scholar Muthayammal Engineering College,Rasipuram ²Professor and Dean Muthayammal Engineering College,Rasipuram.



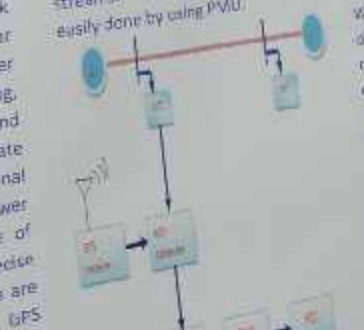
INTRODUCTION

The electric power system is complex man made system which should be reliable and supply electrical energy continuously without any interruption. Black out and outage in the system is to be avoided. One recently used technique is WAMPAC with time synchronized measurement. The main technology used in it is PMU's and is most precise and advanced technology. It gives information about the current and voltage phasor, frequency, rate of change of frequency all this information is synchronized with high accuracy to a common reference time provided by GPS. Its operation is based on mathematical measurement algorithm. This work uses synchronized phasor measurement technology for power system real time monitoring, advanced network protection and control schemes. PMU facilitate innovative solution to traditional utility problems and offer power system engineer a whole range of potential benefits including precise estimates of power system state are obtained through GPS synchronization, it also helps to analyse the vulnerability of system against any contingency. This technology has been made possible by advancement in computer and processing technologies and availability of GPS signals and designed this PMU model in MATLAB SIMULINK and validated in IEEE 9 bus system using MATLAB SIMULINK model.

PROPOSED TECHNIQUE

Synchrophasor vector processor allows us to use synchronized phasor data from various phasor measurement and control unit and relays, transmit data over Ethernet to other clients. This can provide a mechanism for collecting and time correlating synchrophasor data from as many as 20 PMU's.

In PDC we can connect more than 500 PMU inputs with message rates up to 240 per second. Combine data multiple input message rates into a single output stream. Control individually configurable output streams. Wide area protection is easily done by using PMU.



$$\text{Min}(|V_{11}|, |V_{21}|, |V_{31}|, \dots, |V_{n1}|)$$

Where $|V_{ij}|$ is the positive sequence voltage magnitude measured by PMU and located area 1, 2, ... n.

The absolute difference of positive sequence current angles are calculated for all lines connected with faulted area. These absolute angle difference values are selected to identify the faulted line. To find the faulted line we should compare the absolute difference of positive sequence current angles for all the lines connecting faulted area with all other neighboring area and then selecting the maximum one. This can be explained as:

$$\text{Max}(|\Delta\phi_{11}|, |\Delta\phi_{21}|, \dots, |\Delta\phi_{n1}|)$$

Where $|\Delta\phi_{ij}|$ is the absolute difference of positive sequence current angle for a transmission line connecting faulted area "i" with area "j", this can be described by the following equation:

$$|\Delta\phi_{ij}| = |\phi_{ij} - \phi_{ji}|$$

PMU converts the analog voltage, current signals to digital samples synchronized at time of measurement the discrete Fourier transform method. Inside PMU calculates the positive sequence voltages and current phasors.

The main idea of the proposed technique is to identify the faulted area. This is achieved by comparing the measured values of the positive sequence voltage magnitude at the main bus for each area. The minimum voltage value indicates the nearest area to the fault.

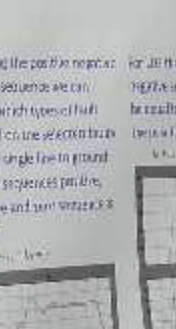
RESULTS AND DISCUSSION

During normal condition, before the fault occurs the waveform of voltage and current will be as shown in figure 1.

With fault, the voltage and current sequence will be as shown in figure 2.

Figure 1

Figure 2



Comparing the positive sequence and zero sequence we can identify which type of fault occurred on the selected bus. For single line to ground fault, a sequence positive, negative and zero voltage sum:

$$V_{11} + V_{21} + V_{31} = 0$$

For the fault location, the zero sequence will be as follows:

$$V_{11} = V_{21} = V_{31}$$

Figure 1

Figure 2

Figure 3

Figure 4

Figure 5

Figure 6

Figure 7

Figure 8

Figure 9

Figure 10

Figure 11

Figure 12

Figure 13

Figure 14

Figure 15

Figure 16

Figure 17

Figure 18

Figure 19

Figure 20

Figure 21

Figure 22

Figure 23

Figure 24

Figure 25

Figure 26

Figure 27

Figure 28

Figure 29

Figure 30

Figure 31

Figure 32

Figure 33

Figure 34

Figure 35

Figure 36

Figure 37

Figure 38

Figure 39

Figure 40

Figure 41

Figure 42

Figure 43

Figure 44

Figure 45

Figure 46

Figure 47

Figure 48

Figure 49

Figure 50

Figure 51

Figure 52

Figure 53

Figure 54

Figure 55

Figure 56

Figure 57

Figure 58

Figure 59

Figure 60

Figure 61

Figure 62

Figure 63

Figure 64

Figure 65

Figure 66

Figure 67

Figure 68

Figure 69

Figure 70

Figure 71

Figure 72

Figure 73

Figure 74

Figure 75

Figure 76

Figure 77

Figure 78

Figure 79

Figure 80

Figure 81

Figure 82

Figure 83

Figure 84

Figure 85

Figure 86

Figure 87

Figure 88

Figure 89

Figure 90

Figure 91

Figure 92

Figure 93

Figure 94

Figure 95

Figure 96

Figure 97

Figure 98

Figure 99

Figure 100

Figure 101

Figure 102

Figure 103

Figure 104

Figure 105

Figure 106

Figure 107

Figure 108

Figure 109

Figure 110

Figure 111

Figure 112

Figure 113

Figure 114

Figure 115

Figure 116

Figure 117

Figure 118

Figure 119

Figure 120

Figure 121

Figure 122

Figure 123

Figure 124

Figure 125

Figure 126

Figure 127

Figure 128

Figure 129

Figure 130

Figure 131

Figure 132

Figure 133

Figure 134

Figure 135

Figure 136

Figure 137

Figure 138

Figure 139

Figure 140

Figure 141

Figure 142

Figure 143

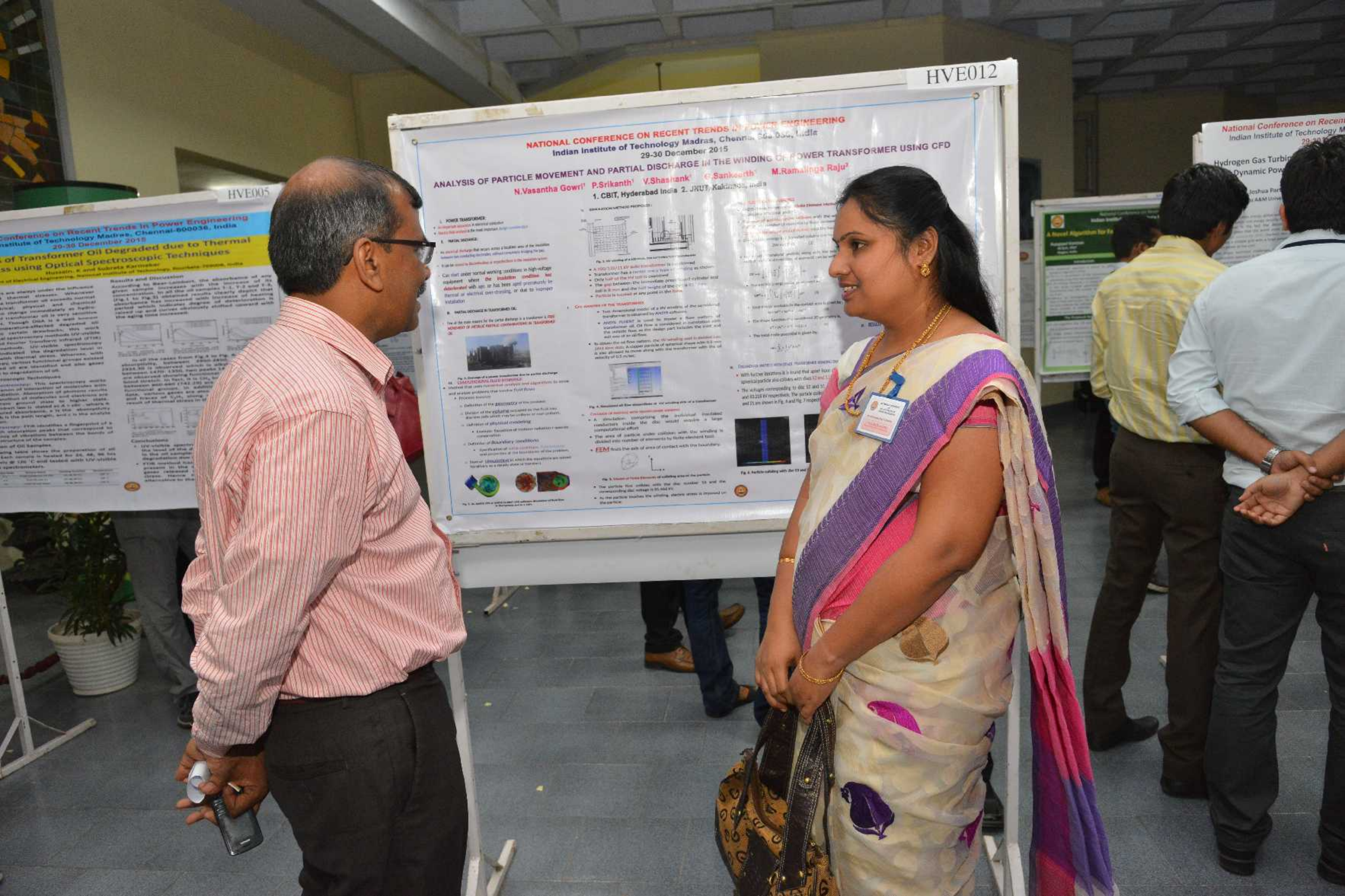
Figure 144

Figure 145

Figure 146

Figure 147

Figure 148





Abstract: Power sector faces a challenge to meet the growing electrical power demand in one of the major problems faced by power sectors operating in developing economies. Power sector aims for certain load shedding to maintain the system demand within its generation limit. Shortages of power forced the end users to install emergency power generation or even to import power from other countries. Thus IBKs storage units operate independently from system with the only objective of power supply to end users with the source of energy. Charging units active as soon as there is any interruption of power supply from the main grid. Similarly, charging of storage units is required at times of power shortage to surge power demand due to a charging load. The independent operation of IBKs burdening the system which is already under stress due to power shortage. In this paper authors demonstrated the impact of IBKs on system peak demand due to uncontrolled operation of IBKs. With a proposal of smart grid (SG) energy storage for IBKs can help with peak demand swapping. The pre-installed infrastructure is extended for the future V2G.

Problem of Uncontrolled Charging

- One out of any power infrastructure is created by its natural generation capacity.
- Excess power demand represented by supply mismatch intended to distribution of excess area.
- Load shedding reduces the system demand within preexisting limits.
- Demand excess generates at 12:00, 13:00, 13:00, 13:00 in 21:00 hours due to changing loads.
- Hour 12:00 was within limit but under IBKs charging effect, its demand exceeds.



$$\text{Min } P_{\text{shd}} = \sum_{i=1}^{10} (P_i + \sum_{j=1}^{20} P_{\text{load},ij} \Delta U_{ij})$$

$$10.9 \geq \Delta t \cdot (\text{State of charge} \geq 0.9; \text{For V2G})$$

$$\epsilon \geq 0.45; \text{For inverter mode } \epsilon \geq 0.1)$$

Figure 2: System Power Demand

Controlled Operation of IBKs

Case 1: Delivered Charging

- 1. Load Shedding Schedule signal is issued beforehand.
- 2. IBKs locally optimised to charging scheme i.e. Delays charging.
- 3. Charging Power demand is reduced.
- 4. Only hour 12:00 and 21:00 hours impose limitation of load shedding.
- 5. IBKs planning equation:

$$P_{\text{shd}} = \sum_{i=1}^{10} \sum_{j=1}^{20} P_{\text{load},ij} \Delta U_{ij} - 46.92$$

$$0.9 \geq \Delta t \cdot (\text{State of charge} \geq 0.9; \text{inverter mode})$$



Figure 3: System Power Demand

Load Shedding Schedule



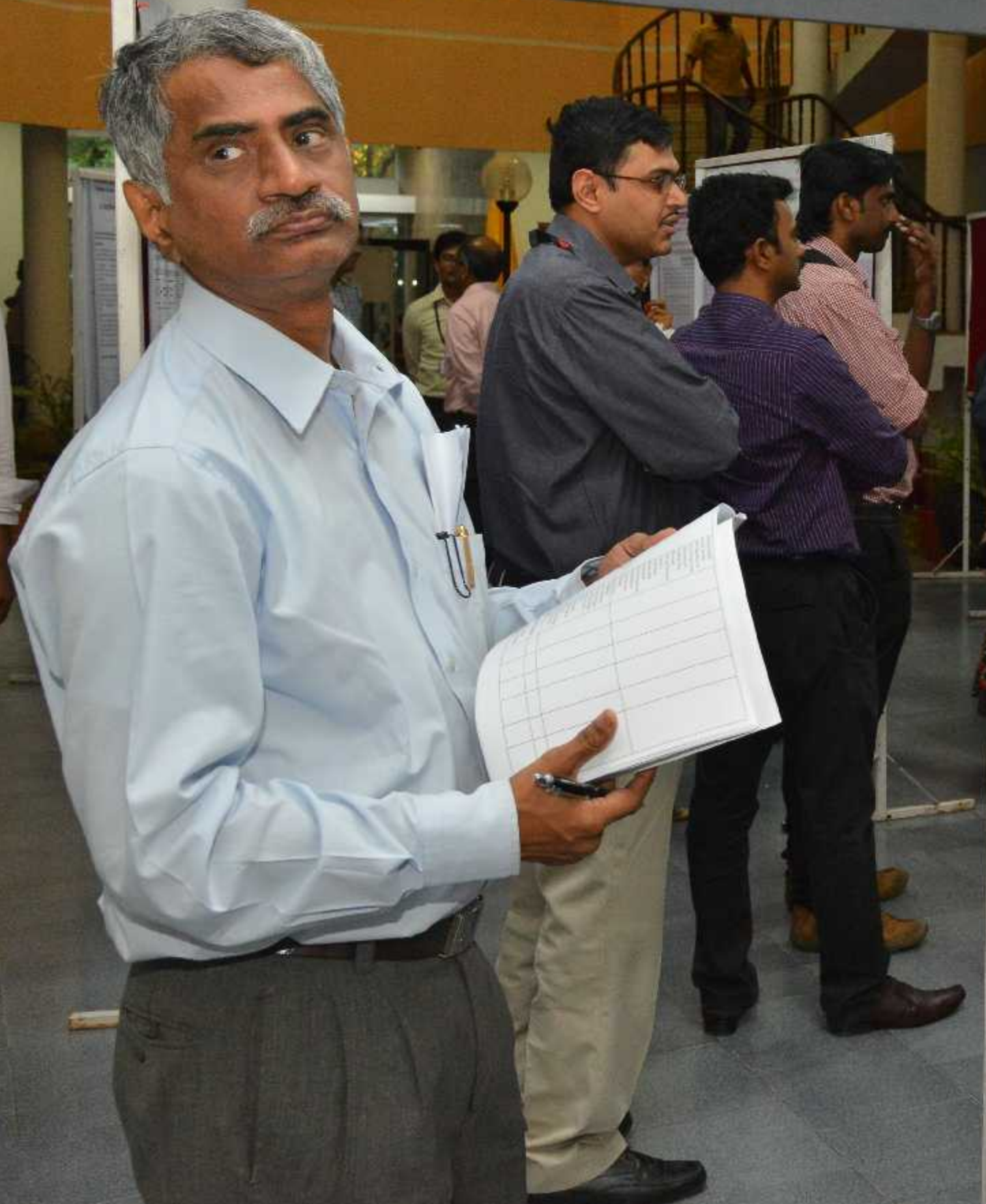
Figure 4: System Load Shedding Schedule

Conclusion

- Charging demand can exceed the peak power due to surplus demand for storage after load shedding.
- Delays charging can help in reduction of peak demand but not sufficient enough to cope with peak power.
- Smart operation of IBKs helps in reduction of frequency of load shedding e.g. a 24 hours schedule but now with 3 hours of load shedding.
- Earlier load shedding was done for 12 hours but is now reduced to 8 hours only.

Forthcoming Research

- IBKs can help V2G in developing countries.
- IBKs infrastructure forms a base for future V2G.
- IBKs acts as fast reserve.
- The capacity can be increased if users participate for power market profit as in V2G market.





DEDICATION

National Conference on Recent Trends in Power Engineering
Indian Institute of Technology Madras, Chennai 600 036, India
29-30 December 2015

ANSYS-Maxwell based Design of High Frequency Link for Grid Connection of Renewable Energy Sources using MLI

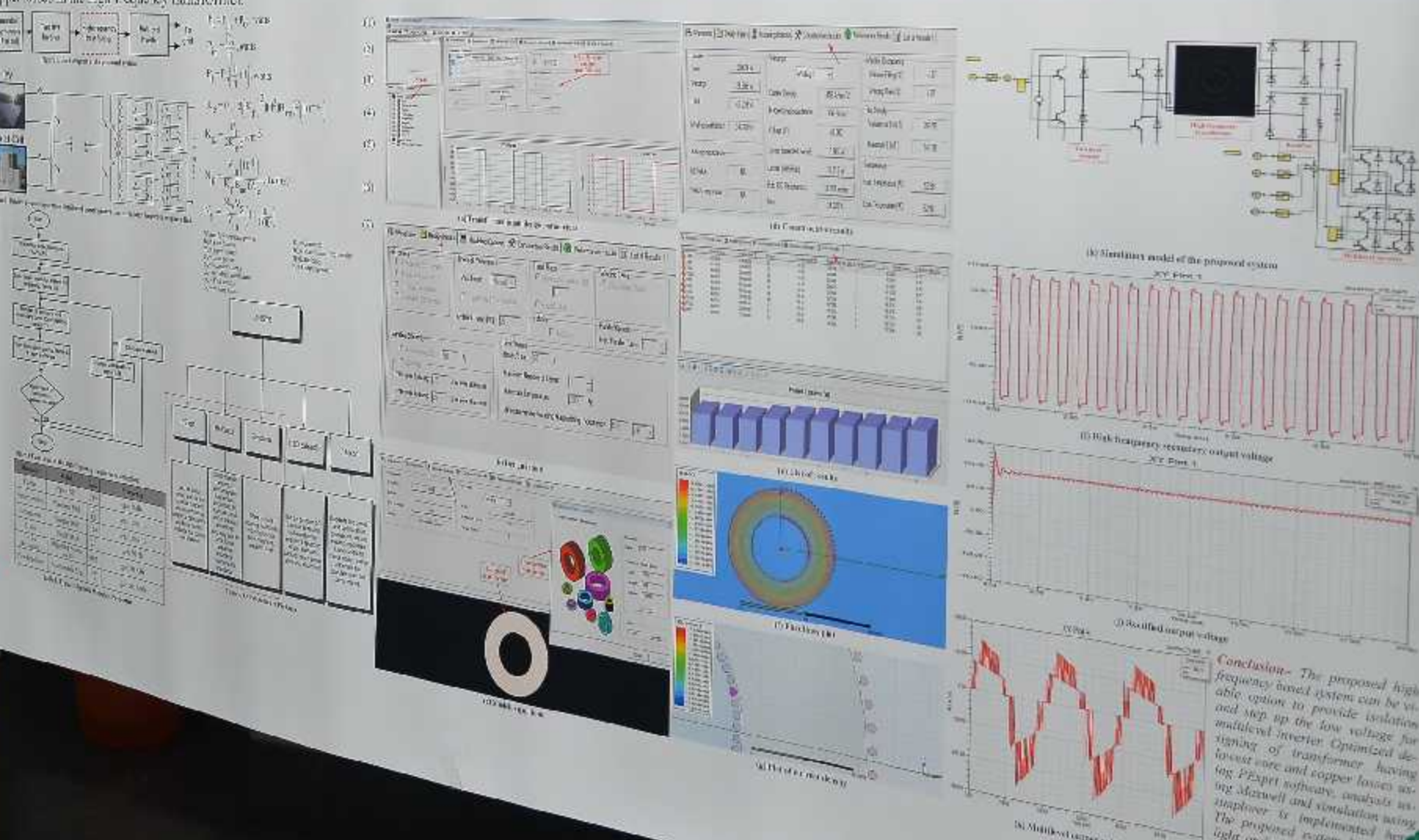
AN

Rekha Agrawal
Student, MANIT Bhopal, MP, India

Shailendra Jain

Professor, MANIT Bhopal, MP, India

Currently, high frequency transformer for power MLI is used for renewable energy interfacing applications. With the advancement in magnetic materials properties have led to the development of high frequency transformers for converters. Recently high frequency based magnetic material offers high saturation flux density and low core losses, used in designing of compact, light weight and efficient transformers. However, the designing of magnetic material is based on electro-magnetic concepts. So here, electro magnetic based software "ANSYS Maxwell" is used to design a high frequency transformer in 2-D geometry. The design methodology is illustrated to optimize it with minimum core losses, copper losses in the high frequency transformer.



Conclusion- The proposed high frequency based system can be viable option to provide isolation and step up the low voltage for medium voltage transformer having minimum core and copper losses using Pspice software, analysis using Maxwell and simulation using Matlab is implemented here. The proposed system leads to a simpler and compact design, which reduces the system size, installation cost and cost.







National Conference on Recent Trends in Power Engineering
Indian Institute of Technology Madras, Chennai 600 036, India
29-30 December 2015

A Systematic Approach towards Developing Proto-type AMI based DSM Model for Load Management

MANJU GUPTA¹, SUSHMA GUPTA², TRIPTA THAKUR³
Maulana Azad National Institute of Technology, Bhopal (M.P.) India

ABSTRACT / INTRODUCTION
Participating in demand response has significant advantages for both consumers and electricity producers, i.e., saving on high electricity prices for the user, and helping utilities in peak load curtailment.

This research paper insight the development of Advanced Metering Infrastructure based Demand Side Management for load Management. The main objective of this application is consumption optimization and automation in operation. This paper proposes a fixed load control strategies with fixed forecasted photovoltaic generation with battery storage system and priority based load curtailment mechanism.

LOAD CONTROL STRATEGIES
(a) Various type of Load Control Angles
(b) Energy Conservation Programme

CONFIGURATION OF ADVANCED METERING SYSTEM FOR DSM MODEL

PROPOSED METHODOLOGY

Fig 3 Architecture of load monitoring system
Fig 4 Graph for modifications in the load curve after load management

DESIGN PARAMETERS OF DSM-AMI MODULE

RF Module with Relay: 2.4GHz or 865MHz ISM band operates Mesh Networking, Point to point, Star Networking topology, Configurable on air data rate of 250kbps, 1Mbps or 2Mbps Relay 5A, 220V, operation voltage 5/12V DC

Fig 5 Single Line diagram
Fig 6 Topology for load management

BASED ON CONSUMER PRIORITY

1. Highest priority load (Active / Critical)
2. Medium priority load (Essential)
3. Lowest priority load (Non-essentials)

SYSTEM DISCRIPTION
The system consists of a load transfer switch, A/D converter, zigbee to send information, current sensor (CT), voltage sensor (PT), control unit. FPGA kit is used for implementation of load control mechanism through HDL coding and design. The real time implementation is proposed through LabVIEW. FPGA generates control signals which are concurrent in nature and 1 KHz clock pulse is used for running of system. The control unit will generate control signal which control the load transfer switch and signal to energy management centre through universal asynchronous transmitter (UART) and zigbee.

Algorithm is based on K factor for selection of source:
specific factor (k) is difference between PV power and load demand
If $K >$ Default value: use power from photovoltaic system
 $K =$ Default value: use power from both sources (utility source and photovoltaic power)
 $K <$ Default Value: use power from the utility source.

CONCLUSION / RESULT
The Proposed design of proto type of AMI based DSM model will manage load and improve the efficiency of PV and utility. The system simulation will be done on LabVIEW.

ACKNOWLEDGEMENT
The authors are highly thankful to Jaswinder Singh Consultant, National Instruments, Bangalore, Pramod Kumar Jainini Superintending Engineer (IT), Japur DISCOM and Nilin Gupta Project Manager Dong Fang Electronics China for their valuable suggestions and guidance.



Date: 29-30 Dec.
Venue : IC & SR Auditorium



**Chief Guest
Prof. Bhaskar Ramamurthi**

(Director, IIT Madras)

&

Plenary Talk on

"Enabling India with Electricity"
by



Prof. Ashok Jhunjhunwala

Department of Electrical Engineering,





NATIONAL CONFERENCE ON
RECENT TRENDS IN POWER ENGINEERING
(for Research Scholars)
Date: 29-30 December 2015
Venue : IC & SR Auditorium



Chief Guest
Prof. Bhaskar Ramamurthi
(Director, IIT Madras)



Research and Development - Where, When and How?

An engineer's odyssey

Dr. V. Jagadeesh Kumar
Professor and Head CEC
Department of Electrical Engineering
IIT Madras Chennai 600036 India

Measurements and Instrumentation Laboratory, Department of Electrical Engineering, IIT Madras





NATIONAL CONFERENCE ON
RECENT TRENDS IN POWER ENGINEERING
(for Research Scholars)
Date: 29-30 December 2015
Venue : IC & SR Auditorium



Chief Guest
Prof. Bhaskar Ramamurthi

(Director, IIT Madras)

&

Plenary Talk on

"Enabling India with Electricity"

by

Prof. Ashok
Department of EEE
IIT

Research and Development - Where, When and How?

An engineer's odyssey

Dr. V. Jagadeesh Kumar
Professor and Head CEC
Department of Electrical Engineering
IIT Madras Chennai 600036 India

Power Electronics and Instrumentation Laboratory, Department of Electrical Engineering, IIT Madras









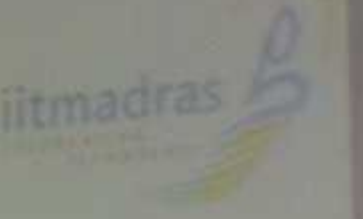






Power Quality Laboratory

Department of Electrical Engineering, IIT
Madras, Chennai - 36



Power Quality Aspects in Renewables Integration and
AC-DC Microgrid System

Dr. Mahesh Kumar
Professor

Power Quality Laboratory
Electrical Engg. Dept. I.I.T. Madras





NATIONAL CONFERENCE ON
RECENT TRENDS IN POWER ENGINEERING
(for Research Scholars)
Date: 29-30 December 2015
Venue : IC & SR Auditorium



Chief Guest
Prof. Bhaskar Ramamurthi

(Director, IIT Madras)

&



Power Electronics and Drives



Driven by: Need for DC Transformers,
Need for AC Batteries





OVERVIEW OF R&D AND RESEARCH SCHEM

J. Sundara Rajan

Joint Director

R&D Management Division and

Centre for Collaborative and Advanced I

Bangalore 560 080

Venue : IC & SR Auditorium
Date : 25th March 2015
Chief Guest
Prof. Bhaskar Venkateswaran

(Direc

Ple

"Enabling In

Prof. Asho

Department c



NATIONAL CONFERENCE ON
RECENT TRENDS IN POWER ENGINEERING
(for Research Scholars)

Date: 29-30 December 2015
Venue : IC & SR Auditorium



Guest
Prof. Balaji Ramamurthi

(Dr. Madras)

Research interests of UK

- Lightning modelling: Modelling of the return stroke evolution; Role of tall objects on ground; Upward connected leaders; ...
- Lightning protection: Definition of stress; Efficacy of different protection schemes; Strike to high voltage lines; Cables on towers and in soil; ...
- Electromagnetics for power engineering: Static fields; RC transient fields; Fields in DC insulation; Eddy current and moving conductor problems; Wave propagation in lightning, transmission lines and windings; ...
- High voltage engineering: Corona; Leader-streamer breakdown; Insulation aspects; Pollution performance of outdoor insulation; Grounding – power system and high voltage; ...

Prof. Umoya Kumar Gupta, IIT, Kharagpur

Thank You...



amurthi
(as)



Chief Guest
Prof. Bhaskar Ramamurti

(Director, IIT Madras)

&

Plenary Talk on
"Enabling India with Electricity"
by



Prof. Ashok Jhunjhunwala

Department of Electrical Engineering
IIT Madras





Mr. S. Jayaraman
R&D Manager
E. I. du Pont de Nemours & Co.
2007-08
2008-09

Mr. S. Jayaraman
R&D Manager
E. I. duPont de Nemours & Co.
2007-08
2008-09

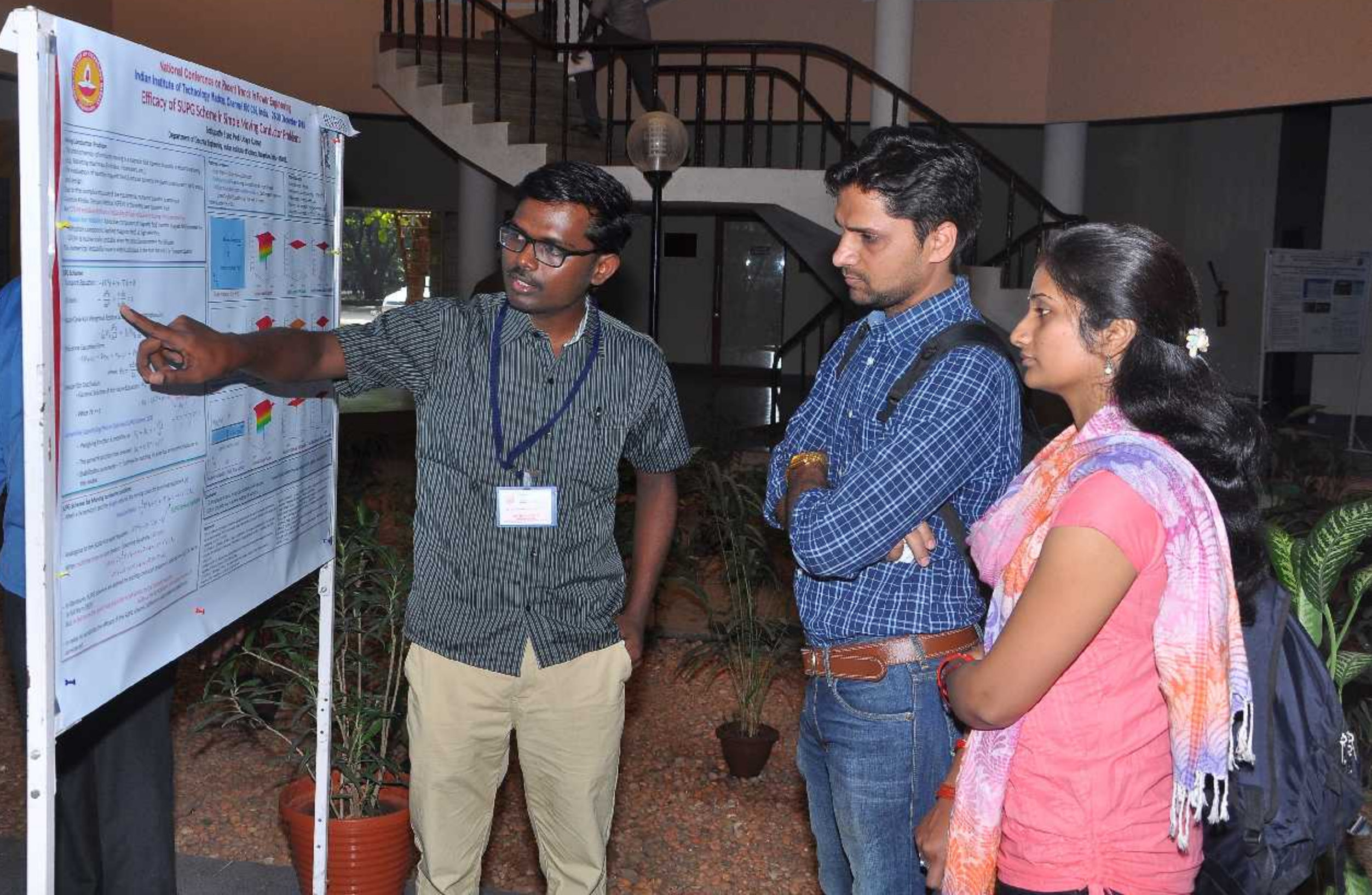


IND

S









PSE065

National Conference on Recent Trends in Power Engineering
Vellore Institute of Technology Maruthi, Chennai 600 036, India.
28-30 December 2015

Development of Andriod Application for
Design of Solar PV System

Author(s): E. Senthil, S. Selvaraj Narayana, Prof. Dr. P.
Srinivasan Aravind, Prof. Dr. R. Balaji



PSE053





IEEE PES INDIA CONFERENCE
2015
"Smart Grids & Renewable Energy Sources
for Sustainable Development"

IEEE PES INDIA CONFERENCE
2015
"Smart Grids & Renewable Energy Sources
for Sustainable Development"



Application Technique in Classification of Multiple
Defects in Oil Cooled Transformer Defect Model

Author Name: Suresh K. V. & Chaitanya
Date: 20 August 2015 at 20 minutes, 10 AM
Session: 1

MR BASED TRANSFORMER
CLASSIFICATION
DEFECTS

Information during COT:

WAT

WAT

PSE082





Chief Guest
Bhaskar Ramamurthi
(Director, IIT Madras)
&
Plenary Talk on

&



**Chief Guest
Prof. Bhaskar Ramamurti
(Director, IIT Madras)
&
Plenary Talk on**



HVE021



National Conference on Recent Trends in Power Engineering
Indian Institute of Technology Madras, Chennai 600 036, India.
29-30 December 2015

Investigation on the Thermal Behaviour of PVC Cable Insulation Material With and without Flame Retardants Under Thermal Ageing Conditions

PRAVEEN T A, Dr. NAGESHWAR RAO B, ARUN JOTHI R and Dr. SUNDARA RAJAN J
Central Power Research Institute, Bangalore – 560080.

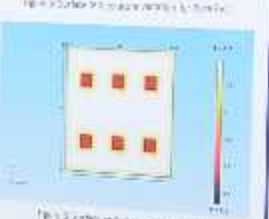
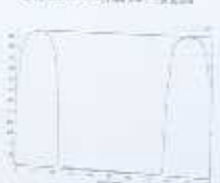
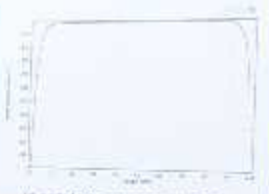
SPR-300

+ Selective Flame Retardant

Material 300C

Chlorinated

- The effect of adding different flame retardants on the PFR of insulation material under thermal ageing conditions.
- The thermal stability of insulation material with and without flame retardants at 300°C.
- The effect of adding different flame retardants on the TGA of PVC cable insulation material under thermal ageing conditions.



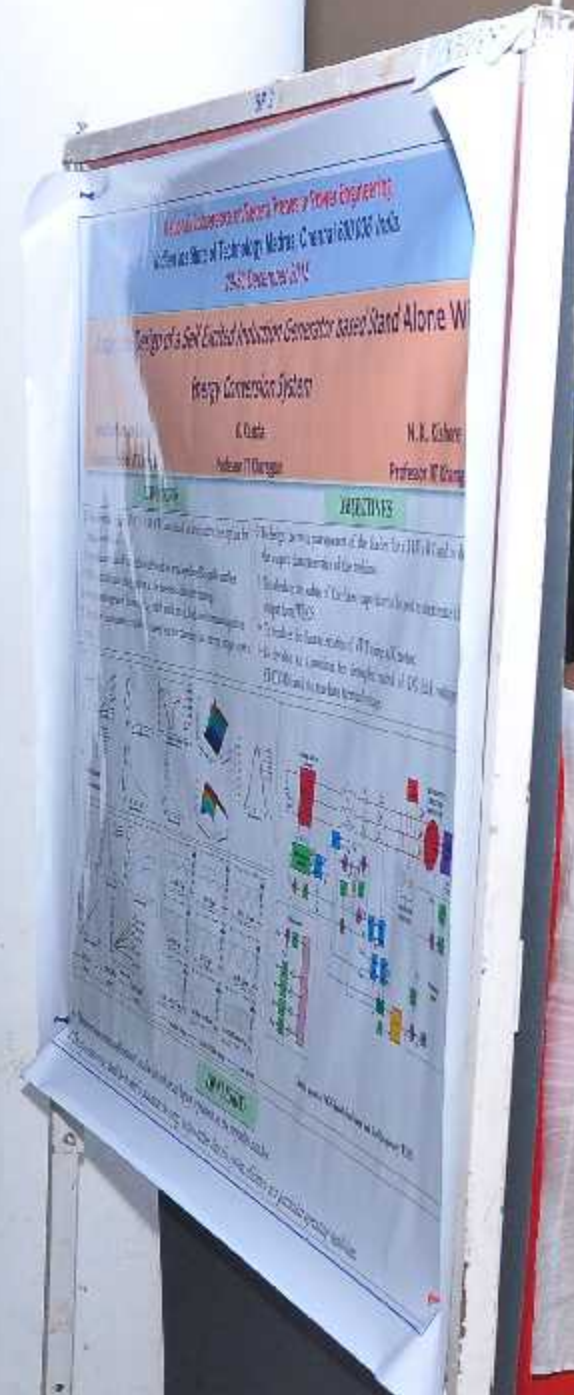
- Maximum PFR of 300C is observed at 300°C in this study.
- The flame retardancy is increased by adding MBH Filter in the order of PVC material > PR material > PR+300C in comparison to the initial temperature of pristine PVC insulation material.
- It is observed that the maximum weight loss of pristine PVC material is 10.1% at 300°C whereas that of PR+300C is 10.1% at 300°C.
- Hence, the addition of flame retardant will also be better for PVC material than to the absence of flame retardant which acts as thermal barrier.
- Weight loss is reduced in comparison with the insulation studied. It is observed that the flame retardant added to the surface and thereby reduces the PVC material at higher temperatures in comparison with the pristine PVC material.
- Due to the reduction in the surface weight, the thermal insulation improved for PVC insulation material in spite of flame retardant studies.

- FTIR analysis was carried out to observe ageing and anti-ageing studies of PVC to study the changes in the look of the sample after ageing.
- For anti-ageing samples, it is explained that the sample undergoes peak shift behaviour due to the formation of new functional groups.

CONCLUSIONS

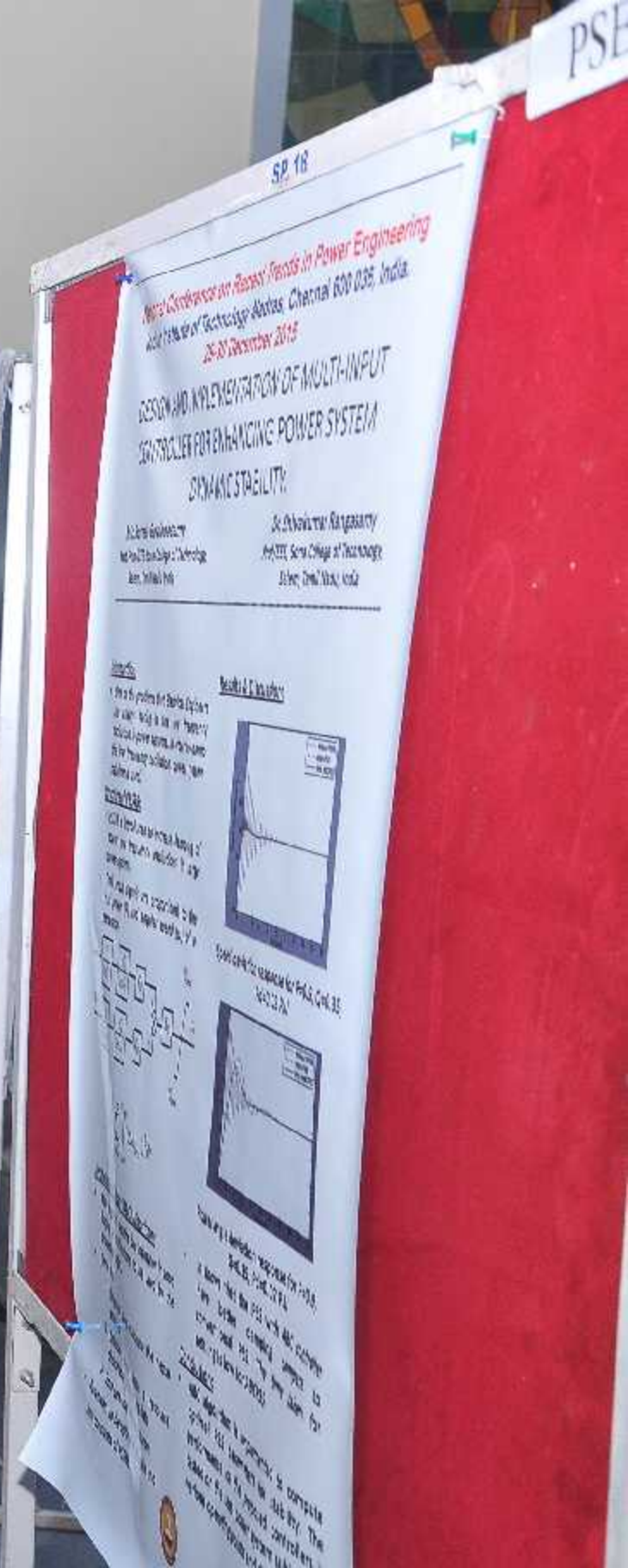
1. The flame retardancy is dependent on the nature of flame retardant and the surface area of the flame retardant.
2. The PFR value is increased by 3%, 13% and 12% for PVC, PR and PR+300C materials respectively.
3. The flame retardancy is increased with thermal ageing as compared to PVC and PR.
4. FTIR analysis shows 10% weight loss with thermal ageing due to progressive ageing.
5. PVC insulation material is more susceptible to thermal ageing than PR and PR+300C.
6. The addition of flame retardant to the insulation material is the most effective way to reduce the thermal ageing.

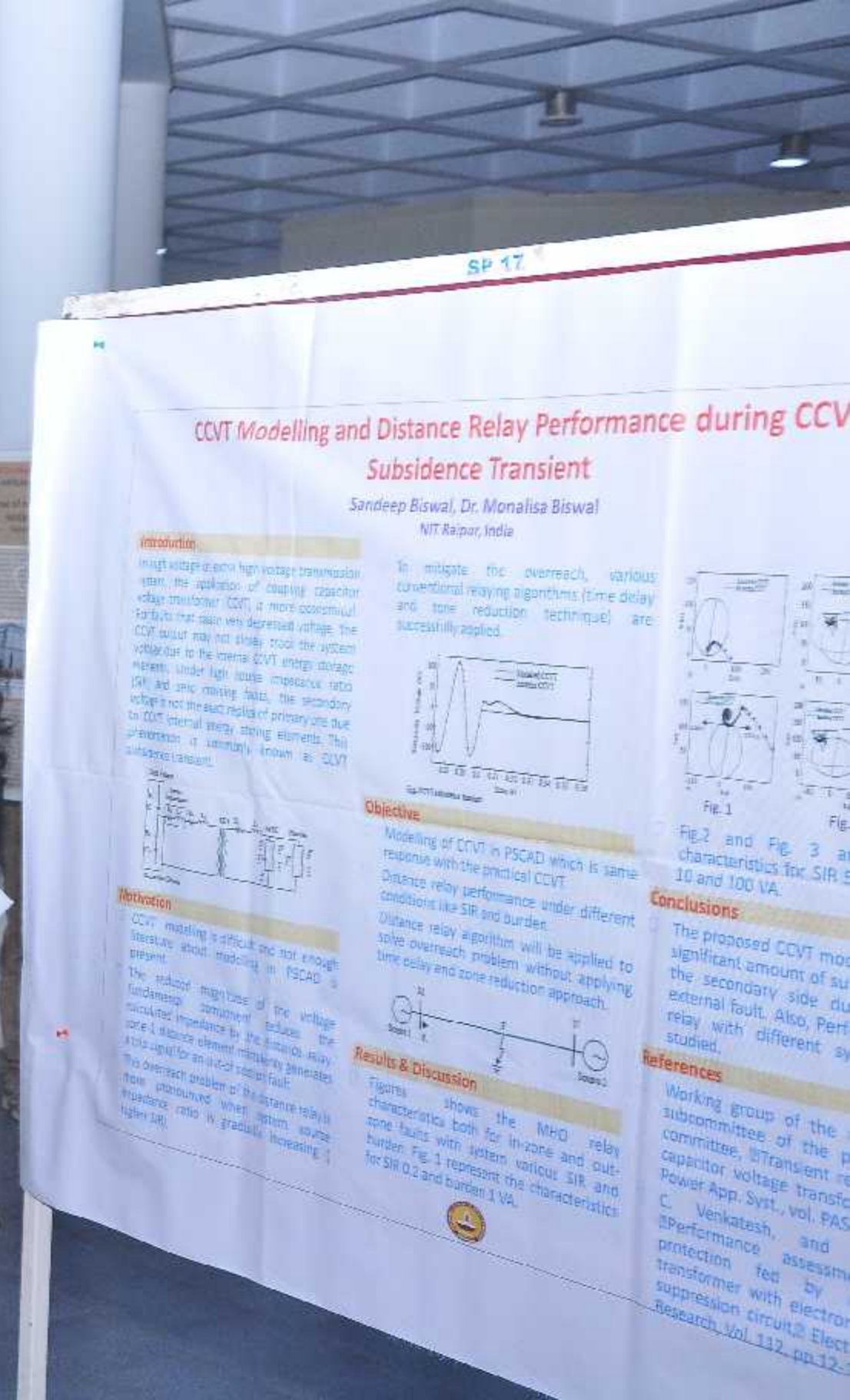






PED063





UVETO29

PP 18

National Conference on Recent Trends in Power Engineering
Indian Institute of Technology Madras, Chennai - 600 036, India
29-30 December 2015

Comparison of Conventional and Phase Shift Methods for
Condition Monitoring of Metal Oxide Surge Arresters

Likhitha S¹ (likitha_jr@iitm.ac.in) Littin Pauly P¹ M. Kanyakumari² R. S. Shivakumara Aradhya²
¹ Central Power Research Institute, Bangalore ² Acharya Institute of Technology, Bangalore

INTRODUCTION

Power providers protect the power system from the effects of over voltages. During this process it is subjected to severe thermal stresses leading to aging. As increasing the resistor leakage current in the arrester, ultimately leading to its failure. It is important to perform the condition monitoring of the power system participants by monitoring current drawn by it. The most common voltage measurement measurement is difficult due to noise. Therefore extraction with noise is very essential.

The total I_2 measured is based on 100 resistors. Based on the reason that the other manufacturers design active arrestor I_2 without I_2 is required for this paper.

SHIFTER

The MOSA electrical circuit consists of a non-linear

METHODOLOGY

A MATLAB code was developed to implement the defined iterative algorithm to detect the resistive damage sectors. The accuracy was carried out up to 2.2% for 100% The details of the results are given in Table 1. The experimental setup is shown in Figure 4.

TABLE I	
RESULTS OF THE MODEL	
Quantity	Value
Resistive damage	100%
Conventional method	100%
Proposed method	99.99%

EXPERIMENTAL RESULTS

CONCLUSIONS

From the concluding data:

The IR compensation using shifted algorithm for non-resistive will give a value which has an error of about 2.2% AD%

The proposed and modified technique I_2 is only 0.02% off

as I_2 is reached and remains at 99.99% of the

resistor, making current repeatable.

No direct current algorithm can be avoided by



Central Power Research Institute

Chennai - 600 036, India

29-30 December 2015

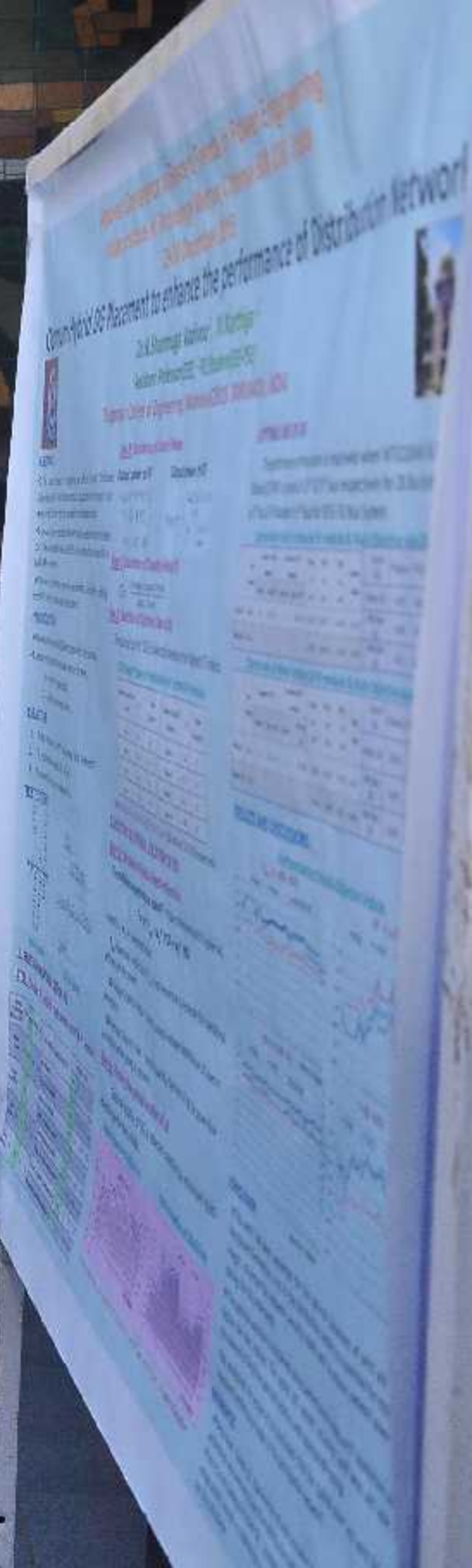
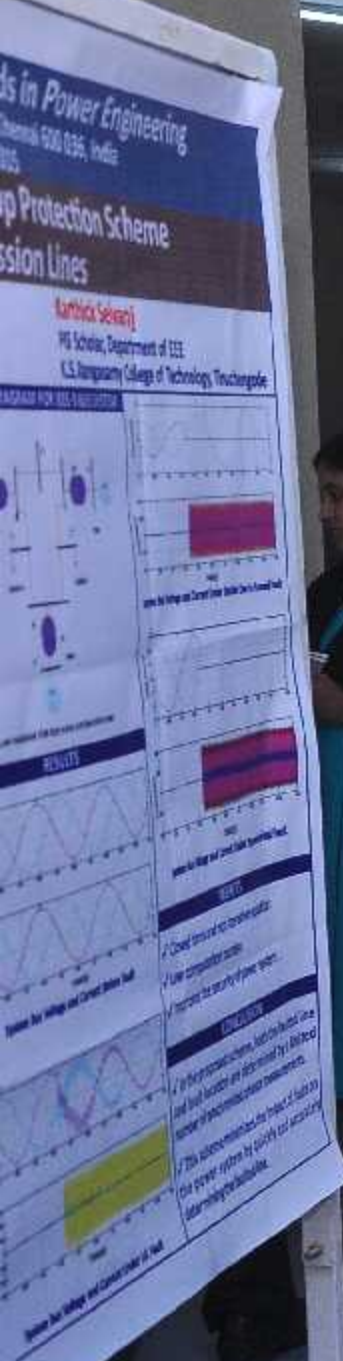
UVETO29

PP 18

सम्मेलन कक्ष 2
CONFERENCE HALL 2

WVE2020
Comparison of Seage ARRS/ERS Specification used in
UTV SYSTEMS
Author: Chaitali and Venkatesh K
Power Systems Institute, Bengaluru, India
E-mail: chaitali.k@psibangalore.com







स
म
ज





Introducing
the
new
method
of
soil
salinity
improvement

Author

1st

2nd

3rd

4th

5th

6th

7th

8th

9th

10th

11th

12th

13th

14th

15th

16th

17th

18th

19th

20th

21st

22nd

23rd

24th

25th

26th

27th

28th

29th

30th

31st

32nd

33rd

34th

35th

36th

37th

38th

39th

40th

41st

42nd

43rd

44th

45th

46th

47th

48th

49th

50th

51st

52nd

53rd

54th

55th

56th

57th

58th

59th

60th

61st

62nd

63rd

64th

65th

66th

67th

68th

69th

70th

71st

72nd

73rd

74th

75th

76th

77th

78th

79th

80th

81st

82nd

83rd

84th

85th

86th

87th

88th

89th

90th

91st

92nd

93rd

94th

95th

96th

97th

98th

99th

100th

101st

102nd

103rd

104th

105th

106th

107th

108th

109th

110th

111th

112th

113th

114th

115th

116th

117th

118th

119th

120th

121st

122nd

123rd

124th

125th

126th

127th

128th

129th

130th

131st

132nd

133rd

134th

135th

136th

137th

138th

139th

140th

141st

142nd

143rd

144th

145th

146th

147th

148th

149th

150th

151st

152nd

153rd

154th

155th

156th

157th

158th

159th

160th

161st

162nd

163rd

164th

165th

166th

167th

168th

169th

170th

171st

172nd

173rd

174th

175th

176th

177th

178th

179th

180th

181st

182nd

183rd

184th

185th

186th

187th

188th

189th

190th

191st

192nd

193rd

194th

195th

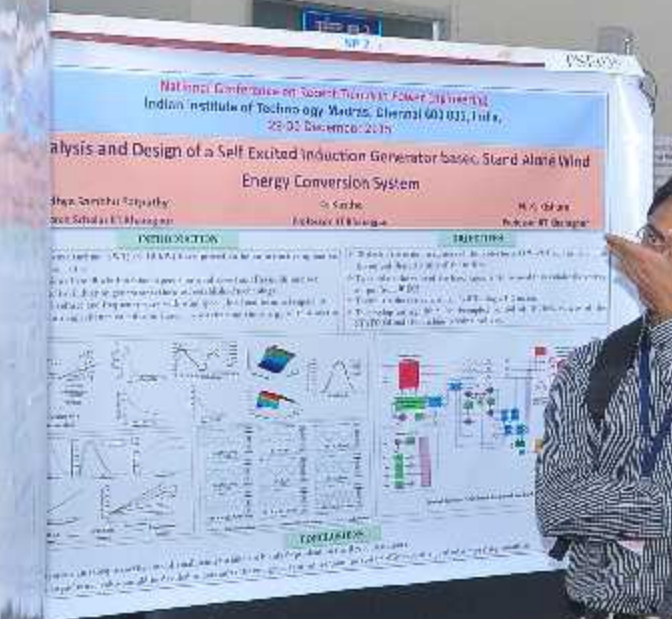
196th

197th

198th

199th

200th





PED049

Impact Of The Layout On The Performance Of A High Frequency Synchronous Buck Converter.

Rajat Channappanavar and Santanu Mishra

Department of Electrical Engineering, Indian Institute of Technology Kanpur, India

IMPORTANT CONSIDERATIONS FOR HIGH FREQUENCY POWER BOARD LAYOUT

- Plan the layout
- Use Thick Cu Trace for power line
- Multiple Vias to reduce resistance
- Small Switch Node Area to reduce EMI
- Large Thermal pads: To Act as Heat Sink
- Maximize Current Loop Surface Area

MAGNETICS OF THE LAYOUT

$$\text{Magnetic Flux} = \text{Magnetic Field} \times \text{Loop Area}$$

$$\theta_B = \frac{\pi}{2} \tan^{-1} \frac{B}{H}$$

B_0 – Magnetic Flux
 H – Magnetic Field
 A – Long Surface Area
 θ – angle between field and area's half vector

CURRENT PATHS ON PCB

Fig. 1: Schematic of Synchronous Buck Converter

Fig. 2: Current paths in SBC

Fig. 3: Current paths in an imperfect layout

Fig. 4: Current paths for improved layout

EXPERIMENTAL VERIFICATION

Fig. 5: Experimental setup of Synchronous Buck Converter with Current Paths marked, Case 1: Imperfect Layout, Case 2: Improved Layout

Fig. 6: Correction introduced to improve the imperfect experimental setup.

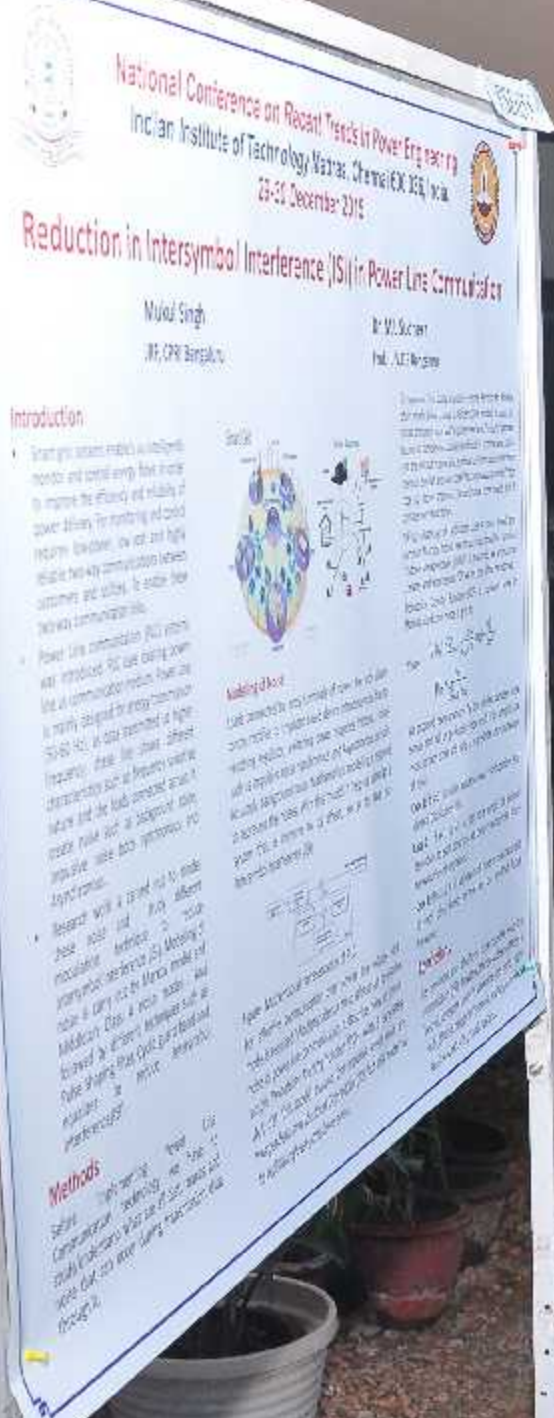
Fig. 7: Switch node voltage and output voltage of the imperfect layout of SBC.

Switch Node spikes: 2 V
Output spikes: 14 V

Fig. 8: Switch node voltage and output voltage of circuit with improvements in Fig. 6.

Switch Node spikes: 2 V
Output spikes: 2 V

POWER MANAGEMENT LAB
Indian Institute of Technology Kanpur





CENTRE FOR
INDUSTRIAL CONSULTANCY



&

APPLIED RESEARCH





NATIONAL CONFERENCE ON RECENT TRENDS IN POWER ENGINEERING

(For Research Scholars)

Date: 29 - 30 December 2015

Venue : IC & SR Auditorium

**Department of Electrical Engineering
Indian Institute of Technology Madras**

10 11 12 1 2
9
8 7 6 5 4





पंजीकरण
REGISTRATION





पंजीकरण
REGISTRATION

**IC & SR
BUILDING**

GROUND FLOOR:
CONFERENCE HALL - 1234
AUDITORIUM
DINING HALLS
FIRST FLOOR:
DEPT. IC & SR
CONFERENCE ROOM
IC & SR OFFICE
PROJECT ACCOUNTS
IC & SR COMPUTER
SECOND FLOOR:
DRAFT. DEPT.
OFFICE OF RESEARCH
PROJECT
PROJECT
THIRD FLOOR:
CENTRE FOR
CONTINUING
EDUCATION



GROUND FLOOR
Conference Halls I, II & III
Auditorium
Exhibition Hall
Dining Hall

FIRST FLOOR
Center for Industrial
Consultancy &
Sponsored Research

SECOND FLOOR
National Institute of
Ocean Technology

THIRD FLOOR
Centres For Continuing
Education









Venue : IC & SR Auditorium





